INFRARED INVESTIGATIONS OF GALACTIC STRUCTURE AND THE X-RAY RAPID BURSTER

by

Anthony Wynn Jones
BSc, ARCS

Astronomy Group
Blackett Laboratory
Imperial College of Science and Technology
London SW7

A thesis submitted for the degree of
Doctor of Philosophy of the University of London
and for the
Diploma of Membership of the Imperial College

May 1982

ABSTRACT

INFRARED INVESTIGATIONS OF GALACTIC STRUCTURE AND THE X-RAY RAPID BURSTER

A. W. Jones

This thesis reports two astronomical projects made with the 1.5 m Tenerife telescope. First, a survey of near-infrared sources in the galactic plane, and second, the detection of bursts of infrared radiation from the X-ray source MXB 1730-335.

The survey was made at 1.65 μm (H band) and 2.2 μm (K band) in 18 small areas on the galactic equator between longitudes 0^{o} and 10^{o}. It is complete to H = 10.5 and K = 9.5. This is equivalent to detecting type M giants at 6-7 kpc. Appendix A lists the equatorial coordinates and H and K magnitudes of 826 sources in a total area of 0.18 deg^{2}. These sources account for 40-50% of the 2.4 μm surface brightness of the galactic disk. The observations are consistent with the presence of supergiants in the putative 5 kpc ring, but are not conclusive. There is evidence for a population (~ 1000 deg^{-2}) of luminous, reddened objects, which may be supergiants within 0.4^{o} (70 pc) of the galactic nucleus. Otherwise, the distribution of survey sources does not depend strongly on longitude.

MXB 1730-335, the Rapid Burster, is inside the globular cluster Liller 1. It is unique in producing thousands of X-ray bursts a day in its active state. In 1979 two bright bursts of 2.2 μm radiation were detected from this object. They are notable for their great luminosity (10^{30} W), accompanying flashes, and high brightness temperature (10^{10} - 10^{18} K). These bursts are most plausibly associated with Type II X-ray bursts, although there were no simultaneous X-ray observations. A concerted international campaign failed to detect any further X-ray or infrared activity. Reports of radio bursts remain unsubstantiated.

Appendix B contains papers written by the author on the Rapid Burster and on the statistics of supposed quasar-galaxy associations.

PREFACE

The work reported in this thesis was carried out by the author in the Astronomy Group at Imperial College, under the supervision of Dr M. J. Selby. It was part of a continuing collaboration between Imperial College and Dr C. Sánchez Magro of the Instituto de Astrofisica de Canarias (IAC), La Laguna.

Chapters 1 to 4 are an account of a survey of near-infrared sources in the galactic plane. The observational part of the project was conducted by the author in collaboration with M. Prieto Muñoz. The analysis and interpretation of the observations are by the author alone.

Chapters 5 and 6 report the detection of bursts of infrared radiation from the X-ray source MXB 1730-335, the Rapid Burster. The observations which form the basis of Chapter 5 were obtained for the author by C. M. Mountain and C. Sánchez Magro. Subsequent monitoring of the source was conducted by the author in collaboration with C. Martinez Roger. All analysis, interpretation and criticism are by the author alone.

Amendments in red are at the request of the Examiners.

ACKNOWLEDGEMENTS

I thank first my supervisor, Mike Selby, for giving me free rein to pursue this work where I saw fit, and Professor Jim Ring for his wise counsel at several critical moments.

Those who have worked at the Observatorio del Teide know well the frustrations, joys, miseries and triumphs of a long observing trip. I must thank my two colleagues at La Laguna who sat through it all with me. Mercedes Prieto assisted with the planning of the galactic plane survey and shared eight interminable weeks of scanning survey blocks and turning cryostats inside out. Carlos Martinez spent many chilly nights gazing at the rosy 2.2 μm glow from the inscrutable globular cluster that hides the Rapid Burster. We saw no bursts, but at least it got him his 'licenciatura'.

Not so Mattias Mountain and Carlos Sánchez, who contrived to be in the right place at the right time to catch the elusive infrared bursts with 15 minutes to spare (and not many people have done that). Those observations spawned Chapters 5 and 6 of this thesis.

For most of this time I was kept alive by a Research Studentship and a Research Assistantship from the Science and Engineering Research Council. I thank, too, Professor Francisco Sánchez for his generous support during a happy month in La Laguna and consequent forced learning of Spanish.

Pat Kerridge typed this thesis to my somewhat precise specifications and still came out smiling.

Finally, I wish to thank those friends and colleagues at Imperial College and La Laguna who have helped in innumerable ways during the course of this work. Above all I am grateful to Bob Joseph for his ideas, moral support and professionalism.

CONTENTS

LIST OF TABLES

LIST OF FIGURES

CHAPTER 1

INVESTIGATION OF GALACTIC STRUCTURE BY INFRARED TECHNIQUES

In recent years our knowledge of the structure of the Galaxy, gleaned from radio and visual observations, has been augmented by a growing series of infrared investigations. The 1-5 μm near-infrared bands provide the only means of detecting ordinary stars at distances ∿ 10 kpc. Two complementary survey techniques have been used; mapping the surface brightness of the Milky Way, and cataloguing of bright, discrete sources. Two important populations of infrared sources have emerged from this work. First the type M giants, which account for the bulk of the infrared radiation in the Galaxy, and second, a population of luminous, dust-shrouded objects, concentrated in the galactic plane and especially in a ring near R = 5 kpc. There is a need for new surveys of discrete sources, reaching deeper into the central region of the Galaxy.

1.1 Introduction

The main features of our Galaxy are now well established (Figure 1.1). There are four components:

(1) The nuclear region (or "core") about 1 pc across, containing the pointlike and highly energetic object in the core of the radio source Sgr A West, and a complex of radio, infrared and X-ray sources surrounding it.

(2) The central bulge (or "hub"); a spheroidal concentration of old stars extending out to ∿ 2 kpc from the centre.

(3) The roughly circular disk, about 25 kpc across and 600 pc thick, containing the spiral arms and dust lanes.

(4) The sparsely populated halo of stars, more or less spherical and centred on the bulge, reaching out to about 15 kpc.

The sun lies in a spiral arm about 10 kpc from the nucleus. Oort (1977) in his review of studies of the galactic centre, says that the distribution of RR Lyrae variables now gives the best measure

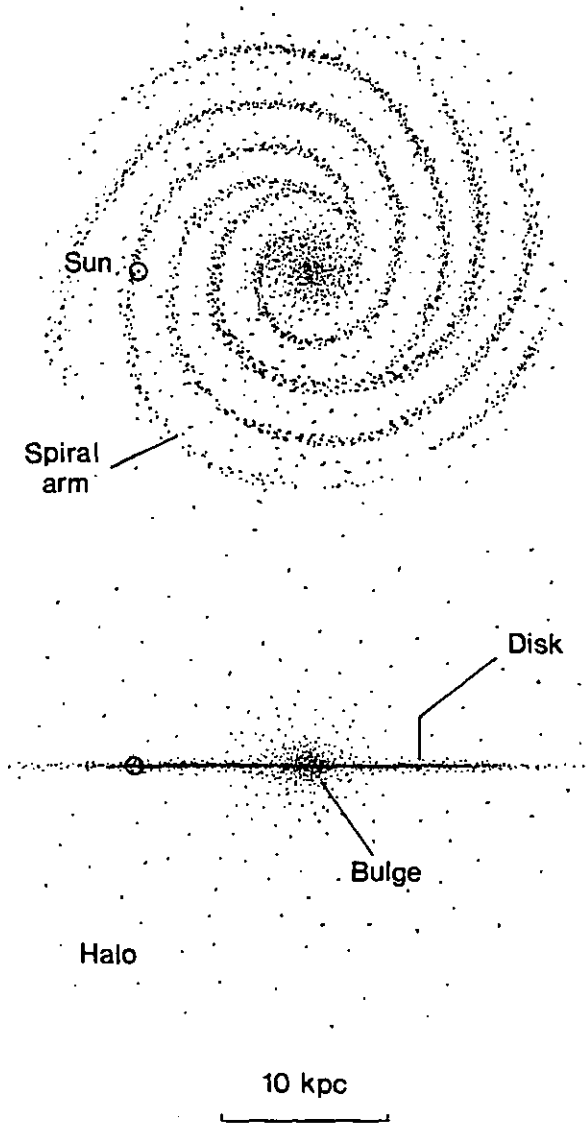

Figure 1.1 - The main features of the Galaxy

of this distance, that is $R_o = 8.7 \pm 0.6$ kpc. However, there is still much disagreement, and for the purposes of this thesis I will assume $R_o = 10$ kpc, as is usual in galactic astronomy.

Almost all our knowledge of the large-scale shape of the Galaxy has been inferred from radio observations. Radio waves ($\lambda > 0.1$ m) pass through interstellar space with negligible attenuation, allowing us to see the entire extent of the Galaxy. HII regions and supernova remnants dominate the galactic radio sky, but clouds of neutral, atomic hydrogen (HI) have proved to be the best spiral tracers. Radio astronomers made the first large-scale

maps of the spiral structure from measurements of the Doppler-shifted 21 cm HI line, interpreted through kinematic models (Schmidt—Kaler 1976).

Visual methods have not been so successful. At the beginning of this century astronomers put much faith in star counts as a means of investigating galactic structure (Bok 1937). They tried to arrive at a model of star distribution by measuring surface number densities in various parts of the sky. Unfortunately, they were not aware of a general interstellar extinction which rendered the method useless over long distances.

To see how visual observations can be thwarted by interstellar extinction, consider the equation relating the apparent magnitude m of a star, and its absolute magnitude M:

$$m = M - 5 + 5 \log r + Ar \qquad (1.1)$$

where r = distance in pc
A = extinction in mag pc^{-1}

Take $M \sim 5$ for a star like the Sun (AQ p.162). Without extinction, its apparent magnitude at r = 10 kpc would be m = 20, easily detectable on photographic plates. But with a mean interstellar extinction of 1.9 mag kpc^{-1} in the galactic plane (AQ p.263), its brightness would be reduced to an unobservable m = 39. Even the brightest supergiants ($M \sim -8$) would appear as a mere $m \sim 26$. Some improvement may be had by looking above and below the galactic plane, or in "windows", where the obscuring dust is not so thick,but even then visual methods are not generally useful beyond $\sim$ 4 kpc (Schmidt-Kaler 1976).

Now consider what happens when we look at the Galaxy in the near infrared, say 2 μm. At this wavelength stars are still dominant (although we see the Rayleigh-Jeans tails of most of them), but the interstellar extinction is now much lower, perhaps 0.2 mag kpc^{-1} (AQ p.264). Over a 10 kpc distance the extinction is therefore a factor of 6.3, compared with $\sim 10^8$ for visible light. To put it another way, 15% of the infrared gets through, but only 10^{-6}% of the visible. Or another way again, the path length for unit optical depth is about 5 kpc at 2 μm, but only 0.6 kpc in the visible. If

we want to study the large-scale distribution of stars in the Galaxy, infrared methods are ideal.

There are two main ways of doing this:

(1) To count discrete infrared sources in a manner analogous to the traditional visual star counts.

(2) To use a large sky aperture to measure the integrated surface brightness of the Milky Way.

Beyond 1 μm there is no infrared counterpart to the photographic plate (photon energies are too small) so the first option would have to be done by direct photometry, which is a slow process. I will return to this in Section 1.3. The second method is much more attractive, and in the next Section I review what it has already taught us about the inner regions of the Galaxy.

1.2 Surveys of diffuse 2.4 μm emission

Conventional infrared photometry from the ground is of little use in mapping the surface brightness of the Milky Way. The problem is OH airglow, which originates in a layer about 90 km above the ground. Even in the 1–5 μm atmospheric windows the sky emission is patchy and changeable, being comparable to the brightness of the Milky Way itself (Hofmann et al. 1978).

A surprising solution, at first sight, is to fly telescopes on balloons at altitudes of $\sim$ 30 km. Although this is below the OH layer, three research groups have successfully exploited a unique gap in the airglow at $\lambda = 2.4$ μm with $\Delta\lambda = 0.1$ μm. In this window, which is not accessible from the ground, OH emission is some 15 times weaker than at 2.2 μm (K band) allowing the Milky Way to be seen clearly, about seven times brighter than the sky itself (Hofmann et al. 1977, 1978).

All three groups, at Nagoya, Kyoto and the Max-Planck-Institut für Astronomie (MPIA), Heidelberg, used similar equipment. The telescopes were 10–20 cm in diameter with lead sulphide (PbS) detectors. Signals were chopped against nitrogen-cooled rotating sectors, which gave an absolute measurement of the integrated radiation entering the sky apertures (0.5–3°). Table 1.1 lists all the 2.4 μm balloon flights for which data have been published, and one rocket flight made as part of the same programme.

Table 1.1 - Near-Infrared Observations of the Milky Way with Balloon-Borne Telescopes

Date	Group	D (cm)	λ (μm)	Beam (deg)	Accuracy (± deg)	Area covered	References
1974 Aug 12	MPIA	15	2.4, 3.4	2	0.5	Bulge	Hofmann et al 1977
1975 June 16	Kyoto	20	2.4	1	0.3	(failure)	Maihara et al 1978, Okuda et al 1977
1975 Sep 9	Nagoya	10	2.4	3	0.5	N. Milky Way	Ito et al 1976, Hayakawa et al 1976, 77
1976 May 30	Nagoya	10	2.4	2	-	Bulge	Ito et al 1977, Hayakawa et al 1977
1976 May 31	Kyoto	20	2.4	1	0.3	Bulge	Okuda et al 1977, Maihara et al 1978
1977 Jan 16	Nagoya	8	2.3	4	-	Anticentre (rocket)	Hayakawa et al 1978
1977 May 21	Kyoto	20	2.4	0.6	0.3	Bulge	Oda et al 1979
1977 June 16	MPIA	15	2.45	1	0.5	Bulge, Aquila	Hofmann et al 1978
1977 Aug 31	Nagoya	10	2.4	1.7	-	Bulge, N. Milky Way	Hayakawa et al 1980
1978 April 25	Nagoya	10	2.4, 3.4	0.5, 0.8, 1.7	0.2	Bulge, S. Milky Way	Hayakawa et al 1979, 80

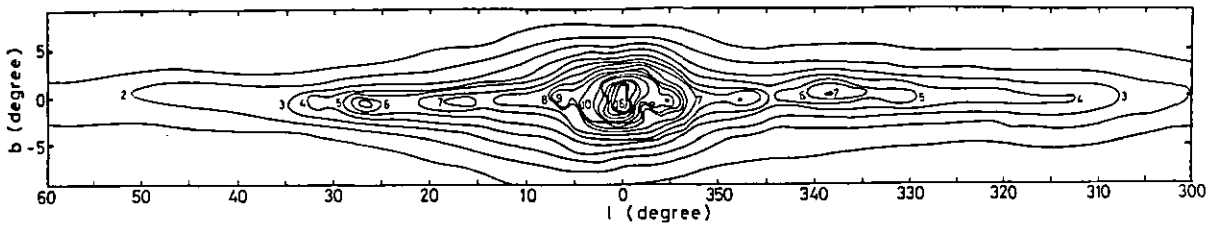

Figure 1.2 - Near-infrared map of the Milky Way

The Milky Way appears as an edge-on spiral galaxy in this composite 2.4 μm map made with 1.7° and 3° beams. The contour unit is 1×10^{-6} W m^{-2} μm^{-1} sr^{-1}. (From Hayakawa et al. 1981.)

Figure 1.2 is one of the many surface brightness maps that came out of this work, and displays the three main features of interest. They are:

(1) The central bulge

(2) The disk

(3) Fine structure and dust.

We now examine these three in detail.

1.2.1 The central bulge

Beginning with the flight of Hofmann et al (1977), the 2.4 μm surveys have revealed the full extent of the central bulge of our Galaxy for the first time (Figure 1.3). Until then astronomers had, at best, glimpsed only small parts of it (e.g. Arp 1965).

The bulge is roughly elliptical, stretching to ± 15° in longitude and ± 7.5° in latitude, corresponding to ± 2.5 and ± 1.3 kpc (Maihara et al., 1978). The half-peak radii are ℓ = 5° and b = 3° (Hofmann et al., 1977).

Maihara et al. (1978) assumed that the bulge behaved as a 4000 K black body and deduced a bolometric luminosity of 2×10^{10} $L_\odot$, similar to the 1.7×10^{10} $L_\odot$ of M31, the Andromeda galaxy. Hofmann et al. (1977) estimated the luminosity of the central 2° of the bulge to be 8×10^{9} $L_\odot$, though only 3% of this appears in the near infrared. The corresponding central mass, derived using M/L = 10 for an Sb galaxy, is 3×10^{10} $M_\odot$, about 20% of the total mass of the Galaxy (AQ p.282).

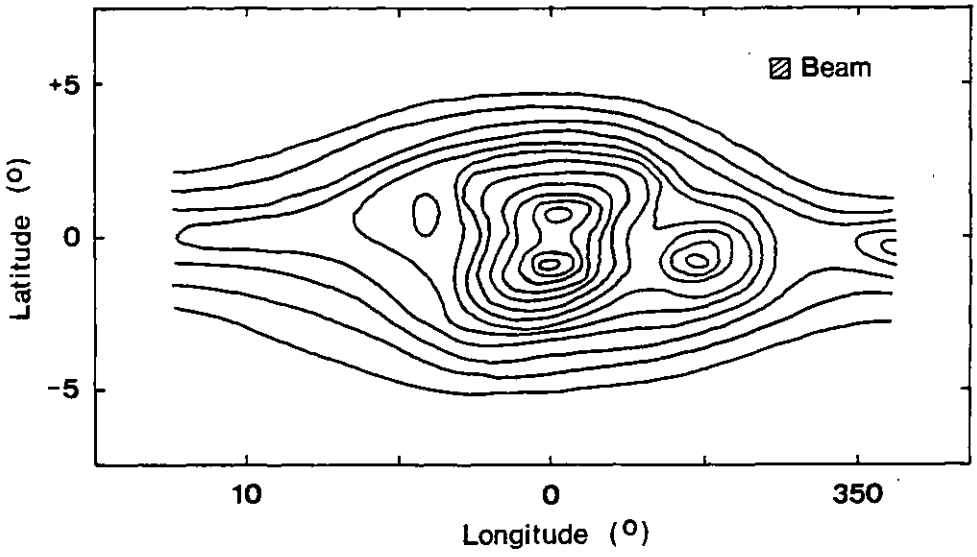

Figure 1.3 - Near-infrared map of the central bulge

Obscuring dust has distorted the oval shape of the bulge and split the central peak into two "islands". The isolated hump at $l = 355^{\circ}$ is most probably a gap in the extinction. Contour units are 1×10^{-6} W m^{-2} μm^{-1} sr^{-1}. The highest contour (in the southern "island") has a value of 15 units. (Adapted from Oda et al. 1979.)

1.2.2 The disk

Until Hayakawa et al. (1979) mapped the southern Milky Way, investigators concentrated on the bulge and the galactic plane to its northern side. The most conspicuous feature is a plateau running from $l = 15^{\circ}$ to a sharp drop at $l = 30^{\circ}$ (see Figure 1.4). Its southern counterpart seems to run to $l = 310^{\circ}$.

On the plateau, the width of the galactic disk (FWHM) is only 3.5° (Maihara et al. 1978) compared to the $\simeq 20^{\circ}$ of late M stars which are believed to contribute most of the near-infrared brightness (Blanco 1965). Surprisingly, there is no evidence of a dip at the peak of the 2.4 μm latitude profile as might be expected from the narrow dust layer in the galactic plane. (Blanco's survey, made in the I band, does show a distinct dip). The 2.4 μm sources must therefore be concentrated towards the galactic plane at least as much as the dust, implying that they are Extreme Population I objects (Hayakawa et al.1977).

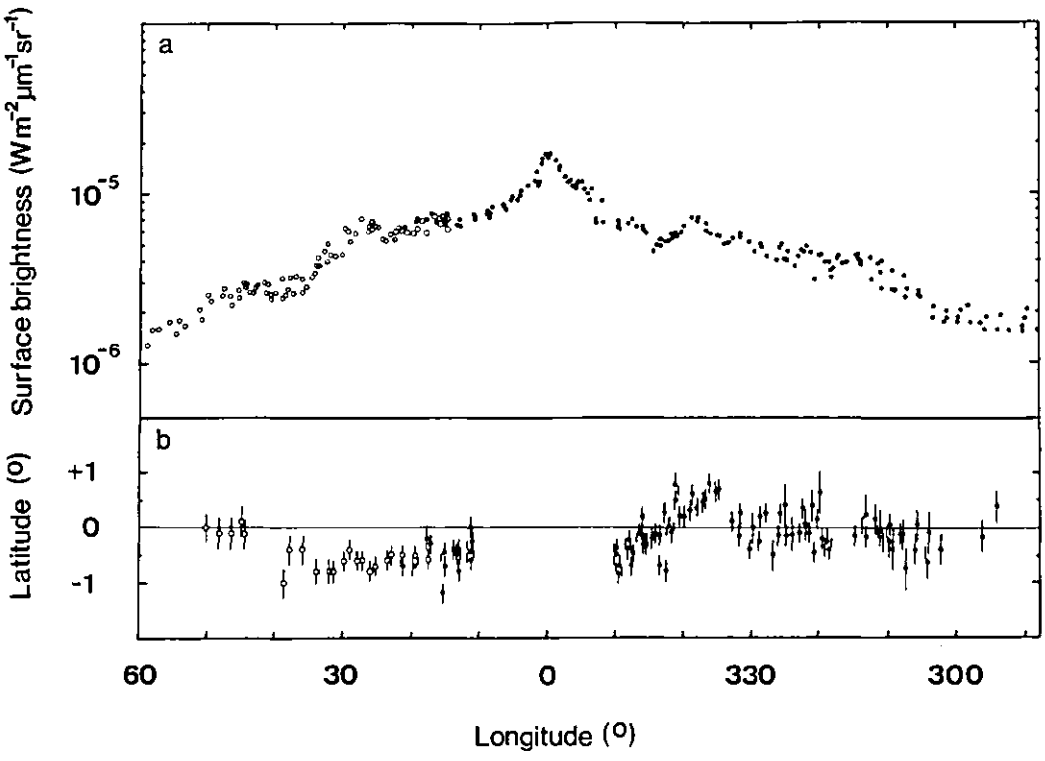

Figure 1.4 - Longitude distribution of near-infrared flux.

a Peak 2.4 μm surface brightness measured with a 1.7° beam. The broad plateau between 310° and 30° is interpreted as a dense ring of young, bright objects about 5 kpc from the galactic centre.

b The latitude of the peak surface brightness.

Both plots are composites of separate observations denoted by the black and white circles. (Adapted from Hayakawa et al. 1979.)

Longitude profiles of CO emission, 408 MHz continuum, gamma-ray emission and far-infrared emission all show peaks at around $\ell = 30^{\circ}$ - the edge of the plateau. The inference is that there is a ring of infrared sources 5 kpc out from the galactic centre, associated with molecular clouds, dust and HII regions (Hayakawa et al. 1976, Okuda et al. 1977). This may be analogous to a 6 kpc ring in M31 (Maihara et al. 1978). Hayakawa et al. (1977, 1980) inferred a width of 300 pc and a scale height of 50-100 pc for the infrared ring, confirming that the sources are Extreme Population I. Such young infrared objects may be protostars, embedded in the dust clouds, or bright supergiants.

Beyond the 5 kpc ring the 2.4 μm longitude profile is fairly well accounted for by the known distributions of M giants (Maihara et al. 1978, Hayakawa et al. 1978), though Hayakawa et al. (1977) have postulated a weaker ring of sources at 7.4 kpc.

1.2.3 Fine structure and dust

Local humps, dips and valleys are superimposed on the ellipse of the bulge and the ridge of the galactic disk. These could be genuine sources close to the Sun, or embedded in the inner parts of the Galaxy, or perhaps they are distortions produced by the clumpy nature of interstellar extinction.

Near the equator the highest contours are distorted to run perpendicular to the plane, even forming little islands. This is interpreted as evidence for a thin layer of strong extinction. Okuda et al. (1977) assumed that our bulge, if unobscured, would have the same shape as that of M31. They deduced the presence of a central core of dust in the region $b = \pm 1^{\circ}$, $\ell = \pm 2^{\circ}$, contributing about a third of the total 2.4 μm extinction to the galactic centre (2.4 mag, equivalent to 30 mag at V).

This was confirmed by Maihara et al. (1978) who, by the same method, estimated the longitude distribution of extinction in the central region, and found that the dust layer in the disk was about 300 pc thick. The mean extinction in the disk is $A_V = 1.5$ mag kpc^{-1}, rising to 2.2 mag kpc^{-1} in the 5 kpc ring. Oda et al. (1979) took this method a stage further and produced a map of the 2.4 μm extinction in the bulge region (Figure 1.5). The core concentration correlates well with far-infrared maps (e.g. Maihara et al. 1979) and has an estimated mass of 10^5 $M_\odot$ of dust (Oda et al. 1979).

One of the most remarkable of these features is an emission hump near $\ell = 355^{\circ}$, $b = -1^{\circ}$ (see Figure 1.3). All three balloon groups noted this anomaly, so it is certainly a real feature, though not so prominent on some maps as on others. It does not coincide with any known object. According to Maihara et al. (1978) and Ito et al. (1977) the nearby open star clusters NGC 6383 and NGC 6405 (M6) are not bright enough to produce the infrared flux, and there is no radio source in that position.

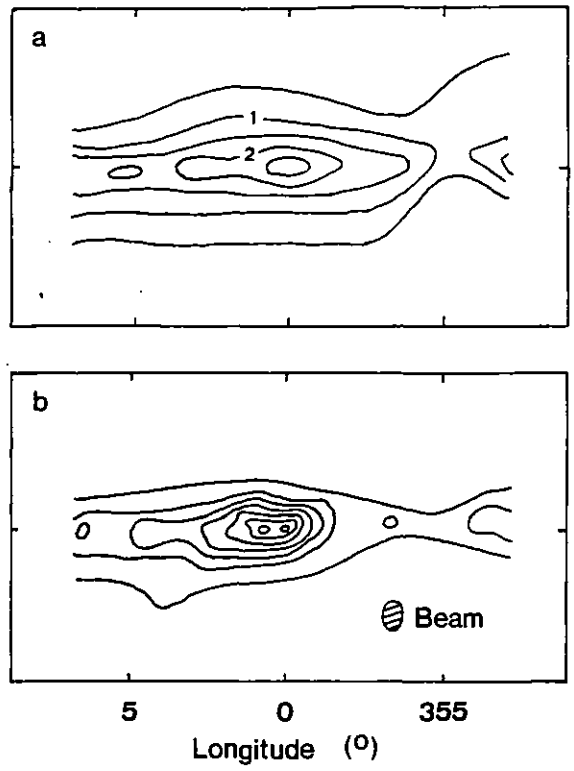

Figure 1.5 - Dust in the central region of the Galaxy

a 2.4 μm extinction (in magnitudes) derived by assuming the unobscured bulge to have the same shape as the bulge of M31. (Adapted from Oda et al. 1979.)

b Far-infrared map (150 μm) of the same region showing good agreement with the extinction map. The contour unit is 1×10^{-7} W m^{-2} μm^{-1} sr^{-1}, and the highest contours are 10 units. (Adapted from Maihara et al. 1979.)

Maihara et al. (1979) in their far-infrared survey of the galactic plane, found a pronounced depression in the 150 μm emission at the position of the 2.4 μm hump (see Figure 1.5). Since far-infrared emission is correlated with the presence of dust, the most likely explanation for the hump is a local reduction of 3-4 magnitudes of visual extinction.

A less prosaic explanation is that the hump is a visually obscured elliptical companion to our Galaxy, similar to the two companions of M31. Oda et al. (1979) have calculated that one of these companions, M32, would appear similar to the hump if placed at a distance of 40 kpc.

1.3 Surveys of discrete infrared sources

We have seen how the surface brightness surveys have revealed much about the inner structure of the Galaxy. But there has been no way to distinguish the different kinds of sources contributing to the integrated flux. As well as many thousands of stars, the wide beams ($\sim 1^{o}$) take in HII regions, hot dust and perhaps sources unknown at present. What are the infrared sources? How are they distributed in space? Can the diffuse emission be accounted for by the known distribution of stars, or are new objects needed?

To answer these questions, we need to survey the sky at higher angular resolutions, in the hope of resolving the discrete objects that are presumed to contribute to the diffuse emission. There have been two comprehensive surveys of the sky at near-infrared wavelengths: the Two Micron Sky Survey (TMSS) and the AFGL Sky Survey.

1.3.1 Two Micron Sky Survey

The TMSS was an unbiased survey covering 77% of the sky at 2.2 μm, down to K = 3. The results of the survey comprise the Infrared Catalogue (IRC) which contains 5612 sources with a mean sky density of $N(3) = 0.18\ \mathrm{deg}^{-2}$ (Neugebauer and Leighton 1969). What are these sources?

Grasdalen and Gaustad (1971) compared the IRC with the Dearborn Catalogue (DC) of Faint Red Stars (i.e. later than K5). Of the 3887 IRC sources in the area of overlap, 93% corresponded to DC stars with a peak around spectral type M4-M5. We conclude that most IRC sources are red stars, but what luminosity class are they?

We can do a quick calculation to show that they must be giants rather than main-sequence dwarfs. From AQ (p.249) we have the space densities in the galactic plane of M giants (ρ_G) and M dwarfs (ρ_D):

$$\rho_G = 3.2 \times 10^{-5}\ \mathrm{pc}^{-3}$$

$$\rho_D = 5.0 \times 10^{-2}\ \mathrm{pc}^{-3}$$

Red dwarfs therefore outnumber red giants by $\sim$ 1500 times.

Now we estimate the distance r out to which the IRC could detect each class. If N(m) is the sky density of sources to a limiting magnitude m, then

$$r = (3\ N(m)/\rho)^{1/3} \qquad (1.2)$$

if extinction can be ignored. For IRC sources in the galactic plane, $N(m) = N(3) \sim 0.5\ deg^{-2}$ or $1600\ sr^{-1}$ (Kleinmann et al. 1981). For each class of star we use Equation 1.2 to calculate r, and then Equation 1.1 to derive the absolute magnitude M_K. We find:

for giants: $r = 530$ pc, $M_K = -5.6$

for dwarfs: $r = 46$ pc, $M_K = -0.3$

Figure 1.6 is a 2.2 μm Hertzsprung-Russell diagram compiled from AQ (p.200) and Johnson (1966). From it we can see that type M giants have M_K in the range −4 to −7, while M dwarfs are much fainter, with an M_K of 5 to 7. The IRC stars must therefore be giants rather than dwarfs.

We conclude that at 2.2 μm the space out to ∼ 0.5 kpc is dominated by type M giants, even though the red dwarfs outnumber them by 3 orders of magnitude. We will take a "typical" IRC star to have $M_K = -5.5$, which corresponds to spectral type M3 III.

1.3.2 AFGL Sky Survey

Following the success of the Two Micron Sky Survey, the US Air Force Cambridge Research Laboratories (AFCRL, now Geophysics Laboratory, AFGL) conducted a rocket survey of most of the sky at the longer wavelengths of 4.2, 11.0, 19.8 and 27.4 μm. The results were published as the AFGL sky survey (Price and Walker 1976), containing 2363 sources.

Kleinmann et al. (1981) have assessed the catalogue in detail. They have three main conclusions about the nature of the AFGL sources.

1. The vast majority of stellar sources are M stars.

2. They are more heavily concentrated toward the galactic plane than are the IRC stars, presumably because of the lower extinction at the longer wavelengths.

3. Beyond 4 μm, a new class of infrared sources emerges. They are highly concentrated in the galactic plane, have a small scale height and low colour temperatures (10^2 to 10^3 K).

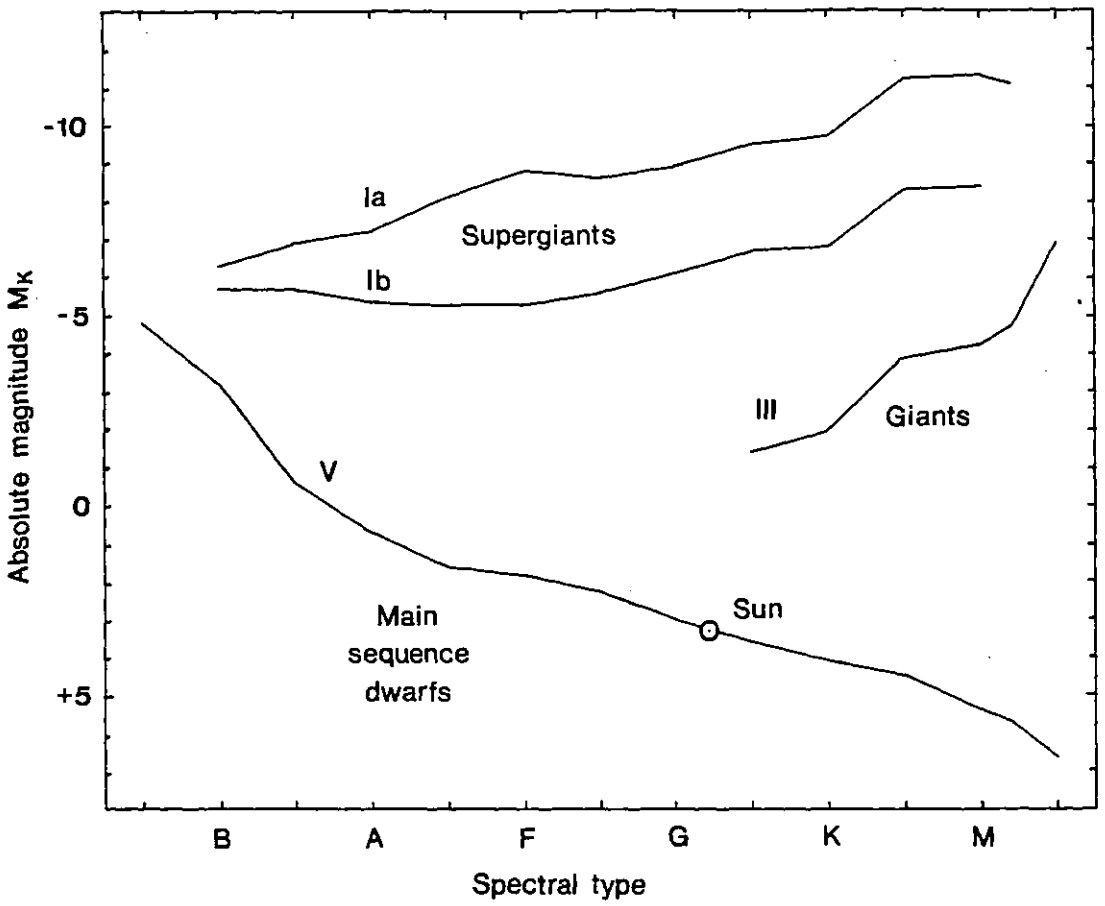

Figure 1.6 - Hertzsprung-Russell diagram at 2.2 μm (K)
(Compiled from AQ p. 200 & 208, and Johnson (1966)

1.4 Consensus of the sky surveys

The two kinds of large-scale survey - mapping of surface brightness and cataloguing of discrete sources - complement each other. From them comes a consensus that there are broadly two classes of important infrared emitters.

First, the infrared sources close to the sun (within our spiral arm) are predominantly type M giants. They can be typified as type M3 III with $M_K = -5.5$. These are old, Population II stars, only moderately concentrated in the galactic plane and may be more-or-less smoothly distributed throughout the disk and bulge of the Galaxy.

Second, there is a new population of infrared emitters, heavily concentrated in the galactic plane and shrouded by dust. They form a narrow ring, or arm, at R = 5 kpc. Almost certainly

they are very young, extreme Population I objects, such as supergiants or protostars, and we may expect them to delineate the spiral arms.

1.5 Objectives for a deep survey

There is a need for a new survey of discrete sources, covering a smaller area of sky than the TMSS or AFGL survey, but looking deeper into the inner parts of the Galaxy (say, within 5 kpc). Such a survey could be designed to answer the following questions:

(1) Can the 2.4 μm diffuse emission be accounted for by a superposition of discrete sources? If so, what kind of sources are required?

(2) Can the Extreme Population I sources in the galactic plane be detected and identified?

From the experience of the Imperial College infrared astronomy group it is an easy matter, without integration, to detect sources down to $m_K = 10$ in uncluttered parts of the sky.

In Table 1.2 I have collected examples of different types of stars and their absolute K magnitudes. The table gives the distance at which each star would have $m_K = 10$, and also values of M_K for distances of 5 and 10 kpc. I assume $A_K = 0.17$ mag kpc^{-1} in the galactic plane, deduced from Maihara et al. (1978).

Type M supergiants are young, rare and among the most luminous stars known. They will be detectable throughout most of the Galaxy. The M3 giants, as we have seen, are representative of the main class of infrared sources in the Galaxy. Type O stars are the hottest and most massive of the main sequence; they are the ionisation source for HII regions. The Becklin-Neugebauer object (BN) is the most famous candidate for a protostar (Becklin and Neugebauer 1967); that is, a star heated by gravitational contraction and which has not yet taken up its place on the main sequence. The Sun, which is included as a representative of the common main sequence stars, would not be detectable much beyond 0.2 kpc. These small stars will not figure much in a deep survey.

Table 1.2 - Visibility of Selected Stars at 2.2 μm

Star type	M_K	r for m_K = 10 (kpc)	m_K for r = 5 kpc	m_K for r = 10 kpc
M Ia	-11	25	3.5	5.5
M Ib	-8.5	15	6	8
M3 III	-5.5	7	9	11
O5 V	-4.5	5	10	12
BN object	-3	3	11.5	13.5
Sun	+3.2	0.2	18	20

The absolute magnitude of the BN object is derived from Becklin and Neugebauer (1967) using a distance of 460 pc to the Orion Nebula (AQ p. 260). Other M_K are from Figure 1.6.

1.6 Conclusions

1. Infrared observations provide the only means of studying the distribution of ordinary stars over distances $\sim$ 10 kpc.

2. A deep survey of infrared sources towards the central region of the Galaxy would be feasible and valuable, especially as a follow-up to previous surveys.

CHAPTER 2

A SURVEY OF INFRARED SOURCES IN THE GALACTIC PLANE

We have used the 1.5 m Tenerife telescope to make a survey of infrared sources in a ∿ 1 deg^2 strip of the sky stretching from $\ell = 0^o$ to $\ell = 10^o$ along the galactic equator. The area was divided into 80 survey blocks of 4 × 12 arcmin. The blocks were scanned at 1.63 μm (H) and 2.20 μm (K) with either 15" or 25" apertures. We secured observations of 14 blocks at H and 18 blocks at K, some 20% of the proposed coverage.

2.1 Introduction

This project arose from a suggestion by Dr. M. J. Selby in the summer of 1977. The infrared group at Imperial College had spent much time searching HII regions (most of which are in the Milky Way) in the hope of finding possible protostars, such as the BN object (see Section 1.5). These searches turned up more background sources than would be expected from simple extrapolations of star distributions near the sun (Jorden 1977).

The new project was to be a deep survey, in the H and K bands, of infrared sources in a strip of sky stretching from $\ell = 0^o$ to 10^o along the galactic equator and with an area of about 1 deg^2 (Figure 2.1). By concentrating the survey in the galactic plane we expected to detect a large number of sources between the sun and the central bulge, particularly in the spiral arms and perhaps in the bulge itself. On the other hand, the galactic plane is exactly where interstellar extinction is the strongest, and so is the worst place to look for objects at large distances.

Justification for this choice comes in hindsight. The surveys outlined in Chapter 1 showed that the most interesting infrared objects were extreme Population I with scale heights as small as 50 pc, corresponding to 0.6^o at a distance of 5 kpc. Figure 2.2 is a schematic representation of the known spiral features in the survey area. Some of these, the ones close to the Sun, are known from visual tracers. The 3 kpc arm is inferred from radio observations. Of most interest to us

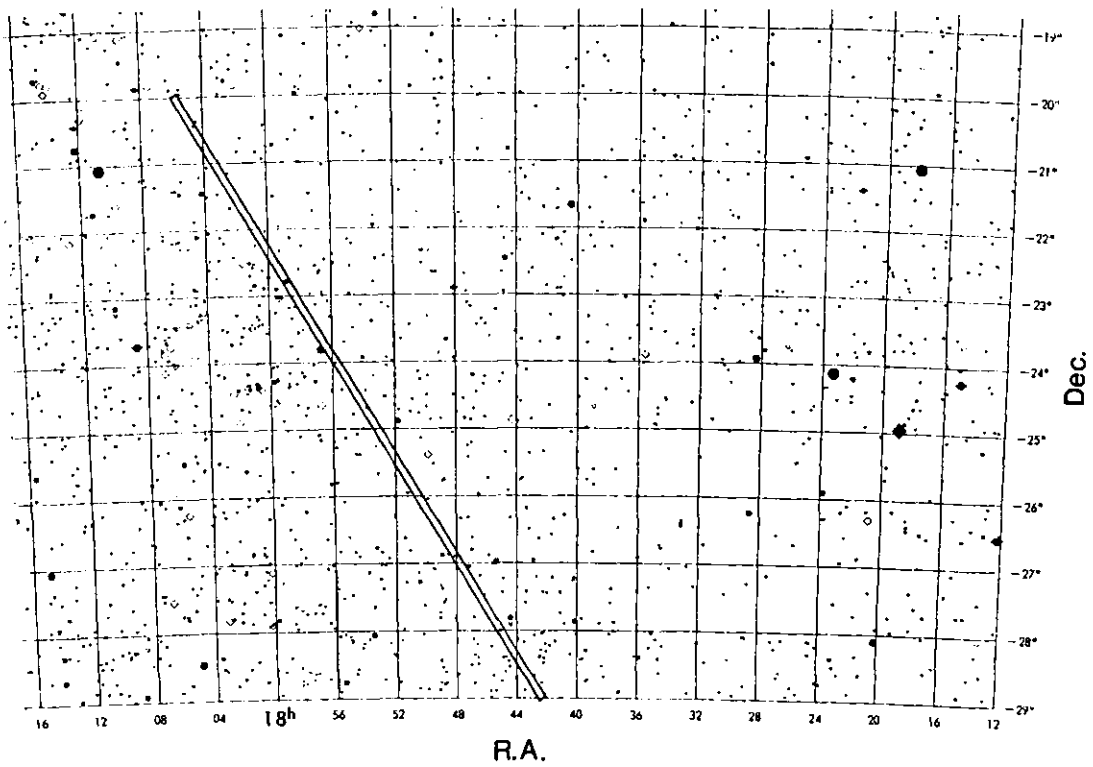

Figure 2.1 - The Proposed Survey Area
(From SAO Atlas, Chart 102.)

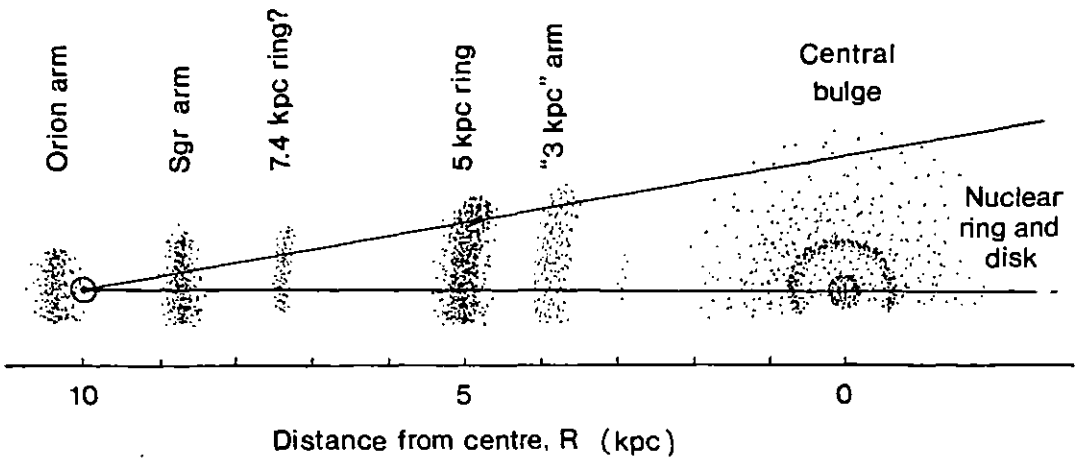

Figure 2.2 - Spiral features in the survey area

The Orion and Sgr arms are from AQ (p. 284), the 5 and 7.4 kpc infrared rings are from Section 1.2 and the 3 kpc arm and nuclear features from Oort (1977).

is the 5 kpc ring (or arm) which seems to be full of the young, dusty and luminous objects reported in Chapter 1. If these are indeed supergiants (Hayakawa et al. 1980) they will be detectable even through several magnitudes of local extinction (see Table 1.2).

This survey project was a collaboration between Imperial College and IAC, La Laguna, being the responsibility of Mercedes Prieto at IAC and myself at Imperial College. In this Chapter I describe the observational part of the project, performed in the summers of 1978 and 1979.

2.2 Survey area

The proposed survey area was a narrow strip inclined at about 30° to the local meridians of right ascension (RA). To make the area more manageable, we divided it into 80 rectangular "blocks", each measuring 4×12 arcmin, with the long side running N-S. (Figure 2.3). A block is the smallest unit of the survey. They are small enough so that several can be scanned in a full night's work, yet big enough to provide a good sample of sources. Each block has its own set of finding and guide stars (see Section 2.4.3) so that it can be searched independently of the others.

To calculate the positions of the blocks on the sky, we began by defining the "true galactic equator". This is the IAU galactic equator shifted 5' 15" south in declination to pass through the core of Sgr A West, the radio source at the physical centre of the Galaxy (Oort 1977). We then strung the 80 blocks along this line, with their separation in RA adjusted to keep the width of each block at 4 arcmin (the positions of completed blocks are in Table 2.3).

2.3 Telescope and photometer

We used the 1.5 m infrared flux collector on Tenerife for the survey. Jorden (1977) and Jones (1978) have described the telescope in some detail, and Jorden has written a comprehensive account of the Imperial College infrared photometry system. Here I briefly outline the equipment used in the survey.

Figure 2.4 is a block diagram tracing the passage of a signal from an astronomical source through the photometry system to a voltage that can be measured. The photometer itself is shown in Figure 2.5. It is a conventional system, employing a differential sky chopper to

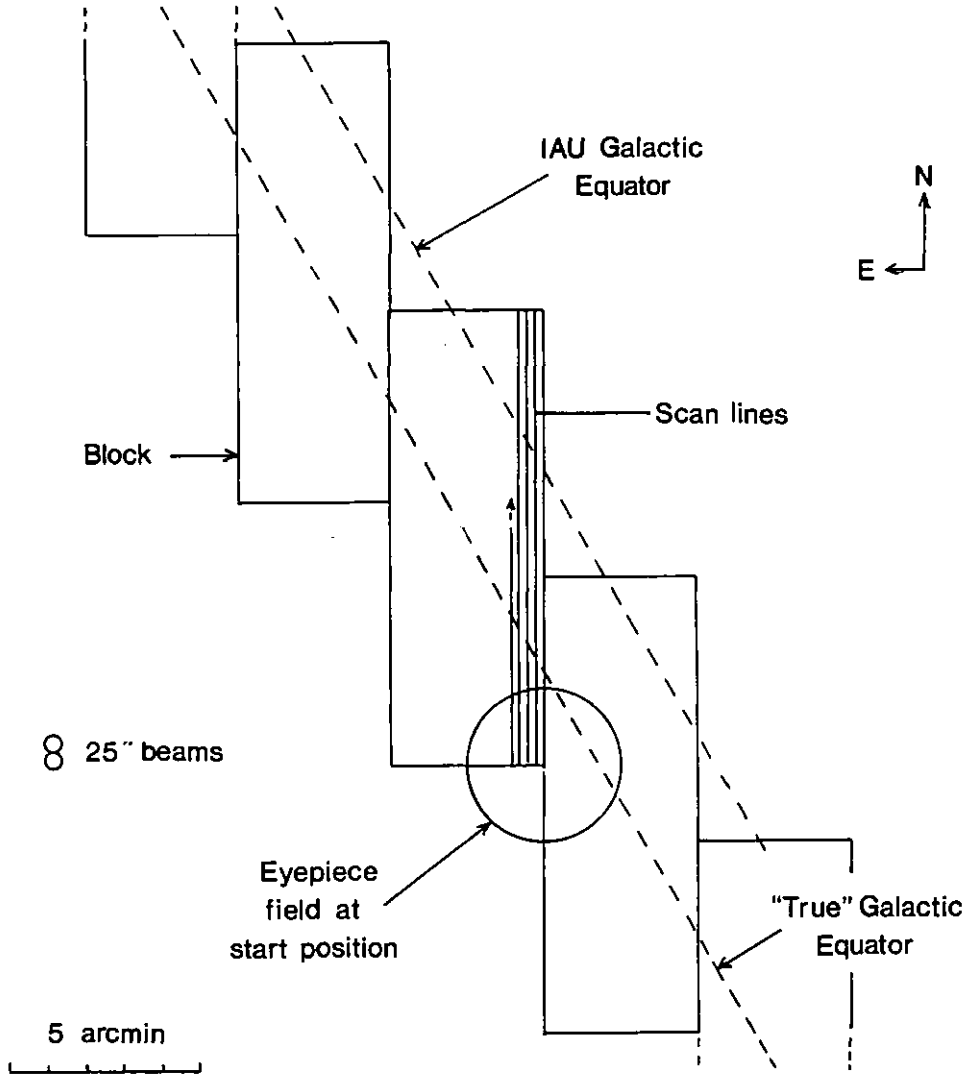

Figure 2.3 - Division of survey area into blocks

modulate the signal, and phase-sensitive detection to extract it.

The detectors are 0.5 mm indium antimonide (InSb) diodes, operated at zero bias with a Hall-type preamplifier (MacGregor 1977). Two liquid-nitrogen cryostats were used; one built by the British Oxygen Company (BOC cryostat) and the other by Oxford Instruments (OI cryostat). Both have JHKLM filter wheels. During the first summer we worked with the nitrogen at ambient pressure (that is, corresponding to a temperature of 75 K at the 2380 m altitude of the observatory), but the following year the nitrogen was pumped to 125 mbar (about 64 K) to reduce thermal noise (see Section 2.4.1).

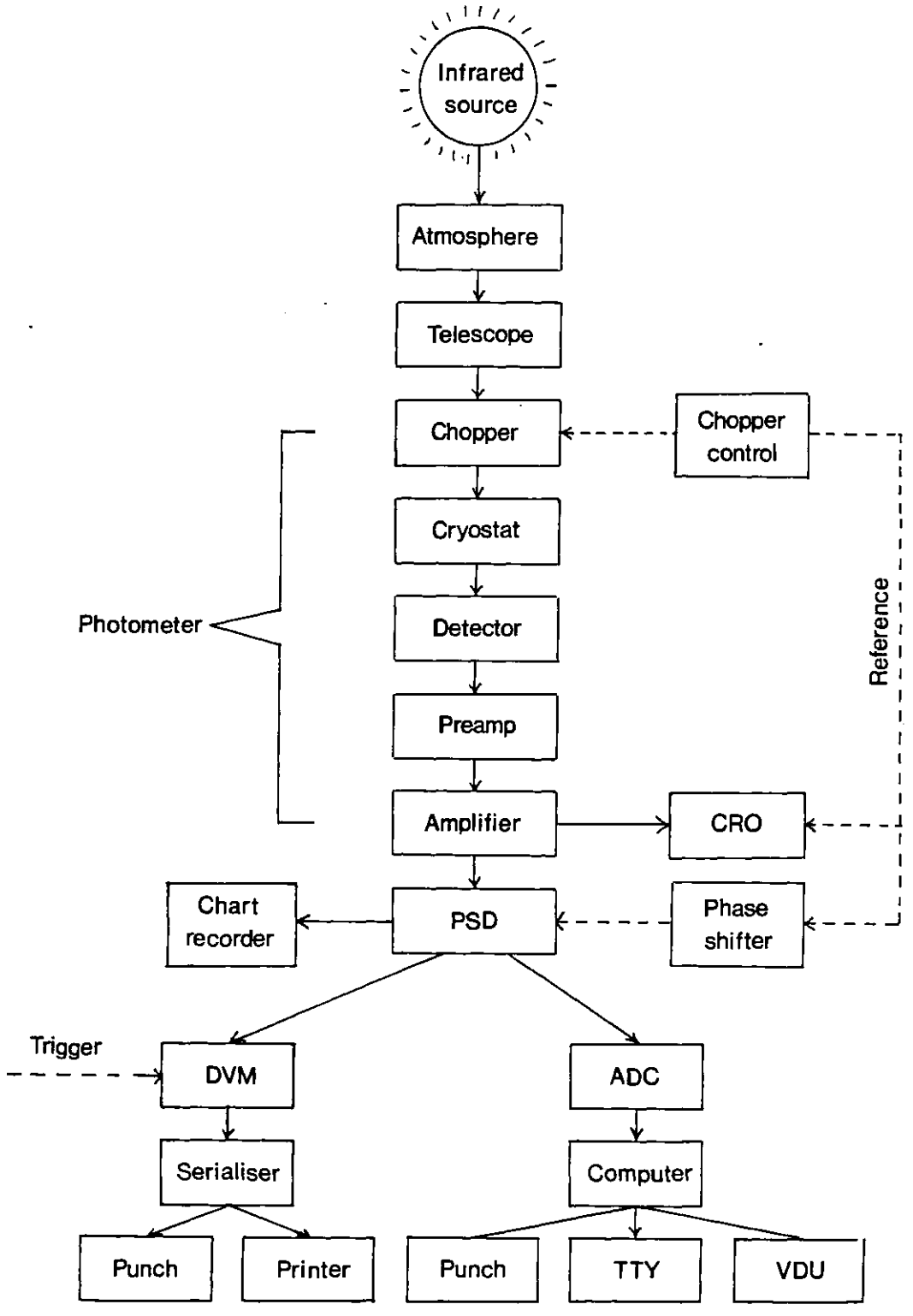

Figure 2.4 - Passage of a signal through the IC photometer system

CRO = oscilloscope, PSD = phase-sensitive detector, DVM = digital voltmeter, ADC = analogue-to-digital convertor, TTY = teletype, VDU = visual display unit. The trigger comes from the scan and sampling controller.

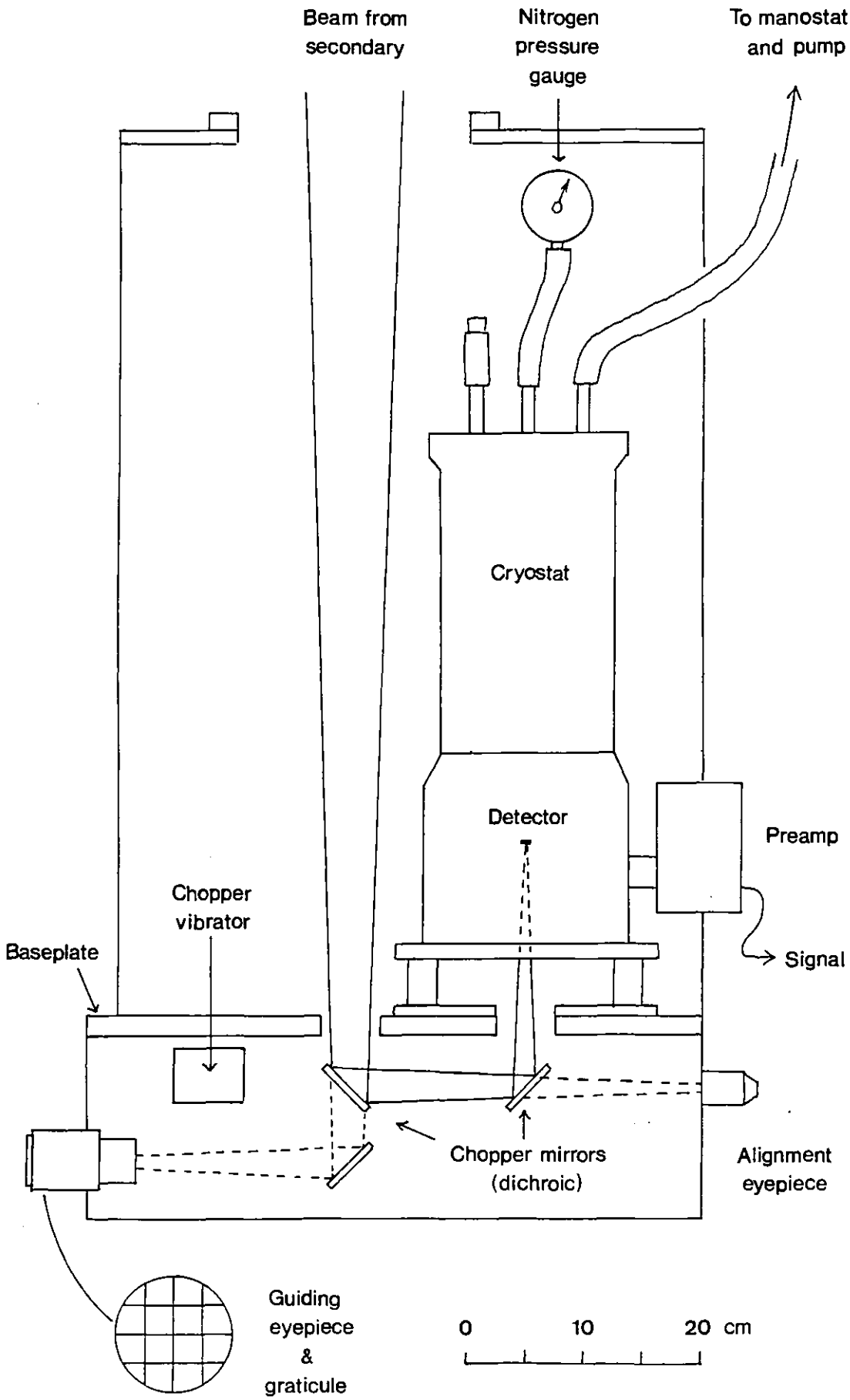

Figure 2.5 - The IC infrared photometer

We recorded the survey data in three forms:

(1) A trace on the chart recorder
(2) A digital record on punched paper tape
(3) A series of printed numbers corresponding to those on the punched tape.

We originally intended to use the Nova computer to collect the data and do some kind of on-line processing. In the event we used the Nova only to synchronise telescope movements with the data sampling. The computer communicates through a CAMAC crate with a scan and sampling controller (see Jorden 1977). This in turn directs telescope movements via the drive control unit and provides sampling pulses from the DVM (Figure 2.4).

2.4 Doing the survey

Early June is the best time of the year for observing the galactic centre, because it is then near the meridian at local midnight. But even so, the southern end of the survey area ($\delta = -29^{\circ}$) has a maximum altitude of only 33° on Tenerife (latitude 28.3°). The telescope cannot be tilted below 20° and this restricts observing time for the galactic centre to $5\frac{1}{2}$ hours a night. The top end of the survey area ($\delta = -20^{\circ}$) is accessible for 7 hours a night.

The survey was conducted during the periods June 9 to 29, 1978; May 25 to June 7, 1979; and June 15 to July 5, 1979, a total of 8 weeks. Some of this time was shared with other projects.

2.4.1 Setting up

At the beginning of each observing trip it was important to get the telescope properly balanced, so that it would scan accurately in a N-S direction without any tendency to drift off to one side.

Once we had observed for a few nights, we settled into something approaching a routine. On a clear evening we would switch on the electronics about sunset, and open the dome to allow the telescope to cool down. We would check and replace consumables (batteries, paper tape, chart paper, and so on), set the clocks (UT and ST) and top up the cryostat with nitrogen.

There is a standard procedure for preparing InSb detectors, which is as follows:

(1) "Flash" the detector through the J filter for 10 minutes (using a 60 W lamp inside the photometer frame).

(2) Pump the nitrogen down to 125 mbar (just above the triple point) and hold it there with the manostat attached to the pump.

(3) Flash the detector again.

Each stage of this procedure raises the impedance of the detector, the biggest improvement coming from pumping on the nitrogen. After the final flash, the impedance was $\sim$ 15 times higher than at the beginning, at about 10^9 to 10^{10} ohm, depending on which detector was in use.

When the sky was dark enough, we would set on a known bright star (such as α Boo) to reset the RA and declination read-outs on the drive unit. A fainter star (usually ν Her) was used to adjust the focus, check the orientation of the cross-wires and note the beam positions. This was followed by the first calibration of the night.

2.4.2 Calibration stars

Table 2.1 shows the calibration stars used in the survey. They are taken from lists of infrared standards kept at the observatory. Unfortunately the sources for the measurements are not well documented. The "primary standards" in Table 2.1 come from a list circulated privately by the California Institute of Technology (CIT) and dated 1972. The "secondary standards" come from other lists.

One of the secondary "standards", RY Scuti, is clearly a variable star. It is listed in the General Catalogue of Variable Stars (Kurkarkin et al. 1970) as a β-Lyrae type eclipsing binary with a visual range of 9.7 to 10.3 mag, and a period of 11.125 days. (There is a comment that "many irregularities are observed in the light variation", suggesting that at least one of the stars is intrinsically variable.) Since the light variation from eclipsing binaries is a geometrical effect, we may expect similar variations in the infrared. It is disturbing that this star should be presented in a list of "standards". (I have traced the infrared magnitudes to Allen (1973) where RY Sct is one of 248 stars measured. There is no mention of variability.) Both the secondary "standards" in Table 2.1 were therefore rejected from the analysis of the survey (Chapter 3).

Table 2.1 - Calibration Stars used in the Survey

Star	Name	RA (1950) (h m s)	Dec (1950) (o ' ")	V	H	K
Primary standards (CIT)						
A	ϕ Oph	16 28 16.4	-16 30 19	4.27	2.33	2.27
B	ν Her	17 56 35.3	+30 11 32	4.41	3.23	3.20
C	ν^2 Sgr	18 52 05.8	-22 44 08	4.98	2.07	2.01
Secondary standards						
D	HD 169454	18 22 24.9	-14 00 25	-	4.02	3.84
E	RY Sct	18 22 42	-12 43	9.7	5.80	5.48

Stars D and E were not used in the data analysis

The first calibration every night was done on νHer, which was usually overhead at the time. Early in the project we made only a single scan of each star at each wavelength to obtain an instrumental profile (see Section 3.1.1). Further into the survey we took 2 or 3 scans to reduce the risk of getting a poor calibration, especially when there was a strong wind.

The second calibration used a star at a similar air mass to that of the survey area. From Tenerife the galactic centre has a minimum air mass of 1.85, and the northernmost survey block has 1.53. At the lowest altitude of the telescope (about 20^{o}) the air mass is about 3. At the time of the survey we did not expect that the magnitudes of detected sources would be precise enough for atmospheric extinction errors to be important ($\sim$ 0.1 mag per air mass), so our only precaution was to use a calibration star at low altitude as a first-order correction.

Further calibrations were made throughout the night; between observing survey blocks and before closing up.

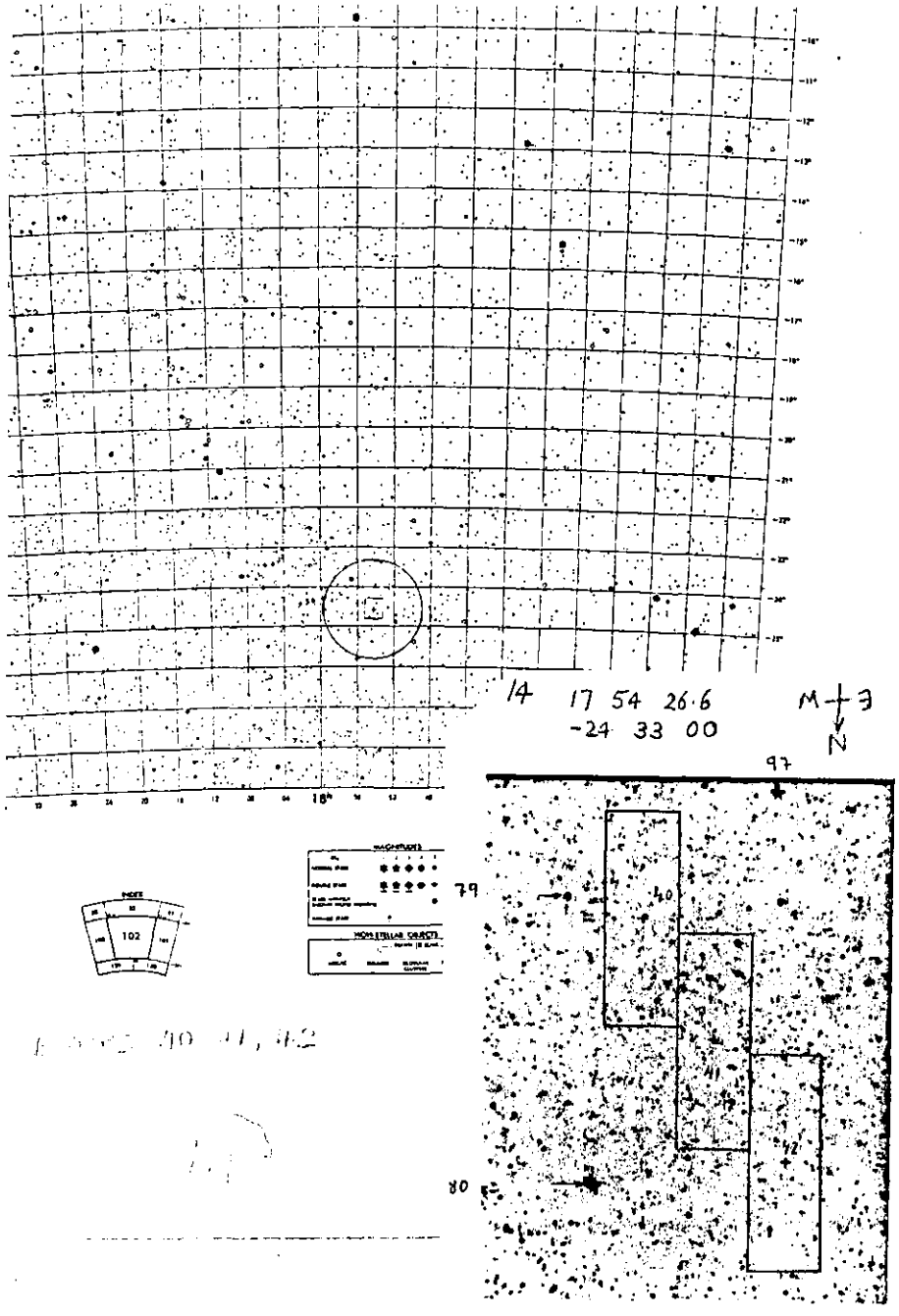

CHART 14 — IC/IAC GALACTIC PLANE SURVEY FINDING SHEET — BLOCKS 40, 41, 42

Star No.	SAO No.	h	m	s	°	′	″	m_v	Sp
20	185920	17	53	47·5	−24	25	04	8·5	A3
79	185979	17	53	50·3	+24	40	57	8·6	K2
97	185997	17	54	41·8	+24	46	49	9·4	A0

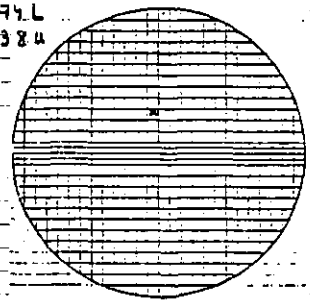

BLOCK NO. 40 Finding Star No. 97
Star : RA = ~~7.5~~ 7.5" Left Dec = 38" up
Start : RA = 17 54 00·2 Dec = −24 35 49
(Centre : RA = Dec =)

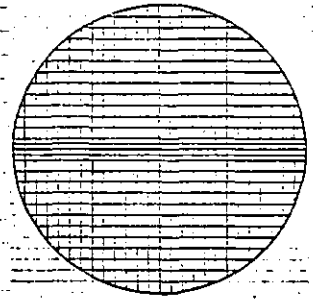

BLOCK NO. 41 Finding Star No. 79
Star : RA = Dec =
Start : RA = 17 54 17·8 Dec = −24 34 09
(Centre : RA = Dec =)

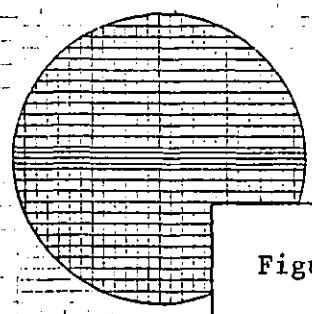

BLOCK NO. 42 Finding Star No. 80
Star : RA = Dec =
Start : RA = 17 54 35·4 Dec = −24 32 09
(Centre : RA = Dec =)

Figure 2.6 – Example of a finding chart

2.4.3 Finding charts

Finding charts are important. Even the most sophisticated observing project will come to nothing if no-one can find the object. This is a great risk on Tenerife, where the 1.5 m telescope has negligible pointing accuracy.

Figure 2.6 is one of the 27 finding charts prepared for the survey. It consists of three parts:

(1) A photocopy from the SAO Atlas marked with primary finding stars and a circle representing the $2\frac{1}{2}^{o}$ field of the 25 cm finder telescope.

(2) A Polaroid print made from the Palomar Observatory Sky Survey (POSS) covering $20' \times 30'$ to a scale of $15''\ mm^{-1}$ (these were supplied by the Royal Greenwich Observatory). We constructed three blocks on each print at positions measured off from nearby SAO stars. In hindsight, this was a needlessly precise method. By insisting that the blocks lay exactly on the "true" galactic equator, we had to make do with whatever guide stars happened to be close to the start of each block. Many of these stars were too faint to be of any use on moonlit nights. We would have saved a lot of time by placing the blocks close to bright guide stars.

(3) Detailed finding instructions. The absolute pointing of the telescope is so bad that for all but the brightest objects (e.g. the Moon), setting is best done by using 2 or 3 finding stars as stepping stones, with a blind offset from the last star to the required position. We listed nearby SAO stars as stepping stones and added diagrams of the expected field in the 4' eyepiece at the start position of each block.

2.4.4 Scan parameters

With the telescope at the start position of a block, the scanning could begin. The chosen method was a compromise between several variables.

First, the chop frequency is more or less independent of the type of observation (except where high time resolution is needed). It is constrained by the bandwidth of the preamplifier and the need to avoid sub-harmonics of mains frequency (50 Hz). We used 14-20 Hz.

Next, the rate at which we could sample the signal was restricted by the maximum speed of the Anadex printer at 2 s^{-1}. Although we could have sampled faster using punched tape alone, we wanted a printed record to back it up. This proved essential (see Section 3.3.1).

Now we invoke the Sampling Theorem, which says that to extract all the information in a signal up to a frequency f_N (the Nyquist frequency), we must sample the signal at a rate:

$$R = 2f_N \tag{2.1}$$

We have R = 2 s^{-1}, so f_N = 1 Hz. The signal from the PSD (Figure 2.4) is smoothed by a low-pass output filter with a time constant τ and a corresponding bandwidth f_m given by

$$f_m = (2\pi\tau)^{-1} \tag{2.2}$$

We require $f_m < f_N$ for all the information to be recorded, so $\tau > 0.16$ s. We chose τ = 0.3 s, giving f_m = 0.5 Hz, half the Nyquist frequency, thus ensuring that the signal was comfortably oversampled (there is still information above f_m because the RC filter does not have a sharp cut-off).

This time constant fixes the maximum scan speed. For a speed v arcsec s^{-1} and a beamwidth w arcsec, most of the signal power in a star profile (Figure 3.1) is near a frequency f_o:

$$f_o \simeq \frac{1}{T} = \frac{v}{2w} \tag{2.3}$$

where T is the time for a star to pass through the two beams. To ensure that the signal is not smoothed too much by the PSD filter, we require $f_m > f_o$, or, from Equations 2.2 and 2.3:

$$w/v > \pi\tau \simeq 1 \text{ s} \tag{2.4}$$

We chose w = 25" and v = 7.6" s^{-1}, giving w/v = 3.3 s or f_o = 0.15 Hz (compare f_m = 0.5 Hz). We intended to use the 25" beam throughout the survey, but had to fall back on a 15" beam for much of the time because of faults with the BOC cryostat (microphonics, jammed

Table 2.2 - Auxiliary Data for Scans

Beamwidth (arcsec)	Step size (arcsec)	Nr of scans in a block	Cryostat
25	12	20	BOC (mainly)
15	8	30	OI

Filters: H (λ_{eff} = 1.63 μm, $\Delta\lambda$ = 0.32 μm)
K (λ_{eff} = 2.20 μm, $\Delta\lambda$ = 0.41 μm)

Number of samples per scan: n = 180

Sampling rate: R = 2 s^{-1}

Speed of scan: v = 7.5" s^{-1}

Length of scan: ℓ = 12'

PSD time constant: τ = 0.3 s

} nominal

Chopper: throw = beamwidth
frequency = 14-20 Hz

wheels and many leaks). For a 15" beam, f_o = 0.25 Hz, which is getting rather close to f_m, though not enough to cause serious loss of signal.

As is usual in declination scanning, we made the chopper throw equal to the beamwidth.

With this combination of scan speed and sampling rate, 180 samples covered the length of a block (12'); with 4" between points.

All these parameters are summarised in Table 2.2.

2.4.5 Scanning procedure

Figure 2.7 shows the two sides of the record sheet used for the survey. A good record sheet is even more important than a good finding chart. The reference number in the top right uniquely identifies the observation and appears on all associated material (charts, tapes, printer rolls, etc). With two observers - a guider and a recorder - the observing procedure was as follows:

Block No.	Filter
52	K

IC/IAC GALACTIC PLANE SURVEY

Record of Scans

Reference Number
W 54

Year: 1978 Month: June Night: 28/29 Begin (UT): 23 h 07 m

Observers: Tony and Mercedes End (UT): h m

Weather: good Seeing: Moon: no

Profile used: W Her Beamwidth: 25" Amp. gain: 100

Chart speed: 30 mm min⁻¹ Scan speed: 7.5 "s⁻¹ PSD int. time: 0.3 s

Chart range: 5 V Sampling interval: 1/2 s DVM range 1 V

Dec. Offset 12' 30" No. of samples: 180 R_{LOAD} 10^{10}

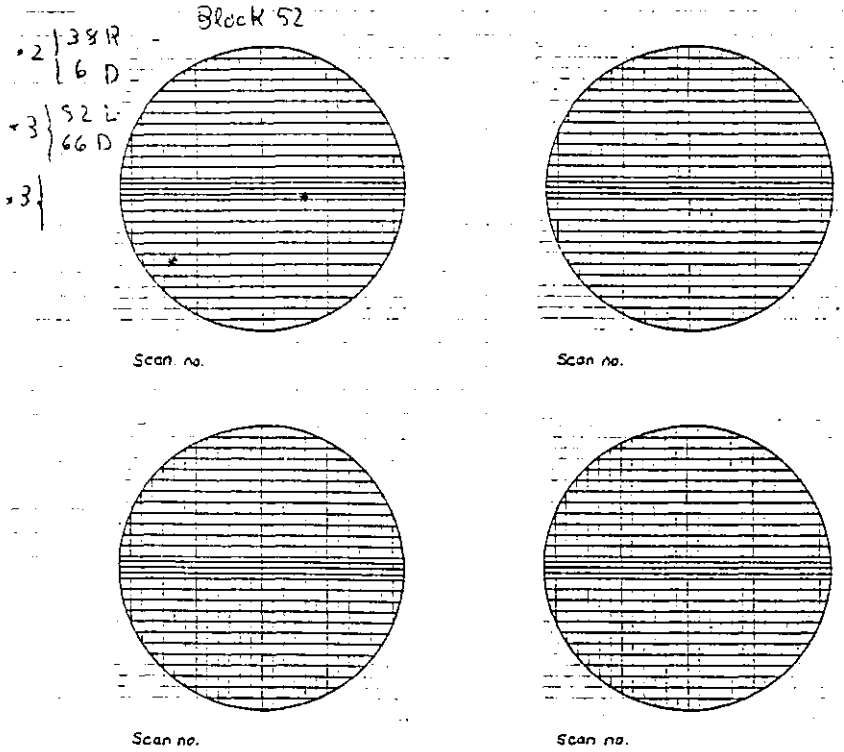

Block: 52, K Ref. No: W 54

General Notes

	Scan no.	Begin (ST)	Guide Star Name	Guide Star Position	Notes	Guider	Punch
S1	1	$16^h 46^m$	3	82L, 6D	star chart stopped at the beginning of the scan	T	
S2	2	16-43	3	760	76 cl. ml 82L, 45D		
S3	3	16-47	3	58,	Star 1 at 124L, 20D at 092	74L, 45D	
S4	4	16-51	1	92L 46 20D		56L, 45D	
S5	5	16-55	"	80L, 20D		45L, 45D	
S6	6	16-58	"	68,		34L, 45L	
S7	7	17-00	"	56		22L, 45	
S8	8	17-03	"	44		10L, 45D	
S9	9	17-06	"	32,		5R, ?	
S10	10	17-09	"	20		17R	
S11	11	17-12	"	8,		30R, 45D	
S12	12	17-15	"	4R,		37R, 45D	
S13	13	17-19	"	16R, 20D			
S14	14	17-22	"	28,		56R 45D	
S15	15	17-25	"	40,		81R, 45D	
S16	16	17-28	"	52		93R ?	
S17	17	17-30	"	64		104R	
S18	18	17-33	"	76,		116R	
S19	19	17-56	"	88			
S20	20	19-59	"	100			

Figure 2.7 - Example of a record sheet

(1) The guider uses the drive handset to place the guide star at the start position shown on the finding chart, taking out the backlash in the direction of scan. In the meantime the recorder prepares the recording equipment.

(2) When all is set, the computer program starts the telescope moving and simultaneously lets the sampling begin. The first sample comes at the start position.

(3) As the scan proceeds, the recorder monitors the signal on the chart trace, while the digitised samples from the DVM appear on the printer and paper tape punch. The scan takes about 3 minutes.

(4) At the end of the scan the drive unit stops the telescope approximately one point beyond the last sample. The guider notes the positions of field stars as a check on the length of the scan (we did not do this often enough in early blocks).

(5) The recorder then returns the telescope to the start position using the manual control on the drive unit (return speed is 15" s^{-1}). The guider moves the dome if need be.

(6) The guider steps the telescope half a beamwidth in RA (12" for a 25" beam, 8" for a 15" beam) and is ready for the next scan.

2.5 Outcome of the observations

Of the 80 blocks in the survey area, we observed 14 at H and 18 at K. This is 20% of the proposed coverage. On average, we covered about half a block a night, or one block for every 12 hours that the survey area was above the telescope's horizon. On a good night we could survey a block in 2 hours, so the overall efficiency was only 17%. Some of this can be attributed to bad weather or occasional nights given over to other projects. This is discussed further in Chapter 4.

Table 2.3 lists the positions of the survey blocks for which we have verifiable data, and the dates on which the observations were made. The next chapter is an account of how these observations were processed.

Table 2.3 - Observations of Survey Blocks

Block	RA & dec of nominal centre (1950)		H band		K band	
	(h m s)	(o ' ")	Ref	Date	Ref	Date
1	17 42 29	-28 59 20	W1	78 June 15	W5	78 June 16
2	17 42 48	-28 52 50	W49	78 June 27	W37	78 June 25
3	17 43 06	-28 46 20	W42	78 June 26	W13	78 June 18
4	17 43 24	-28 39 50	W55	78 June 28	W14	78 June 18
9	17 44 55	-28 07 10	Z99	79 July 2	Z98	79 July 2
16	17 47 02	-27 21 10	-	-	Z20	79 June 4
23	17 49 07	-26 34 30	W62	78 June 29	W29	78 June 22
31	17 51 30	-25 40 50	-	-	Z27 Z31	79 June 5 79 June 6
32	17 51 48	-25 34 10	Z51	79 June 17	Z44 Z46	79 June 15 79 June 16
40	17 54 09	-24 39 50	-	-	Z94	79 July 1
42	17 54 44	-24 26 10	W51 W57	78 June 27 78 June 28	W63	78 June 29
52	17 57 39	-23 17 20	Z53	79 June 17	W54	78 June 28
56	17 58 49	-22 49 40	Z16 Z22	79 June 3 79 June 4	Z10 Z15	79 June 2 79 June 3
59	17 59 41	-22 28 40	W43 W48	78 June 26 78 June 27	W20	78 June 19
60	17 59 58	-22 21 40	Z69 Z80	79 June 19 79 June 23	Z61 Z66	79 June 18 79 June 19
62	18 00 33	-22 07 50	W50	78 June 27	W19	78 June 19
70	18 02 50	-21 11 30	-	-	Z34 Z38	79 June 6 79 June 7
72	18 03 25	-20 57 20	W38	78 June 25	W9	78 June 17

The dates are UT at the beginning of the night

CHAPTER 3

REDUCTION OF THE SURVEY DATA

The object of data reduction is to determine the position and brightness of each object detected in the survey. We used two methods: deconvolution (at IAC) and correlation detection (at IC). This chapter is concerned only with correlation detection. A series of computer programs reduced the raw data to a unified catalogue of sources for each survey block. The catalogues list, for each source, its right ascension, declination, H and K magnitudes and the separation between H and K positions.

3.1 The nature of the signal

We begin this chapter with a consideration of the characteristic signal observed in the survey, and the information contained within it.

3.1.1 The instrumental profile

Differential sky chopping causes the beam incident on the detector to be alternately switched between two adjacent patches of sky (Figure 3.1a). In normal photometry one beam contains the object of interest and the other is the reference beam. In a scan mode, however, the telescope is moving in declination parallel to the direction of chop. Any sources in the path of the telescope enter the leading beam (causing the signal to rise) pass into the following beam (causing the signal to fall and go negative) and finally leave (causing the signal to return to zero). This produces a characteristic shape known as the instrumental profile (Figure 3.1b). It is the system's response to a star.

One important consequence of this particular shape is flux cancellation. Where sources are so close together that their profiles overlap, the negative part of one may cancel the positive part of the other. The integrated measured flux from a crowded field will therefore be a lower limit on the true flux. This is not so where the instrumental profile is wholly positive. For example, the large beams used in surface-brightness mapping (Chapter 1) were too big to distinguish individual stars, yet the integrated flux could still be measured accurately. The effects of source confusion will be discussed in Chapter 4.

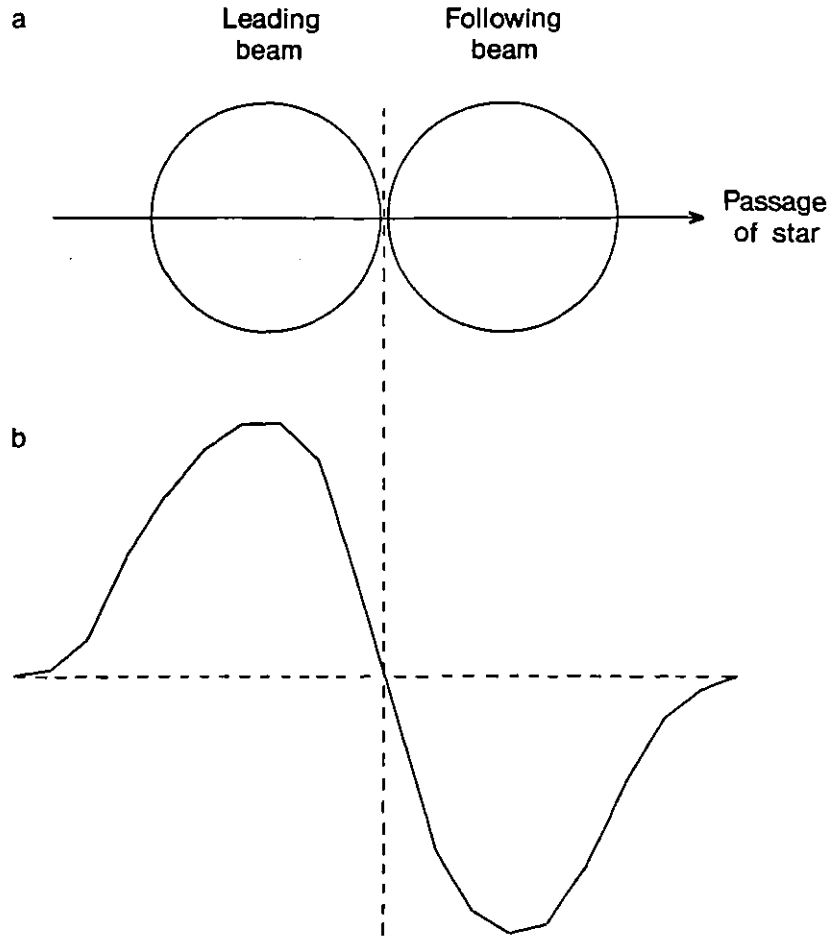

Figure 3.1 - The instrumental profile

a Passage of a star through the two beams

b Signal response, the instrumental profile

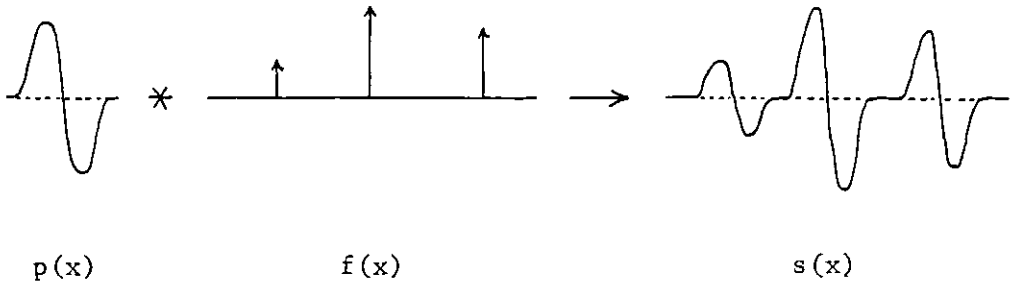

Figure 3.2 - Representation of a scan as a convolution

3.1.2 Scans on the sky

A scan contains information on a series of stars. For each star we are interested in two things: its position (x_o) and its brightness, (a_o). These quantities can be conveniently represented by an impulse (delta) function, $a_o\ \delta(x - x_o)$. The signal $s(x)$ which appears on the chart recorder during the course of a scan can be thought of as the convolution of the instrumental profile $p(x)$ with $f(x)$, where $f(x)$ is a row of impulses $a_i\ \delta(x - x_i)$ representing the stars in the scan.

$$s(x) = p(x) * f(x) \tag{3.1}$$

This is shown schematically in Figure 3.2. The objective of the data reduction is to extract values of x_i and a_i for all the sources detected in the survey.

3.2 Extracting the signal

The most straightforward way of determining x_i and a_i is to use a ruler to measure the positions of stars on a chart trace, and the peak-to-peak heights of their profiles. These measurements can then be calibrated to yield equatorial coordinates and source magnitudes. This is feasible for a small number of bright stars in uncluttered fields. However, when there are many faint sources in a noisy background a more objective procedure is required.

We decided to process the survey observations by computer. Two methods were used: deconvolution (at IAC) and correlation detection (at Imperial College).

3.2.1 Deconvolution

Deconvolution, sometimes known as Fourier restoration, is a theoretical means of recovering information that has been distorted and smoothed by the aberrations and finite resolution of the observing instrument. In the present case it would mean restoring the pointlike images of stars, $f(x)$, from their bipolar signals $s(x)$ (Figure 3.2). The process is essentially an "unfolding" of Equation 3.1 by taking Fourier Transforms:

$$f(x) = \mathcal{F}^{-1} \{ \mathcal{F}[s(x)] / \mathcal{F}[p(x)] \} \qquad (3.2)$$

Here $\mathcal{F}$ represents a Fourier Transform, and $\mathcal{F}^{-1}$ its inverse. Although deconvolution is attractive in principle, there are two reasons why, in practice, it does not lead to efficient restoration of the original signal.

(1) Real observations are band-limited, either by physical filtering (such as the output filter of a PSD) or by a finite sampling frequency, or both. Information in the higher Fourier components will not be recorded and so cannot be restored. The ideal impulse functions in f(x) can never be attained.

(2) Real observations are contaminated by noise. Brault and White (1971) have vividly demonstrated how a small amount of noise on the signal can be disastrously amplified by a straightforward application of Equation 3.2. The usual solutionis to apply some kind of filter in the Fourier domain to reject the noise components while preserving the signal. As it is not usually possible to separate uniquely signal and noise components, the result is almost always a compromise.

Despite these complications, deconvolution can be an effective way of restoring data, especially with the advent of Fast Fourier Transform (FFT) algorithms that reduce computing time to acceptable levels. This was the method chosen by the IAC group to reduce the survey data.

3.2.2 Correlation detection

Correlation detection, which is equivalent to matched filtering, is the most efficient way of detecting a signal of known shape in the presence of noise (Lynn 1973, pp. 145 and 208). It is thus ideally suited to reduction of the survey data, where we expect signals to have the same shape as the instrumental profile.

The method employs the cross correlation of the observed scan with the IP. The cross-correlation integral is similar to the convolution integral, except that the two functions are not reversed with respect to each other.

$$c(x) = \int_{-t_o}^{t_o} s(x + t)\, p(t)\, dt \qquad (3.3)$$

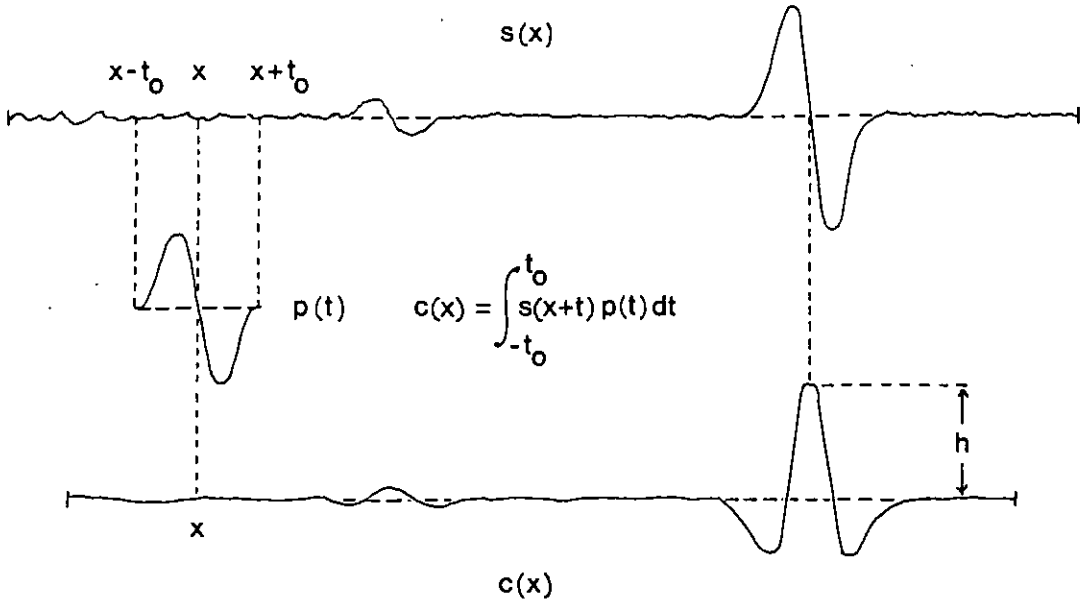

Figure 3.3 - The cross-correlation integral

Here, s(x) is the observed scan which is transformed into the cross-correlation function c(x) through integration with the instrumental profile p(t). The bipolar signal from a star (right) becomes a central peak at the position of the star with a trough on either side. The signal strength is proportional to h, the height of the peak.

Here, t is a dummy variable integrated over $\pm t_o$, where $2t_o$ is the width of the IP. This process is shown schematically in Figure 3.3. The cross-correlation, c(x), reaches a peak when the signal has the same shape as the IP. Although the height of the peak is proportional to the brightness of the star, the detailed shape of c(x) has no physical significance. It is an instrumental artifact determined by the form of the IP. (Contrast this with deconvolution, where the aim is to completely unravel the IP from the observed scan.)

Apart from its simplicity, correlation detection is attractive because it is equivalent to matched filtering. That is, the signal s(x) is smoothed so as to produce the best possible improvement of signal-to-noise ratio (SNR) in c(x) over s(x).

The problem of signal detection is then reduced to looking for peaks in c(x). The heights of the peaks give a_i, and their positions x_i.

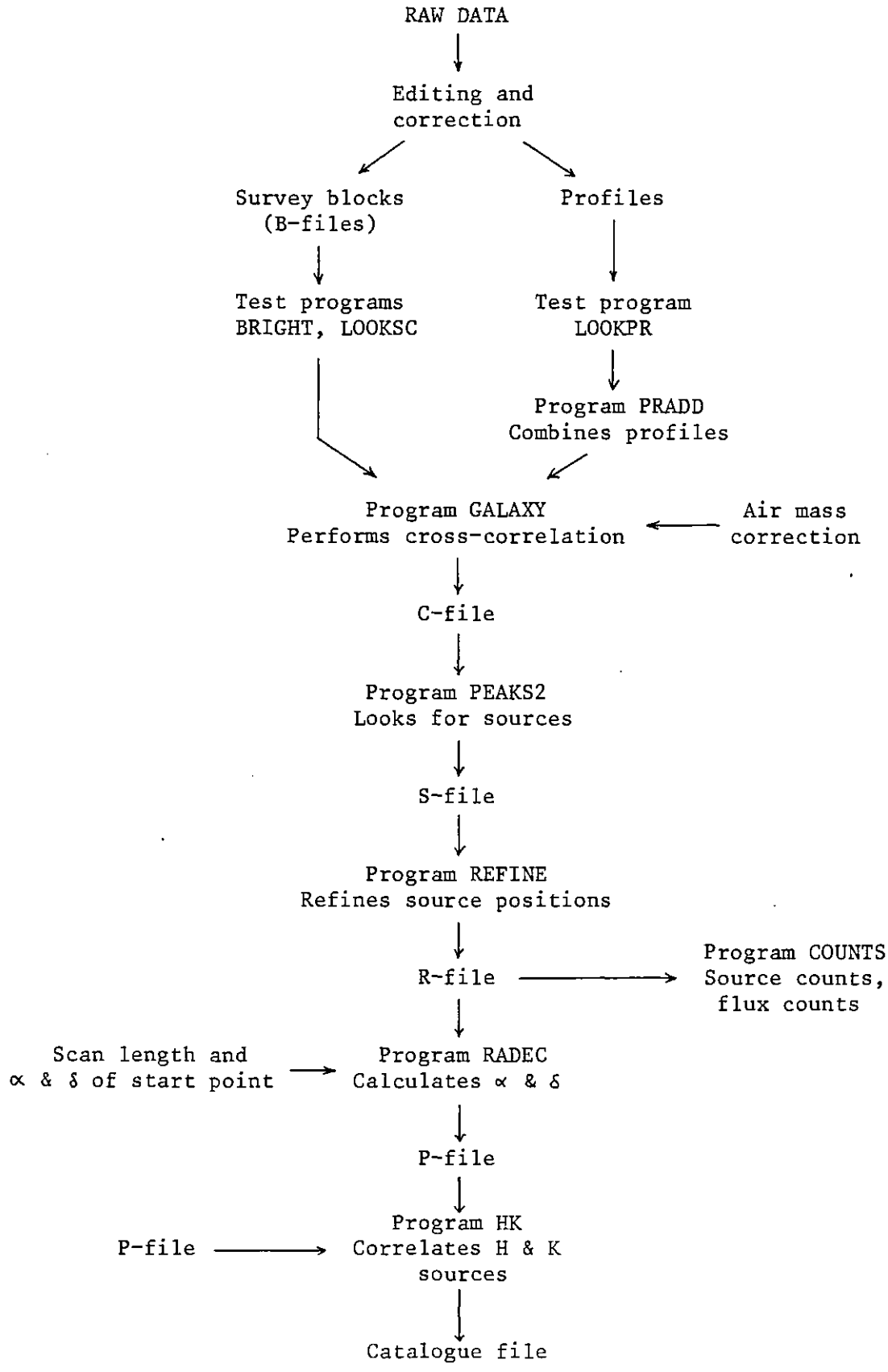

Figure 3.4 - Reduction of the survey data

For these reasons, but especially because of its simplicity, I chose correlation detection for the reduction of the survey data. The rest of this chapter explains how this was done in practice.

3.3 Data reduction

The objective was to take the raw data in the form of numbers on punched tape, and convert it into a working catalogue of infrared sources, ideally listing RA, declination, and H and K magnitude for each source. Figure 3.4 outlines the chosen scheme. All the programs were written in Fortran, using the IC Astronomy Group's PDP 11/80 minicomputer.

3.3.1 Preparation of the raw data

Each night's observations (Table 2.3) were recorded in three forms: punched tape, lists of printed numbers, and chart recordings. The survey data, calibration stars, test runs and false starts were all mixed up together. The first step in sorting them out was to read the paper tapes into disk files on the PDP 11.

The survey blocks were then edited and corrected for punching errors with reference to the printed lists, and compiled into files of 20 or 30 scans of 180 points each, known as B-files (B for "block"). Data values in the B-files are stored in the integer form ± DDDDD, where D is a decimal digit (0–9) and the unit is 0.1 mV.

A test program (BRIGHT) runs through a whole B-file to make sure all the numbers are readable and to identify points where a strong signal has saturated the DVM (outside the range ± 2 V). Another program, (LOOKSC) displays a graph of any chosen scan on the Tektronix 1010-1 terminal, so that any obvious errors can be spotted.

Likewise, the calibration scans were edited into instrumental profiles identified by their reference numbers. A program (PRADD) combines scans from the same observation into a single profile where necessary. Finally, there is a viewing program (LOOKPR, similar to LOOKSC) to check the appearance of the profiles before they are used.

In this way I am confident that the edited and tidied data are free of significant errors.

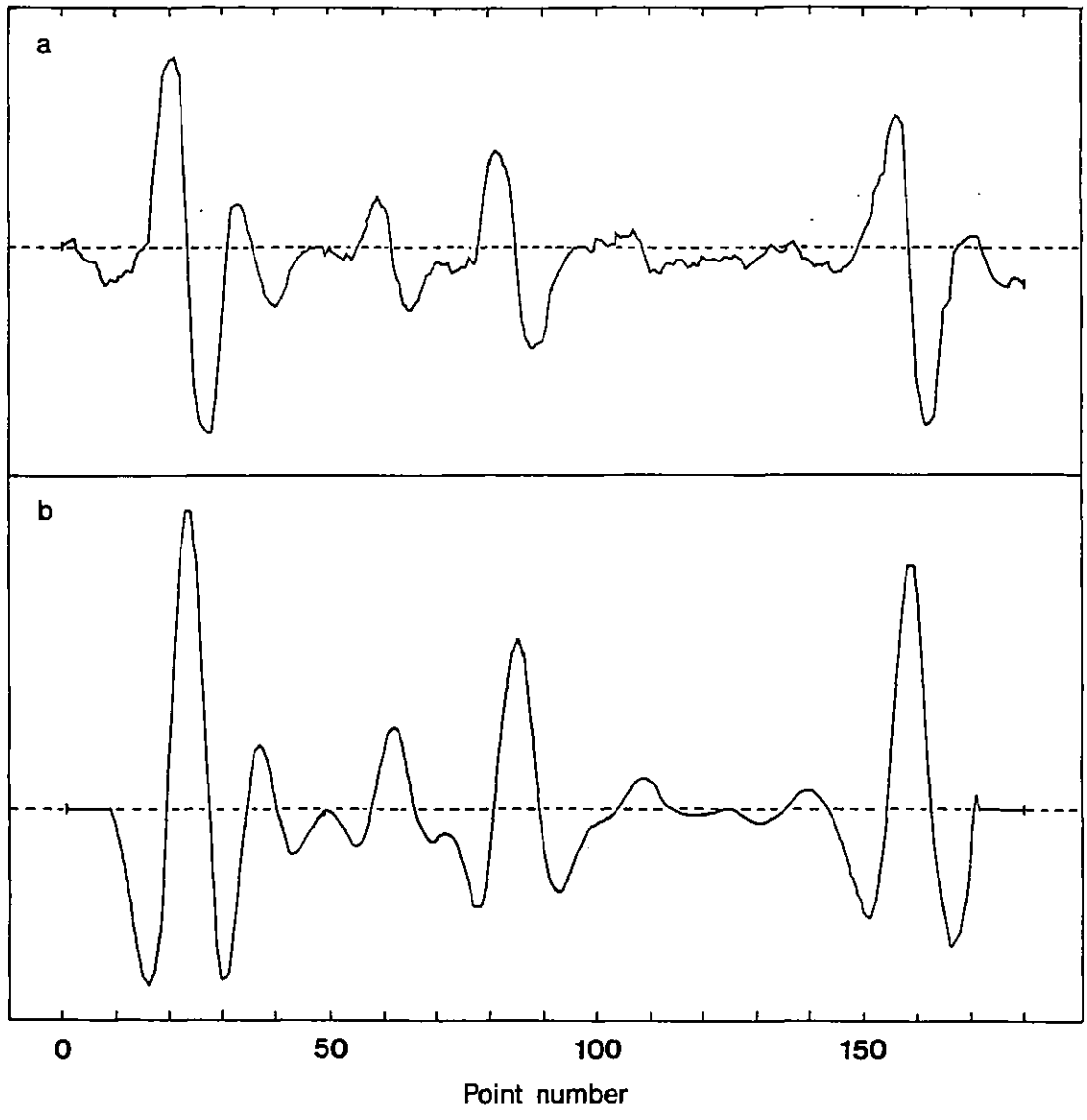

Figure 3.5 - Example of a scan and its cross-correlation

a Scan 4 of Block 59K showing several star profiles.

b The cross-correlation of the same scan with an instrumental profile (IP).

The dashed lines represent zero levels. Note the smoothness of the cross-correlation compared to the original scan. The null regions at either end correspond to half the width of the IP. The brightest star has a K magnitude of 7.4.

3.3.2 Cross-correlation

Program GALAXY reads in a whole B-file and performs a cross-correlation of each scan with an IP. The output is stored in a C-file (C for "cross-correlation").

The program first adjusts the IP so that its mean is zero (this is equivalent to saying that the area beneath it is zero). It can be shown that the cross-correlation of such an IP with a scan is not affected by an arbitrary zero level in s(x).

Next, the cross-correlation is performed using the discrete version of Equation 3.3:

$$c_i = \sum_{j=-j_o}^{j_o} s_{i+j}\, p_j \qquad (3.4)$$

where c_i is the value of the cross-correlation function corresponding to s_i in the observed scan, and p_j is the IP of $2j_o + 1$ points (the centre point is point 0). The C-file contains 20 or 30 cross-correlated scans of 180 points each, the first and last j_o points being zeroes (c_i cannot be calculated in these regions because i + j would lie outside the range of the scan). An example of a scan and its cross-correlation is shown in Figure 3.5.

3.3.3 Magnitude calibration

Values of c_i from Equation 3.4 are in arbitrary units. To calibrate them, GALAXY calculates the peak height of the autocorrelation of the calibration profile, and then scales c_i so that

$$c_i = 10^{-0.4\, m_i} \qquad (3.5)$$

where m_i is the calibrated magnitude of point i in the C-file (this is merely a convenience: values of m_i will not in general correspond to the magnitude of a source).

Two corrections are incorporated into Equation 3.5.

(1) The peak sample will not, usually, coincide with the peak signal, thus tending to underestimate the brightness of sources. To allow for this, the height of the profile autocorrelation is calculated

Table 3.1 - Calibration of Survey Blocks (H)

B-file	Beam (arcsec)	Data			Calibration			C-file
		Ref.	Scan numbers	Air mass	Ref.	Star	Air mass	
B01H	25	W1	1-20	2.0	W2	C	1.8	C01H
					W3	B	1.2	
B02H	25	W49	1-20	1.9	W47	B	1.2	C02H
B03H	25	W42	1-20	2.1	W45	B	1.4	C03H
B04H	25	W55	1-20	1.9	W53	B	1.1	C04H
B23H	25	W62	1-20	1.7	W61	B	1.0	C23H
B32H	25	Z51	1-20	1.7	Z49	B	1.1	C32H
					Z55	B	1.4	
B42H	25	W51	1-13	2.2	W47	B	1.2	C42H
		W57	14-20	2.5	W53	B	1.1	
B52H	25	Z53	1-20	1.9	Z49	B	1.1	C52H
					Z55	B	1.4	
B56H	15	Z16	1-25	2.1	Z13	B	1.1	C56H
					Z14	A	1.4	
					Z17	B	1.3	
		Z22	26-30	2.1	Z18	B	1.1	
					Z19	A	1.4	
					Z21	A	2.6	
					Z23	B	1.3	
B59H	25	W43	1-11	2.3	W45	B	1.4	C59H
		W48	12-20	1.9	W47	B	1.2	
B62H	25	W50	1-20	1.7	W47	B	1.2	C62H
B72H	15	W38	1-20	2.2	W40	B	1.6	C72H

Notes to Tables 3.1 and 3.2 (overleaf):

Codes for calibration stars are A = ϕ Oph, B = ν Her, C = ν^2 Sgr (see Table 2.1 for details).

Block 9 H & K - Not used because of inconsistent calibrations believed due to a faulty cryostat.

Block 31 K - Partial coverage, 24 scans out of 30.

Block 60 H & K - Could not be edited and corrected because the printed lists were not available.

Block 72 H - Partial coverage, 20 scans out of 30.

Block 72 K - Partial coverage, 12 scans out of 20.

Table 3.2 - Calibration of Survey Blocks (K)

B-file	Beam (arcsec)	Data			Calibration			C-file
		Ref.	Scan numbers	Air mass	Ref.	Star	Air mass	
B01K	25	W5	1-20	2.4	W6	C	1.9	C01K
B02K	15	W37	1-30	1.9	W40	B	1.6	C02K
B03K	25	W13	1-20	1.9	W11	B	1.2	C03K
B04K	25	W11	1-20	2.3	W11	B	1.2	C04K
B16K	15	Z20	1-30	1.9	Z18	B	1.1	C16K
					Z19	A	1.4	
					Z21	A	2.5	
					Z23	B	1.3	
B23K	15	W29	1-30	1.8	W28	B	1.0	C23K
B31K	15	Z31	7-30	1.8	Z29	B	1.3	C31K
					Z30	A	1.5	
					Z32	A	2.1	
					Z33	B	1.1	
B32K	25	Z44	1-14	2.3	Z42	B	1.0	C32K
					Z43	A	1.7	
					Z45a	B	1.3	
		Z46	15-20	2.2	Z45b	B	1.0	
					Z47	B	1.2	
B40K	25	Z94	1-20	1.9	Z92	B	1.0	C40K
B42K	25	W63	1-20	1.8	W61	B	1.0	C42K
B52K	25	W54	1-20	1.7	W53	B	1.1	C52K
B56K	15	Z10	1-17	2.1	Z5	B	1.2	C56K
					Z6	A	1.4	
					Z8	A	1.9	
					Z9	B	1.0	
					Z11	B	1.3	
		Z15	18-30	1.6	Z13	B	1.1	
					Z14	A	1.4	
					Z17	B	1.3	
B59K	25	W20	1-20	1.8	W18	B	1.5	C59K
B62K	25	W19	1-20	1.6	W18	B	1.5	C62K
B70K	15	Z34	1-6	2.3	Same as for B31K			C70K
					+Z35	B	1.4	
		Z38	7-30	1.6	Z36	B	1.6	
					Z37	A	1.4	
					Z39	B	1.1	
B72K	25	W9	9-20	1.7	W7	B	1.8	C72K

For notes see Table 3.1

as a weighted mean of the peak and its two neighbouring points:

$$\text{Height} = \frac{1}{6}(p_{-1} + 4p_o + p_{+1}) \qquad (3.6)$$

where p_o is the peak value, and p_{-1} and p_{+1} those on either side. The corrected height is typically 97% of the peak for a 25" beam and 92% for a 15" beam. This adjustment converts a systematic error into a random error of about ± 0.03 mag (25") or ± 0.08 mag (15").

(2) A correction of 0.1 mag per air mass is made for differential atmospheric extinction at both H and K. There are few occasions when the difference in air mass between a block and a calibration star is as great as 1.0. Here, I define the mean air mass of a block as

$$AM = \frac{1}{3}(AM_{\text{first scan}} + AM_{\text{min}} + AM_{\text{last scan}}) \qquad (3.7)$$

When more than one calibration star was available, C-files were produced with each one, and then the average taken.

A further source of error is that a star may not pass through the centre of the beam. But since scans overlap by 8" or 12", the star will be less than 4" or 6" from the position of peak transmission. From Figure 3.6, which shows examples of beam profiles, we see that this error is unlikely to be more than 5% or 0.05 mag.

I estimate that the final errors in magnitude would be about ± 0.2 mag. See Section 4.2.2 for the effects of noise.

Tables 3.1 and 3.2 document the calibrations for each block.

3.3.4 Detection of peaks

At this stage we have a set of C-files containing calibrated cross-correlations of the survey scans. From Figure 3.5 we see how each star in the original scan has been transformed into a peak in the cross-correlation. Each peak can be located by a change in sign of the slope, and there is a program (PEAKS) to do this.

However, it is not correct to identify each peak in a scan as a star. Neighbouring scans overlap by half a beamwidth, so sources will be detected at least twice. The source detection program (PEAKS 2)

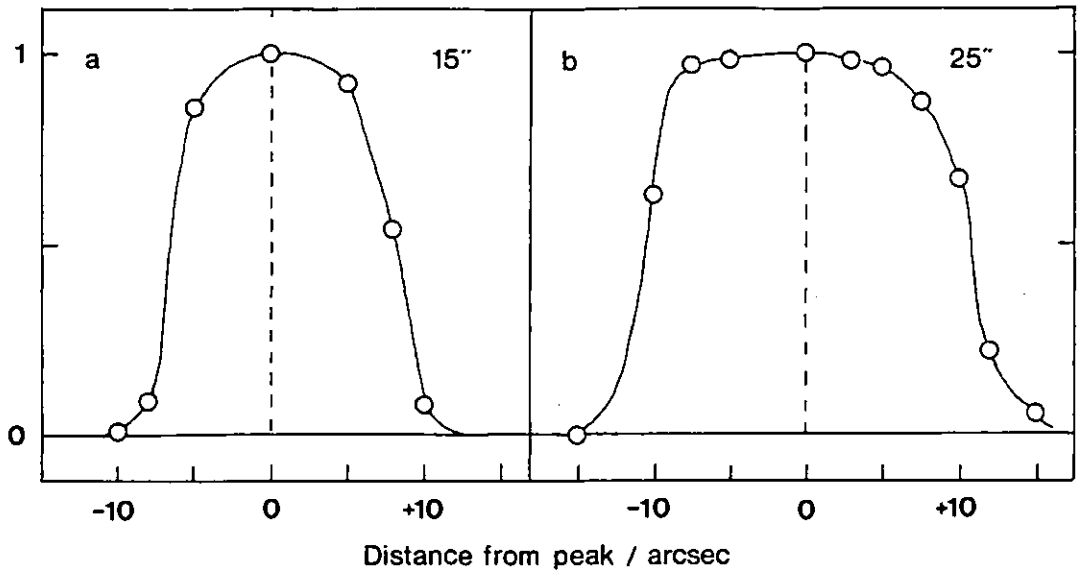

Figure 3.6 - Cross-beam profiles for 15" and 25" apertures

These profiles, made with the star ν Her, represent the signal strength measured away from the centre of the beam.

a Ref. Z12, 1979 June 3 b Ref. Z49, 1979 June 17

therefore looks for peaks across the scans as well as along them. The criterion for a "source" is this: if the value of the cross-correlation at a point is higher than at its eight neighbours, then there is a source at that point. Figure 3.7 illustrates this definition. Sources in the first and last scans of each block are defined with respect to their five neighbours, but because this introduces a bias, they are reconsidered by the REFINE program (see next section).

Figure 3.8 is a rough contour map (made on a line printer) of part of the C-file of a survey block. The rounded blobs represent stars, and crosses mark the positions of sources found by PEAKS 2. Sources identified in this fashion correspond closely to those judged by the eye.

The output of PEAKS 2 is stored in an S-file (S for "source") listing the scan number, point number and magnitude of each source.

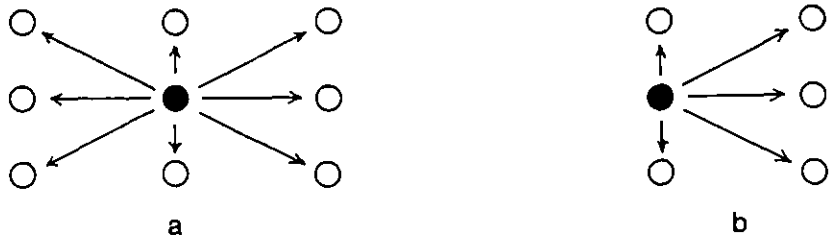

Figure 3.7 - Definition of a source

a If the value of the cross-correlation at a point in a block is higher than at its eight neighbours, then there is a source at that point.

b A source at the edge of a block is defined with respect to its five neighbouring points.

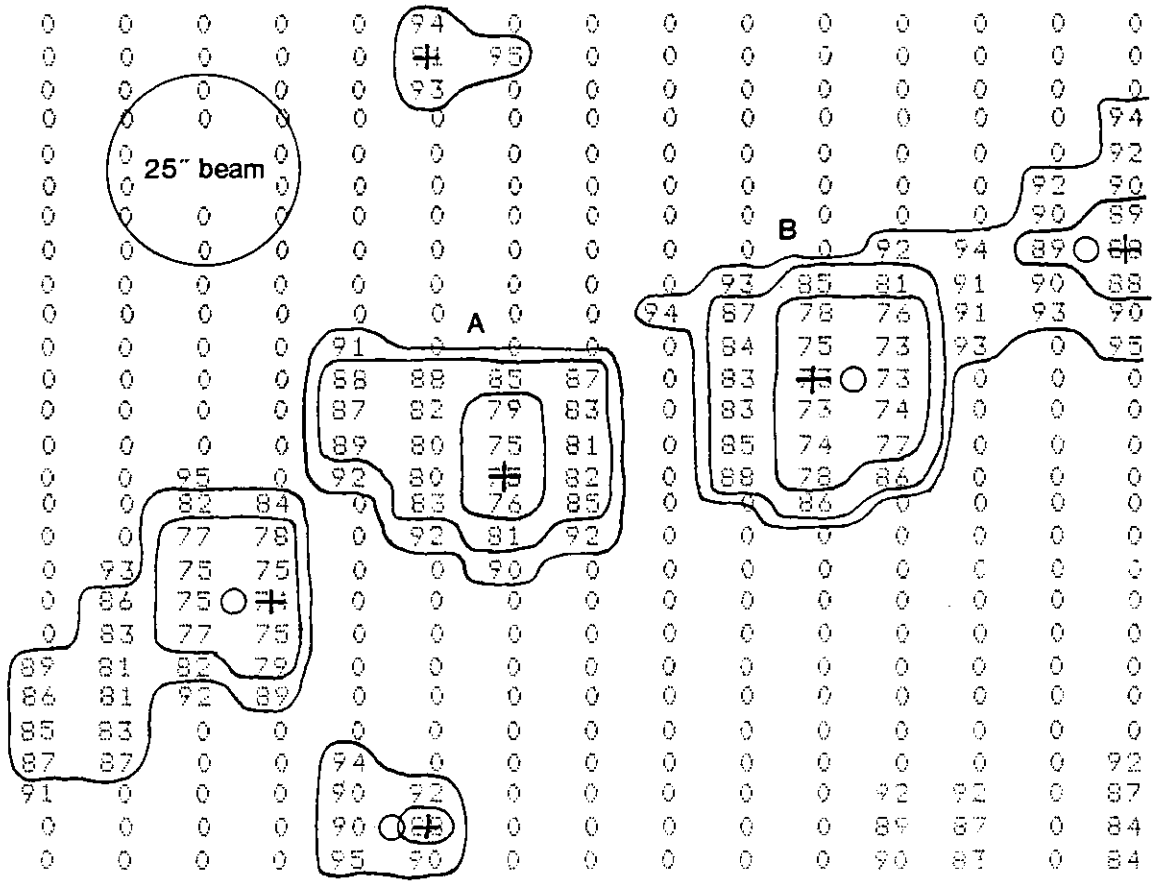

Figure 3.8 - Refinement of source positions

This is a crude contour map of part of the C-file for Block 3 K. Scans run vertically. The numbers are the cross-correlation at each point in units of 0.1 mag, for points brighter than 9.5 mag. Crosses mark sources identified by PEAKS2, and small circles show adjusted positions produced by REFINE.

3.3.5 Refinement of source positions

From Figure 3.7 we can see how the separation between scans (8" or 12") is bigger than that between the samples in a scan (4"). It is possible to refine the position in RA by a crude interpolation between the scan lines; that is, to decide whether a source is closer to a scan line or closer to the mid-point between two scan lines. In Figure 3.8 for instance, source A is symmetrical about a strong central peak, so the star must be close to the central scan line. Source B, on the other hand, has two similar central peaks, so the star must be about half-way between them.

The main task of the interpolation program (REFINE) is to read a C-file and an S-file, examine the cross-correlation on either side of each source, and decide whether to move the source to a mid-point or not. The criterion is this: if the magnitude drop to a neighbouring scan is less than 0.35, then the source is half-way to that scan. If the drops on either side are both less than 0.35, then the source is moved towards the smaller drop. (The value of 0.35 was chosen by trial-and-error to leave half the sources in a block on the scan lines, and half between them. It works for both 25" and 15" beams.)

REFINE also deals with sources in the first and last scans. Any sources that are not moved inwards are skimmed off and discarded.

Finally, REFINE looks out for sources in neighbouring scans that are almost in the same position. Scans may be slightly misaligned, so that the peaks of a single source do not appear at the same point. Peaks within 2 points of each other are deemed to be the same source and the fainter one is discarded.

The output from REFINE is stored in an R-file (R for "refined") listing the position of each source in units of half-scans, and point numbers, together with its magnitude. This file is already suitable for statistical analysis.

3.3.6 Position calibration

In some respects, position calibration is a luxury. We do not need to know the equatorial coordinates of the sources within a block to proceed with a statistical analysis, nor to match up H and K

observations of the same block. However, positional information is present in the observations and it would be a waste not to make use of it. Absolute positions would be especially valuable in comparing these observations with others.

The first step is to determine the positions of the guide stars for each block surveyed. I used the method of dependences (McNally 1974, p.262) to measure positions with respect to three SAO stars. Working from an enlargement of the blue POSS prints (to 8" mm^{-1}) I could get positions reproducible to better than 3". Since the "pixel" size is Δx = 4" or 6" and Δy = 4", this is quite good enough.

Program RADEC then calculates the equatorial coordinates of all the stars in an R-file, given the length of the block and the RA and declination of one point inside it. These quantities were calculated from the positions of the guide stars and using data from the record sheets (Figure 2.7). The reference point was usually the start position, but it is possible to use any other point, such as the position of a known source within the block.

Where there are both H and K observations of the same block, the scan length of one set is usually better determined than the other. To ensure good registration between the H and K scans, I identified about a dozen sources in each block which appeared at both wavelengths, and used these to calculate the relative lengths of the H and K scans by a least squares fit, and any offset between them. In this way, one accurate set of positions could calibrate both wavelengths.

The main sources of error in source positions are likely to be irregularities in the telescope movements. A sample of 71 scans made over both summers showed that drift in RA due to poor tracking had a σ of $\pm$ 2-3" from the mean over a 12' offset. Some deviations could be much greater than this, particularly on windy nights. However, scan lengths were usually reproducible to about 5".

I estimate that the positional error for registration between H and K observations should be about 10". The absolute positions should be almost as good as this where the start and end points are well determined. Otherwise, deviations bigger than this will be systematic (see next Chapter).

Output from RADEC is stored in a P-file (P for "position") containing for each source, RA and declination (both in degrees), magnitude and scan and point numbers.

3.3.7 Matching H and K sources

The final step in the data reduction process is to merge the P-files from the H and K observations of each block into a unified catalogue file. This is the job of program HK.

It reads two P-files, one for each filter, and stores the sources brighter than a defined limiting magnitude. Sources which coincide to within some specified distance (say 10") are deemed to be the same object. A system of flags ensures that the matches recorded are the best possible, and that no sources are paired more than once. The program continues until all sources are flagged as either paired or unpaired. It then lists the mean positions of the pairs, their H and K magnitudes, and their separations, along with the positions and magnitudes of remaining unpaired sources. This merged list is then ordered in increasing RA, and deposited in a CAT-file (CAT for "catalogue").

HK does not treat the two P-files symmetrically and so provides a useful check. Happily, the results are the same when the two files are interchanged.

3.4 Presentation of the reduced data

Merged catalogues (CAT-files) are available for the twelve blocks for which both H and K observations have been reduced. They are Blocks 1, 2, 3, 4, 23, 32, 42, 52, 56, 59, 62 and 72. Blocks 16, 31, 40 and 70 have K observations only. These are stored as P-files. All the brighter sources in the survey are listed in Appendix A, and form the basis for the analysis in the next chapter.

CHAPTER 4

PRELIMINARY RESULTS FROM THE SURVEY

The survey is complete to H = 10.5 and K = 9.5. This is equivalent to detecting M giants at 6-7 kpc. Source confusion, rather than sensitivity or noise, is the limiting factor. Merged catalogues of H and K observations contain about 800 sources brighter than these limits in 0.18 deg^2, but the calibration of Block 1 is probably in error.

The integrated 2.2 μm surface brightness is 40-50% of the 2.4 μm disk brightness measured from balloons. There is no sign of the central bulge. Our observations are consistent with the presence of supergiants in the 5 kpc ring, but are not conclusive. A study of the distributions of surface number densities, surface brightness and H-K colour indices points to a population of supergiants (∿1000 deg^{-2}) within 0.4^o (70 pc) of the galactic centre. Otherwise the source distributions show no strong longitude dependence. One IRC source is newly identified with a faint red star.

4.1 Introduction

In this chapter I will present some preliminary results from the galactic plane survey. My strategy is to start with the simplest observation (the number of sources) and then move to progressively more detailed results. Thus, I first use the magnitude distributions to estimate the completeness and depth of the survey. Second, I look at the surface number densities and how they depend on longitude. Third, the sources are integrated to produce surface brightness measurements and I compare these with the large-scale maps of Chapter 1. The fourth stage is to look at the H-K colour indices of the sources and what they reveal about the nature of the emitting objects. Fifth I compare the survey catalogue with other infrared catalogues and with other observations of the galactic centre. Finally we ask, have we detected supergiants in the 5 kpc ring? I conclude the chapter with suggestions for further work and recommendations for others contemplating similar investigations.

Table 4.1 - Analysis of Source Counts (H)

Block	Beam	H Magnitude																
	(")	≤5.5	6.0	6.5	7.0	7.5	8.0	8.5	9.0	9.5	10.0	10.5	11.0	11.5	12.0	12.5	13.0	13.5
1	25							1	1	1	2	5	12	11	30	23	11	6
2	25				2	0	2	2	2	5	12	11	21	10	4	0	1	1
3	25				1	0	0	3	6	2	9	7	14	13	4	3	2	
4	25					1	2	1	0	3	15	13	16	11	9	3	0	3
23	25			$\hat{1}$	0	0	2	0	2	7	6	11	18	9	10	7	2	1
32	25						1	3	4	6	14	15	16	15	15	10	1	3
42	25			$\hat{1}$	3	2	0	1	2	6	10	13	13	7	7	8	4	2
52	25							1	3	10	12	13	12	14	16	7	3	1
56	15		$\hat{1}$	1	0	0	2	4	3	9	12	20	45	44	40	21	12	4
59	25				1	0	0	5	2	4	5	14	15	19	4	4	4	1
62	25			$\hat{1}$	1	2	1	0	7	5	9	24	7	4	6	1		
72	15						2	0	1	3	5	20	40	44	17	8	2	1
All 15"	a(H)		$\hat{1}$	1	0	0	4	4	4	12	17	40	85	88	57	29	14	5
	n(H)		1	2	2	2	6	10	14	26	43	83	168	256	313	342	356	361
All 25"	a(H)			$\hat{3}$	8	5	8	16	28	48	92	121	132	102	75	43	17	12
	n(H)			3	11	16	24	40	68	116	208	329	461	563	638	681	698	710
All H	a(H)		$\hat{1}$	$\hat{3}$,1	8	5	12	20	32	60	109	161	217	190	132	72	31	17
	n(H)			5	13	18	30	50	82	142	251	412	629	819	951	1023	1054	1071

Table 4.2 - Analysis of Source Counts (K)

Block	Beam	K Magnitude																
	(")	≤5.5	6.0	6.5	7.0	7.5	8.0	8.5	9.0	9.5	10.0	10.5	11.0	11.5	12.0	12.5	13.0	13.5
1	25			1	0	2	2	0	6	7	9	14	14	7	4	4	4	
2	15			$\hat{3}$,1	1	3	10	14	25	35	35	25	6	7	3			
3	25			$\hat{2}$	2	8	5	14	7	13	2	8	3	3	1	1		
4	25			$\hat{1}$	0	5	6	12	9	16	12	5	4	0	1			
16	15		1	1	0	1	2	4	15	33	39	38	33	24	7	8	1	
23	15		$\hat{1}$	0	1	0	3	5	9	23	34	28	32	20	13	5	5	4
31	15			1	0	1	3	2	12	15	22	23	30	26	6	7	3	
32	25			1	0	4	4	9	10	18	10	9	12	8	4			
40	25	$\hat{1}$				1	2	5	8	14	28	25	23	6	2	2	2	
42	25		$\hat{2}$	$\hat{2}$	3	0	1	5	15	12	8	10	7	2	4	3	1	
52	25					3	5	10	6	9	7	7	10	7	6	1	1	2
56	15	$\hat{1}$	1	0	1	4	3	13	10	11	19	31	51	34	17	12	1	
59	25			$\hat{1}$	0	2	4	4	7	11	16	5	7	4	4	0	0	1
62	25			$\hat{3}$	1	2	3	7	14	6	12	9	2	0	0	1		
70	15		$\hat{1}$	0	1	0	7	10	20	15	20	37	28	28	14	6	5	3
72	25					1	4	1	4	6	3	4	7	2	7	2	1	1
All 15"	a(K)		$\hat{2}$,2	$\hat{3}$,3	4	9	28	48	91	132	169	182	180	139	60	38	15	7
	n(K)	1	5	11	15	24	52	100	191	323	492	674	854	993	1053	1091	1106	1113
All 25"	a(K)		$\hat{2}$	$\hat{8}$,2	6	26	34	67	80	105	98	82	75	32	29	10	5	4
	n(K)	1	3	13	19	45	79	146	226	331	429	511	586	618	647	657	662	666
All K	a(K)		$\hat{4}$,2	$\hat{11}$,5	10	35	62	115	171	237	267	264	255	171	89	48	20	11
	n(K)	2	8	24	34	69	131	246	417	654	921	1185	1440	1611	1700	1748	1748	1779

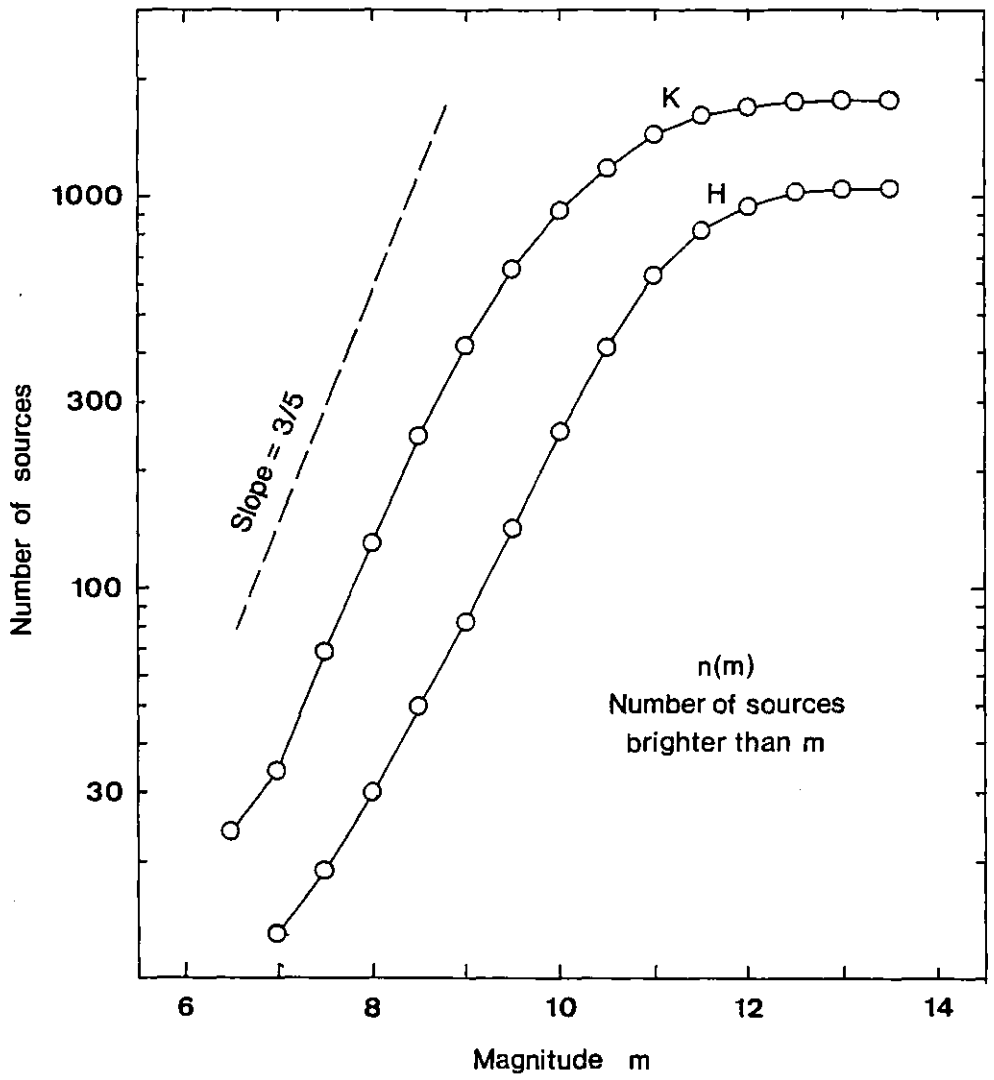

Figure 4.1 - Survey source counts: n(m)

These are the cumulative totals, n(m), of 1071 H sources and 1779 K sources. The sources from Block 1 have been excluded.

Notes to Tables 4.1 and 4.2:

Two quantities are tabulated: a(m), the number of sources in the range m to m - 0.5, and n(m), the number of sources brighter than m. Each Table is divided in two by a horizontal line. The top part contains a(m) for each block. In the bottom part a(m) and n(m) are summed by beamwidth, and for all blocks together (except Block 1). A number with a hat (e. g. $\hat{2}$) is the number of saturated sources in that magnitude range.

4.2 Assessment of the survey results

We begin with a statistical analysis. Tables 4.1 and 4.2 show how the sources are distributed in magnitude. Two quantities are tabulated: a(m), the number of sources in the range m to m - Δm, where Δm = 0.5; and n(m), the number of sources brighter than m. See the notes following the Tables for more explanation.

Figure 4.1 is a plot of n(m) for both H and K bands. Figure 4.2 shows a(m) plotted for both filters and for both beamwidths (15" and 25"). We can use these plots to assess the reliability of the survey results. First we examine the completeness and depth of the survey, and then the limitations on it.

4.2.1 Completeness

We will define the completeness limit as the magnitude above which n(m) and a(m) depart from linearity (this is a conventional definition used, for instance, by Kleinmann et al. (1981) to assess the IRC, AFGL and Bright Star catalogues). The survey is then presumed to have detected almost all sources brighter than this limit. The criterion of linearity arises in the following way. Suppose the survey sources have a homogeneous luminosity function, are spread uniformly through space, and extinction can be ignored. Then

$$\log n(m) = \frac{3}{5}m + \text{constant} \qquad (4.1a)$$

$$\log a(m) = \frac{3}{5}m + \text{constant} \qquad (4.1b)$$

Figures 4.1 and 4.2 contain a slope of $^3/5$ to represent this ideal condition. The agreement with the plotted curves is good until n(m) flattens off and a(m) turns over.

In the examples of Kleinmann et al. (1981) the completeness limits are well defined, with n(m) flattening over less than one magnitude. In Figure 4.1 the flattening is gentler, perhaps 2-3 magnitudes (this is probably a confusion effect; see next Section). For this reason I have used Figure 4.2 to set the limits, putting them just to the bright side of the peaks. The limits are H = 10.5 and K = 9.5. There are 412 H sources and 654 K sources brighter than these

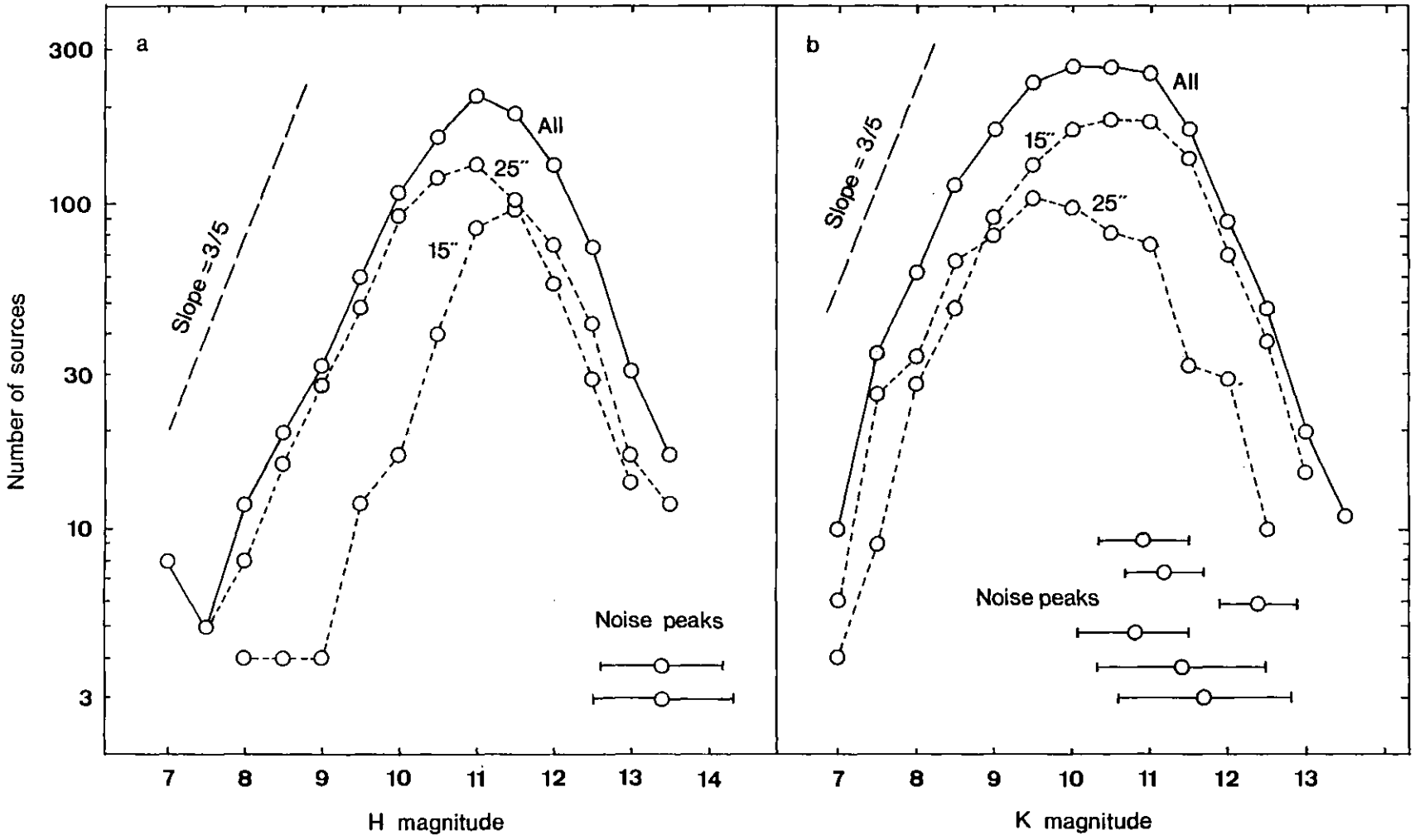

Figure 4.2 - Survey source counts: a(m). Here, a(m) is the number of sources in the interval m to m - 0.5 for (a) H and (b) K. Data are from Tables 4.1 and 4.2, but sources from Block 1 are excluded.

limits, excluding those of Block 1. (Block 1 is omitted because it may have a calibration error. I come back to it in Section 4.6).

Many sources are too bright to be measured, because they saturated the DVM. This sets an upper limit on the brightness range of the survey, which varies according to the degree of saturation, but it is always brighter than magnitude 6.5 at both H and K.

These limits correspond to detecting type M giants between 2 kpc and 6–7 kpc from the sun.

Appendix A contains the equatorial coordinates and H and K magnitudes of all sources brighter than H = 10.5 and K = 9.5. A detailed description of this catalogue will also be found in the Appendix.

4.2.2 Limiting effects

Confusion, rather than background noise or sensitivity, appears to be the limiting factor in this survey. During the observations we made several "noise scans" which were identical to the survey scans except that the telescope was stationary. They were processed in exactly the same way as the rest of the data. Since these scans contain no sources, any peaks found in them must be spurious. Figure 4.2 shows the distributions of 143 noise peaks; 32 at H and 111 at K. These spurious sources cluster well below the completeness limits, so background noise is unlikely to be an important limitation. This is what we expected. The faintest detectable stars are swamped by the brighter ones, causing the a(m) plots in Figure 4.2 to peak and fall off.

We can test the confusion hypothesis by comparing the a(m) plots for the 15" and 25" beams. The smaller beam should reach to fainter magnitudes before confusion becomes dominant. Figure 4.2 shows that the 15" peak is about a magnitude fainter than the 25" peak.

In Section 3.1.1 we saw that the shape of the instrumental profile leads to flux cancellation where sources are crowded together. This effect will tend to dim sources, pushing them to fainter magnitudes and so make n(m) flatten off more gently, as is apparent in Figure 4.1.

Table 4.3 - Longitudes, Extents and Areas of Survey Blocks

Blk	Long	H							K						
		RA (1950)			Declination (1950)			Area	RA (1950)			Declination (1950)			Area
	o	h m s			o ' "			min^2	h m s			o ' "			min^2
1	-0.06	17 42 20.1			-29 04 29			41.0	17 42 20.1			-29 04 32			40.3
2	+0.07	17 42 38.3			-28 58 15			40.5	17 42 38.3			-28 58 28			42.6
3	0.20	17 42 57.1			-28 51 42			40.6	17 42 57.1			-28 51 40			40.6
4	0.32	17 43 15.2			-28 44 49			41.1	17 43 15.2			-28 44 57			40.8
16	1.86	-			-			-	17 46 52.4			-27 26 40			46.3
23	2.77	17 49 02.3			-26 40 29			40.8	17 49 02.3			-26 40 45			42.8
31	3.81	-			-			-	17 51 25.2			-25 46 15			36.2
32	3.94	17 51 38.8			-25 39 20			42.6	17 51 38.8			-25 39 27			43.6
40	4.99	-			-			-	17 54 00.0			-24 45 10			44.9
42	5.25	17 54 35.7			-24 31 43			41.1	17 54 35.7			-24 31 39			41.1
52	6.58	17 57 29.9			-23 22 44			43.9	17 57 29.9			-23 22 36			41.4
56	7.12	17 58 39.5			-22 55 10			44.4	17 58 39.5			-22 55 10			44.7
59	7.52	17 59 31.8			-22 34 12			41.2	17 59 31.8			-22 34 16			40.7
62	7.92	18 00 23.8			-22 13 04			40.2	18 00 23.8			-22 13 09			41.2
70	9.00	-			-			-	18 02 41.7			-21 17 02			45.9
72	9.27	18 03 15.4			-21 02 59			28.1	18 03 22.3			-21 02 41			24.1

Longitudes refer to nominal block centres. Latitude is -0.04^{o}. Equatorial coordinates are those of the edges of the surveyed areas. Total areas are 485.5 $arcmin^2$ (H) and 656.6 $arcmin^2$ (K).

4.3 Surface number densities

We next calculate the surface number densities N(m) for each block, using the data from Tables 4.1 and 4.2 and the block areas in Table 4.3. N(m), in units of sources deg^{-2} brighter than m, is plotted against longitude in Figure 4.3.

There are three interesting features in the longitude distribution: the absence of a general trend, the jaggedness of the plots, and a peak near $\ell = 0^{\circ}$.

(1) At first sight there is little evidence for a general trend in longitude. This is not too surprising, since the survey only reaches to 6–7 kpc, somewhat short of the central bulge which, with a radius of 2.5 kpc (Section 1.2.1), should come into view at about 7.5 kpc. Nevertheless, there is some sign of a falling off in longitude at K = 9.5 which may mean that some of the outer bulge stars have been detected.

(2) Both sets of curves are jagged. They become smoother with fainter magnitude, presumably because more stars then contribute to each data point and so reduce Poissonian fluctuations. But some of the roughness must be due to irregularities in the star distributions or in the interstellar extinction.

(3) There appears to be a sharp peak near $\ell = 0^{\circ}$ in the N(K) distribution, but this is not so clear in N(H). This may be a selection effect, since a sharp peak will only be apparent where data points are close together (Blocks 2, 3 and 4). If this peak represents sources clustering around the core of the Galaxy, then they must have $M_K < -9$ to be visible at $K < 8$. From Figure 1.6 (the 2.2 μm H–R diagram) we see that only late-type supergiants are luminous enough to be these sources. At 10 kpc they should be about 1.6 mag fainter at H than at K, (Section 4.4), but there is no clear evidence for a peak in N(H) at $H < 9.5$.

4.4 Surface brightness

We now wish to compare the present observations with the 2.4 μm surface brightness maps of Chapter 1.

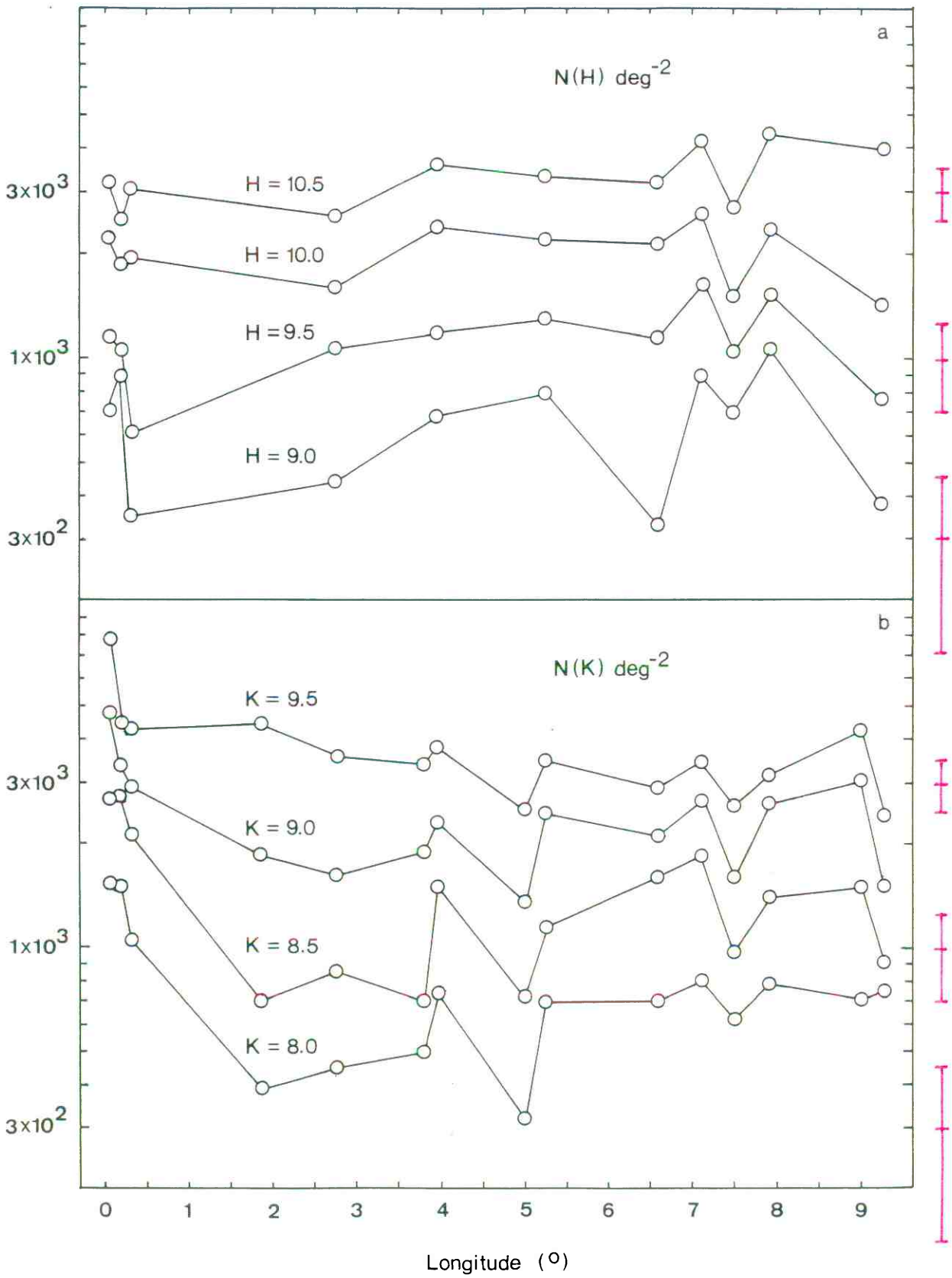

Figure 4.3 - Distribution of surface number density with longitude
Error bars are an indication of the Poissonian standard deviation at N = 300, 1000 and 3000 deg^{-2}.

4.4.1 Distribution in longitude

Figure 4.4 shows the surface brightness of each of the survey blocks, calculated by adding the fluxes of all the sources down to the completeness limits. Because the blocks are so small (about 40 arcmin^2), one or two bright objects can severely bias the brightness of a block. Moreover, many of the bright sources are saturated, making the surface brightness even less reliable. Points formed in this crude manner are joined by dashed lines in Figure 4.4.

To make the plots more representative, I have subtracted all the sources brighter than H = 6.5 and K = 6.5, to leave a uniform sample of sources in each block. These points are joined by solid lines in Figure 4.4. The new distribution is somewhat smoother.

There is a clear peak near $\ell = 0^\circ$, corresponding to the peak in N(m) (Figure 4.3). The jagged shape of the plots is reflected also. But surprisingly, the noticeable slope in N(K) for K = 9.5 is not present in the surface brightness distribution. Away from the galactic centre the curve is more or less flat. This must mean that the sources tend to be brighter with increasing longitude. Figure 4.5 shows how the mean brightness of sources depends on longitude. For K, the mean flux increases by about a half from $\ell = 2^\circ$ to 9°, whereas H sources do not change very much.

4.4.2 Comparison with 2.4 μm observations

Figure 4.6 shows the 2.4 μm surface brightness of the galactic plane between $\ell = 0^\circ$ and $\ell = 9^\circ$ measured by Hayakawa et al. (1979). The curve is for $b = 0^\circ$, which is close to the $b = -0.04^\circ$ of the present survey. The 2.2 m curve from Figure 4.4 is shown for comparison, with a constant 1.2×10^{-6} W m^{-2} μm^{-1} sr^{-1} added as the contribution from stars brighter than K = 6.5 (this figure was obtained by interpolating between the N(m) distribution for the IRC in the galactic centre region and that of the present survey).

We note the following

(1) The 2.2 μm distribution shows no sign of the steep slope in the 2.4 μm curve. Whatever is producing the slope cannot be composed of stars brighter than K = 9.5, and cannot be M giants within 7 kpc.

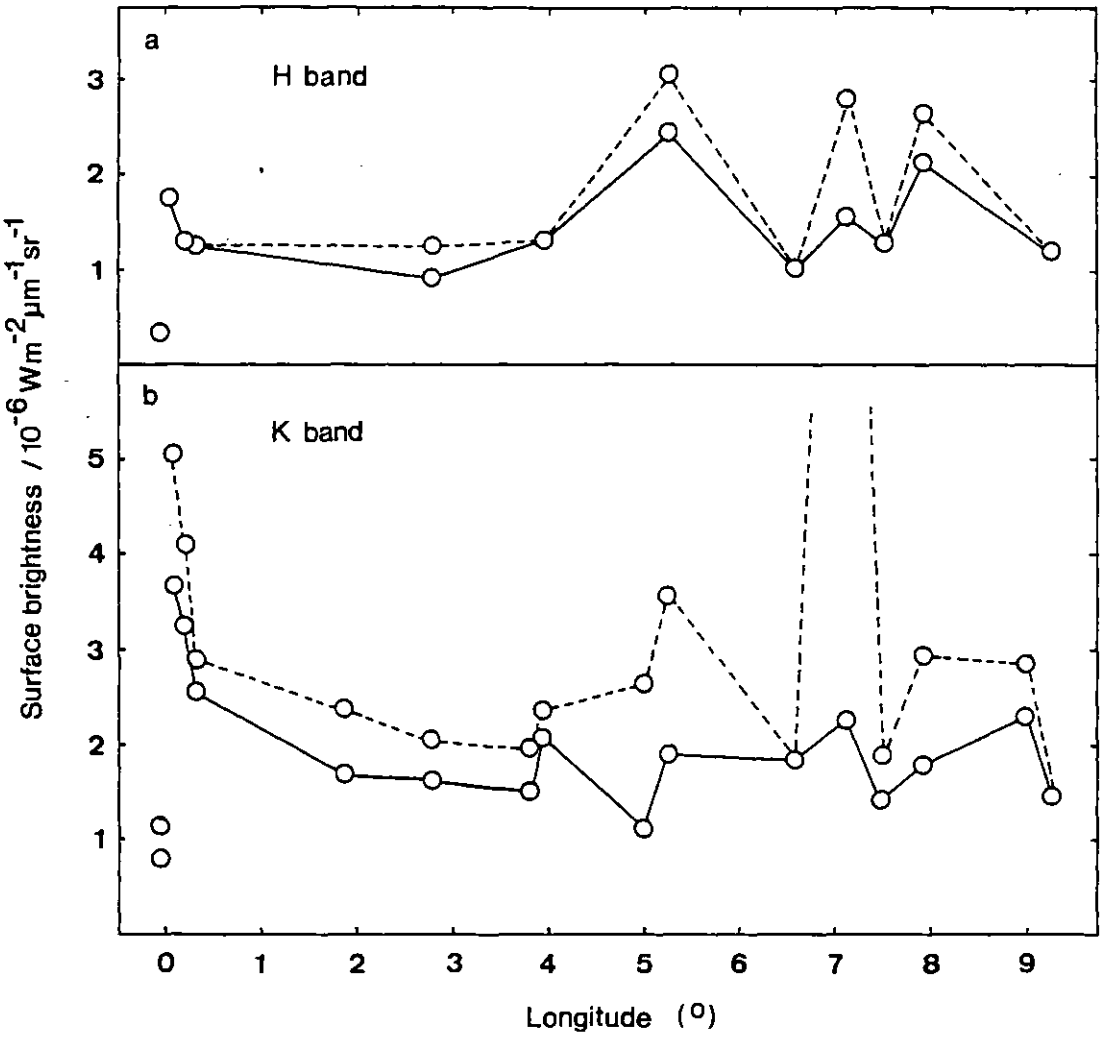

Figure 4.4 - Distribution of surface brightness with longitude

The dashed lines join points calculated by adding the fluxes from all the sources brighter than H = 10.5 and K = 9.5 in each block (absolute calibration is from Johnson, 1966). A few bright sources, many of them saturated, dominate these points and distort the distribution. To correct for this, the points joined by solid lines are formed from sources fainter than magnitude 6.5. None of these is saturated. Block 1 , at the bottom left of the plots, appears anomalously faint (see text).

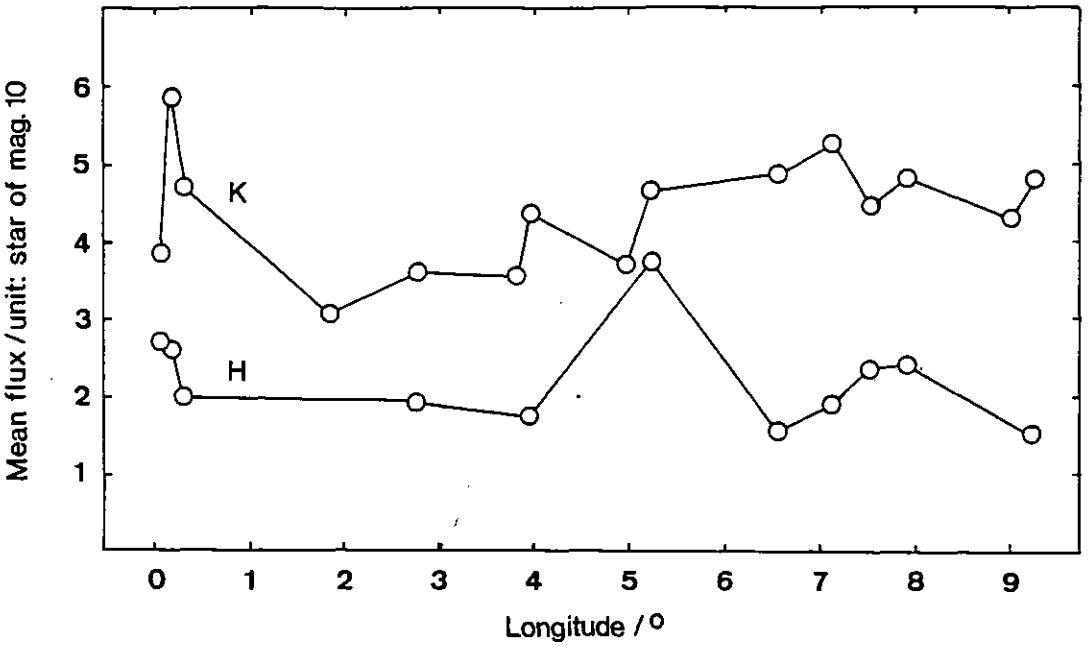

Figure 4.5 - Mean brightness of sources as a function of longitude

The mean flux is summed over the sources fainter than H = K = 6.5, and brighter than H = 10.5, K = 9.5.

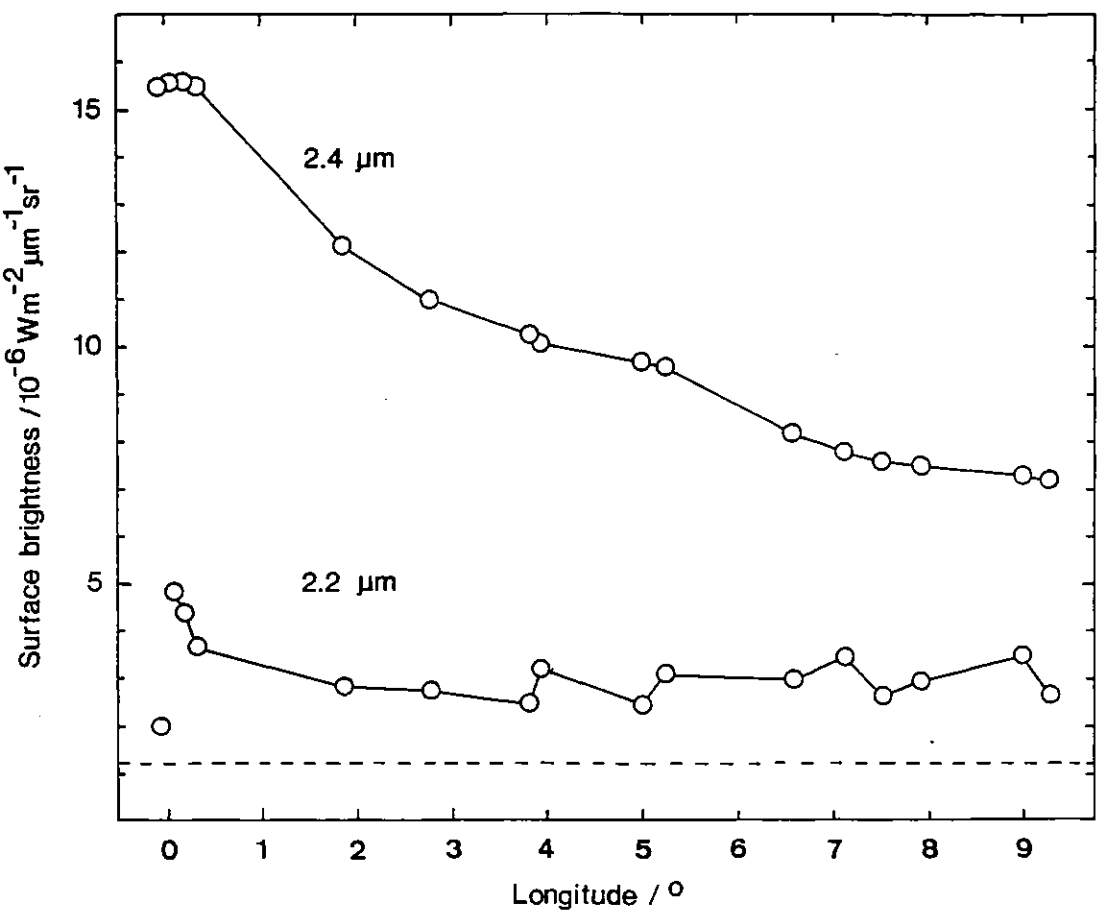

Figure 4.6 - Comparison of 2.2 μm and 2.4 μm surface brightness

The 2.4 μm points are measured from Figure 3a of Hayakawa et al. (1979) and represent the surface brightness at b = 0°. The dashed line is the estimated 2.2 μm contribution from stars of K ≤ 6.5.

These observations confirm that the slope is from the central bulge of the Galaxy.

(2) There is no sharp peak in the 2.4 μm curve near $\ell = 0^{\circ}$. This could be because of the large aperture (1.7°), or because the bright core has been swamped by the rest of the bulge.

(3) After subtracting the bulge component from Figures 1.2 and 1.4, I estimate that the residual 2.4 μm disk brightness is $6\text{-}7 \times 10^{-6}$ W m^{-2} μm^{-1} sr^{-1}. In Figure 4.6 the integrated 2.2 μm surface brightness is about 3 of these units. Therefore, 40-50% of the disk emission comes from discrete sources brighter than K = 9.5, or M giants within 6-7 kpc.

We should add a note of caution about the difference in wavelength between the two observations. If M giants have an effective temperature of $\sim$ 3000K, then the flux ratio is $F_{2.2}/F_{2.4} \simeq 1.25$. The 2.4 μm curve would need to be raised by about 25% to correct it to 2.2 μm. However, the effects of differential extinction (reddening) act the other way and would drop the 2.4 μm curve by about 20% over 10 kpc. Because of this uncertainty I have not made any corrections to Figure 4.6.

4.5 H-K colours

The merged catalogues of H and K observations allow us to study the H-K colour indices of the survey objects.

4.5.1 Contributions to H-K

An H-K colour has two components:

(1) Intrinsic colour. This is the H-K of the star's photosphere, and covers a range from 0.0 for type B stars, to 0.3 for late type M stars (these figures are from the CIT list of calibrations and Becklin et al. (1978)).

(2) Differential extinction, or "reddening". Dust extinction is stronger at H than at K, and makes stars appear redder than they really are. The accepted model for reddening is van de Hulst's curve number 15 (Johnson 1968, Becklin et al. 1978),which predicts the following relation of H and K extinction to that at V:

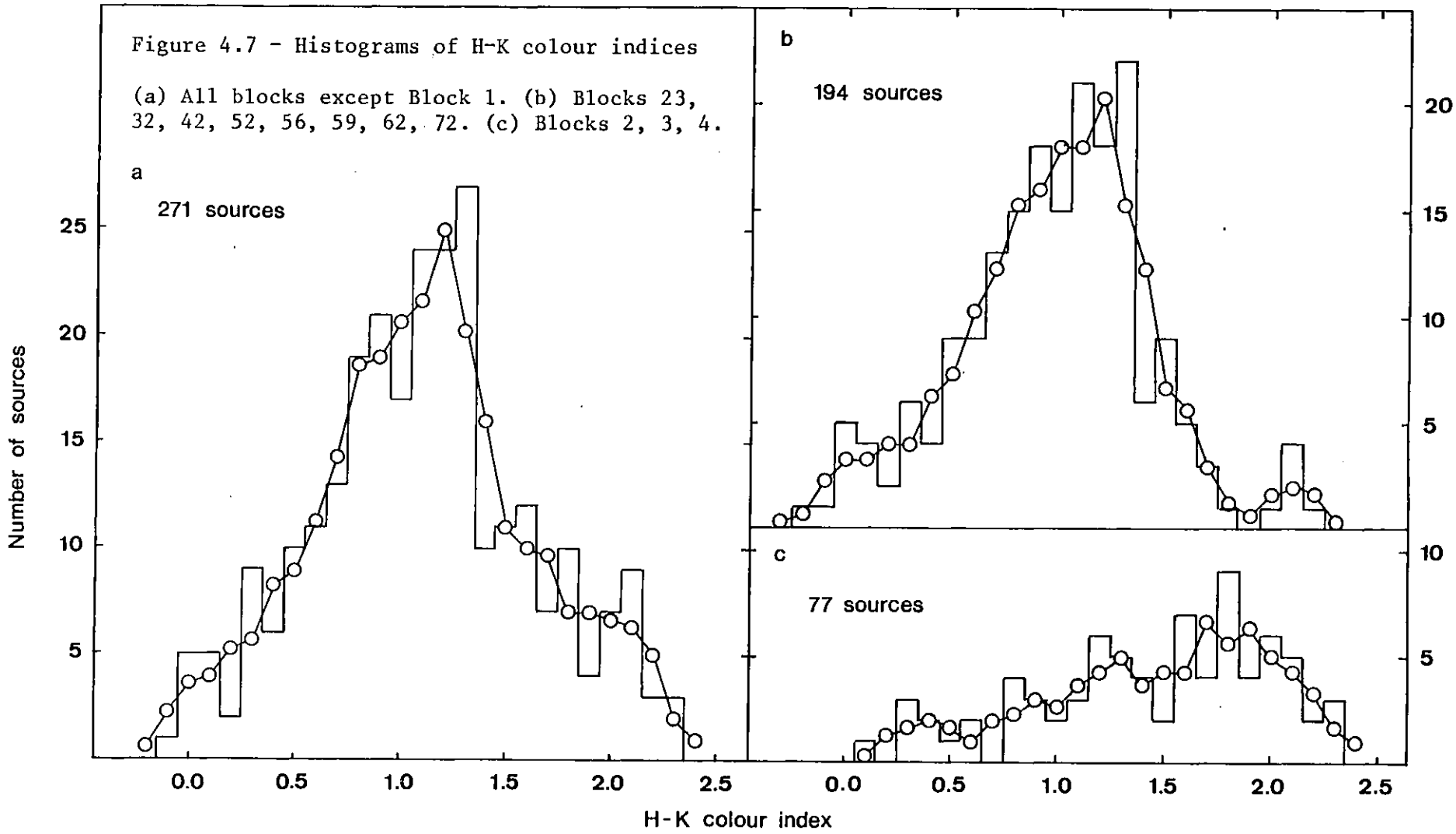

Figure 4.7 - Histograms of H-K colour indices

(a) All blocks except Block 1. (b) Blocks 23, 32, 42, 52, 56, 59, 62, 72. (c) Blocks 2, 3, 4.

The circles are smoothed values, obtained by averaging each point with its two neighbours.

$$A_H = 0.16\ A_V$$

$$A_K = 0.09\ A_V$$

$$A_{H-K} = 0.07\ A_V \qquad (4.2)$$

The reddening, A_{H-K} is proportional to the amount of visual extinction, and so can be used as an indicator of distance. I assume $A_V = 1.9$ mag kpc^{-1} (AQ p.263).

4.5.2 Distribution of H-K colours

Figure 4.7a is a histogram of 271 H-K values taken from all the blocks except the first. The error in an individual H-K is likely to be ± 0.1 at least, and so I have smoothed the histogram by averaging each point with its two neighbours. There are two striking features: a sharp peak near H-K = 1.2-1.3, and a broad shoulder to the right of it.

The peak is caused by the arbitrary survey limit of H = 10.5 and K = 9.5. The faintest sources are seen through about 13 magnitudes of visual extinction. From Equation 4.2 the maximum reddening should be about 0.9 mag. For stars with an intrinsic H-K of 0.3, the histogram should cut-off after H-K ≈ 1.2, close to the observed peak.

If this interpretation is correct, the broad shoulder beyond H-K = 1.5 requires another explanation. In Figures 4.7b and 4.7c I have plotted separate histograms for the three central blocks (2, 3 and 4) and for all the others. The two curves are remarkably different. Almost all the objects with excess H-K are in the galactic centre blocks.

4.5.3 Supergiants near the galactic centre?

Could these reddened objects be the conjectured supergiants clustering around the core of the Galaxy (Section 4.3)? At 10 kpc, the observed H-K of a star cannot be much more than 1.6, yet there are many objects with H-K up to 2.3. Another 0.7 mag remains unexplained. However, in Chapter 1 we found that the infrared mapping of the Milky Way had revealed a dense core of dust within 2° of the galactic centre, contributing about 10 mag of visual

extinction. This would produce an H-K reddening of up to 0.7 mag, which is the observed discrepancy, and is consistent with the H-K of 2.3 for the galactic centre complex (Becklin et al. 1978; see next Section). Objects with H-K = 2.3 would appear with K < 8.2 in the present survey, and require $M_K < 9$. These can only be supergiants.

We can estimate the numbers of these objects. The mean number density of sources with H-K > 1.6 is 1180 deg^{-2} in the central blocks and 180 deg^{-2} in the others. In the galactic centre the reddened objects are therefore in excess by 1000 deg^{-2}.

Is this figure consistent with the peak in the N(K) distribution (Figure 4.3)? For H-K in the range 1.6 to 2.3, K lies between 8.2 and 8.9. The mean excesses in the central blocks over the others are N(8) = 740, N(8.5) = 1370 and N(9.0) = 1620 deg^{-2}. This good agreement strengthens the inference that there is a population of luminous, reddened objects within 0.4° (70 pc) of the galactic centre, with $N \sim 1000$ deg^{-2}.

4.6 Block 1 and the galactic centre

Of the 16 blocks in the present survey, only one covers an area for which comparable observations exist. This is Block 1, which is centred on the galactic nucleus. It has so far been omitted from the analysis because it is peculiar in several ways, and may have a calibration error at both wavelengths.

4.6.1 Peculiarity of Block 1

There are three main anomalies:

(1) Surface number densities are only 28% of the mean for the neighbouring blocks (2, 3 and 4) at both H and K. This is equivalent to a magnitude error of $\Delta H = 1.3$ mag and $\Delta K = 1.5$ mag.

(2) Surface brightnesses are also lower: 21% at H ($\Delta H = 1.1$) and 25% at K ($\Delta K = 1.1$)

(3) The peaks of a(H) and a(K) in Tables 4.1 and 4.2 are displaced by $\Delta H \sim 1$ mag and $\Delta K \sim 1$ mag compared with the 25" a(m) plots in Figure 4.2.

At first sight, there appears to be a calibration error in Block 1, making the sources appear 1-1.5 mag too faint. This would be consistent with a misreported amplifier gain, which changes in factors of 3 (1.2 mag) or 0.3 (1.3 mag). However, it is odd that both H and K should have similar errors, since they were done on different (though successive) nights.

Perhaps there is no error, and there really are fewer and fainter objects in Block 1 than in the neighbouring blocks. The galactic centre is a unique place and we should not be surprised to find unique properties. However, these properties cannot be expected to extend several kpc towards the sun and affect foreground objects. If Block 1 really is unusual, then it must be for reasons unconnected with the presence of the galactic nucleus, and therefore coincidental.

One formal possibility is the intervention of a dark cloud. If ΔK = 1.0-1.5 mag, then ΔV = 11 to 17 mag, over half the extinction on a 10 kpc line of sight. To dim all the sources in Block 1 fainter than K = 7.5, it would have to be within 3 kpc of the Sun. Moreover, it must be shaped to blot out Block 1 without encroaching on Block 2. This seems unlikely.

4.6.2 Comparison with Becklin and Neugebauer's observations

Fortunately, there already exist observations of this region. Becklin and Neugebauer (1968, B & N) mapped the core at 2.2 μm with a range of beamwidths. In Figure 4.8 I show their map made with a 15" beam. It remains the most comparable observation to the present survey, even though it records extended emission rather than discriminating in favour of discrete sources. Superimposed on this map are the brighter K sources discovered in the survey. Because the region is so complex, some of them may be clumps in the diffuse background rather than true discrete objects.

The central complex has three important components:

(1) A diffuse source, elongated along the galactic plane, and with H-K = 2.3

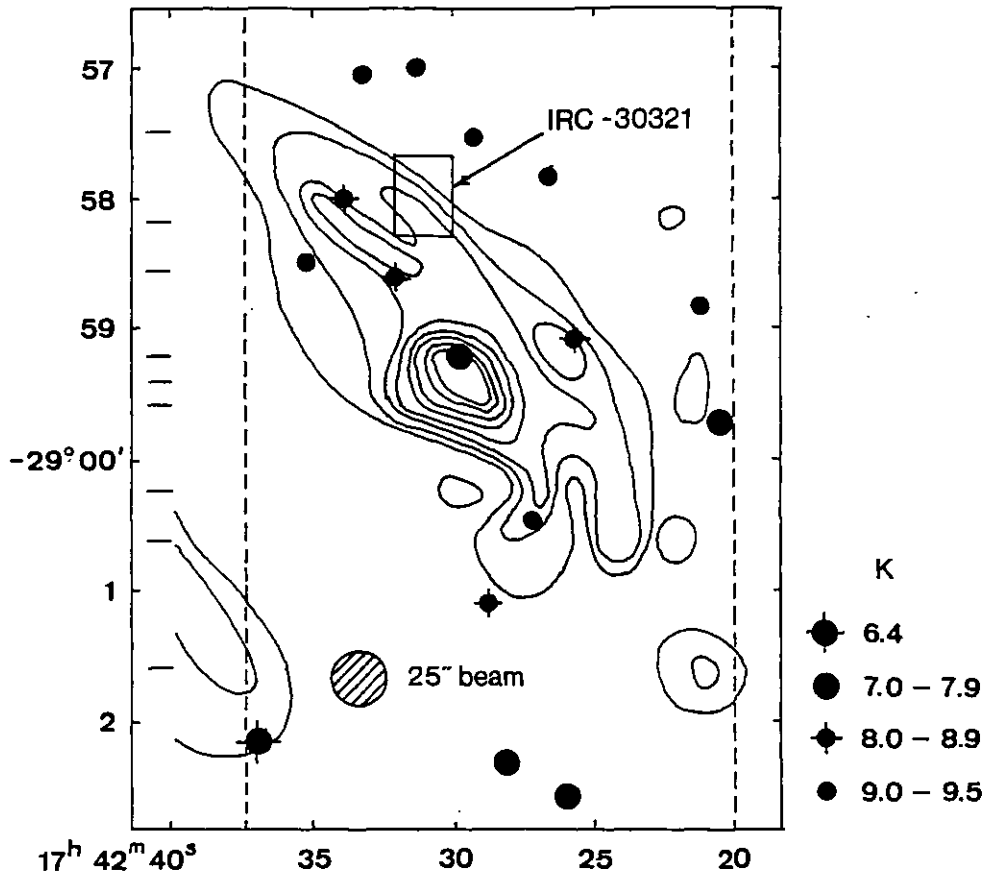

Figure 4.8 - Infrared map of the galactic centre

Survey sources (mapped with a 25" beam) are superimposed on this 2.2 μm map made with a 15" beam by Becklin and Neugebauer (1968). The contour interval is 2×10^{-5} W m^{-2} μm^{-1} sr^{-1}. Bars on the left mark the declinations of the B & N scans. The vertical dashed lines are the bounds of Block 1.

(2) A 20" core source that was later found to contain a cluster of pointlike objects.

(3) A bright, starlike object within the core and known as IRS7 (after B & N). It has K = 6.7, H-K = 2.6 and is probably a supergiant (Becklin et al. 1978).

How do the B & N observations compare with the survey? IRS 134 (Appendix A) coincides closely with the B & N core, but has K = 7.4, H-K = 1.7. If this is IRS7, and is free of confusion, then we require $\Delta H = 0.2$ and $\Delta K = 0.7$ to match the two observations.

But although the main source (1) is diffuse, it is strongly peaked and will dominate over IRS7 in the present survey. B & N (1969) derive a power low of $F \propto D^{1.2\pm0.1}$ where F is the flux contained in an aperture of diameter D (see their Figure 2). From this it is possible to estimate the apparent flux measured by a 25" beam passing across the source with a 25" chop. I obtain K = 5.8 and H-K = 2.2 ($\Delta H = 1.1$, $\Delta K = 1.6$). Even in this complex and confused region, it is difficult to see how such a bright source could be missed.

It seems, then, that the block calibration is in error. There is a simple way to check it. The brightest object in the block is not, surprisingly, the galactic nucleus, but IRS151 (K = 6.4, H-K = 1.6) about 3' to the SE. It lies in a relatively barren part of the field and B & N missed it because none of their scans passed nearby. (Figure 4.8). A single photometric measurement of this source will be sufficient to recalibrate the whole block.

4.7 Comparison with other catalogues

Two catalogues were searched: the IRC (the two-micron survey) and the AFGL catalogue (see Section 1.3 for more details). Four sources were found within the surveyed area, and two more were close enough that their error boxes overlapped survey blocks. One SAO star is also in the area. These sources are listed in Table 4.4.

4.7.1 IRC -30321 / AFGL 2003

The error box of the IRC source is contained entirely within that of the AFGL object, and the AFGL catalogue identifies them as one and the same. Although IRC -30321 is listed with K = 2.78, there is certainly no discrete source as bright as that in or near the error box (Figure 4.8). These sources can only be the broad, diffuse emission discovered by B & N, although the centre of this object lies well outside both error boxes.

4.7.2 AFGL 2004

According to the catalogue, this extended source coincides with the HII region Sharpless 17, and is therefore likely to originate in hot gas or dust, rather than a discrete object. Fourteen sources lie in the overlap between Block 3 and the error box.

Table 4.4 - Comparison of Survey Sources with Existing Catalogues

	Object	Equatorial coordinates (1950) h m s	o '	Notes
A	IRC -30321	17 42 31 ± 1	-28 58.0 ± 0.3	K = 2.78
	AFGL 2003	17 42 32 ± 9	-28 56.0 ± 2.7	
	Core	17 42 29.3 ± 0.15	-28 59.30 ± 0.05	Oort (1977)
	IRS 134	17 42 29.7 ± 0.7	-28 59.2 ± 0.2	K = 7.4?
B	AFGL 2004	17 43 00 ± 9	-28 50.8 ± 2.7	Sharpless 17
C	IRC -20416	17 58 50 ± 2	-22 44.9 ± 0.3	K = 2.42
	IRS 5644	17 58 50.5 ± 0.7	-22 44.7 ± 0.2	K = 2.5
	Red star	17 58 50.6 ± 0.1	-22 44.73 ± 0.03	B ~ 16, R ~ 13
D	SAO 186135	17 58 52.52	-22 46.85	V = 5.73, BO II
	IRS 5649	17 58 52.4 ± 0.7	-22 46.7 ± 0.2	K = 6.0, H = 6.1
E	IRC -20427	18 02 38 ± 2	-21 14.0 ± 0.7	K = 2.58
	AFGL 2062	18 02 36 ± 8	-21 13.4 ± 2.1	

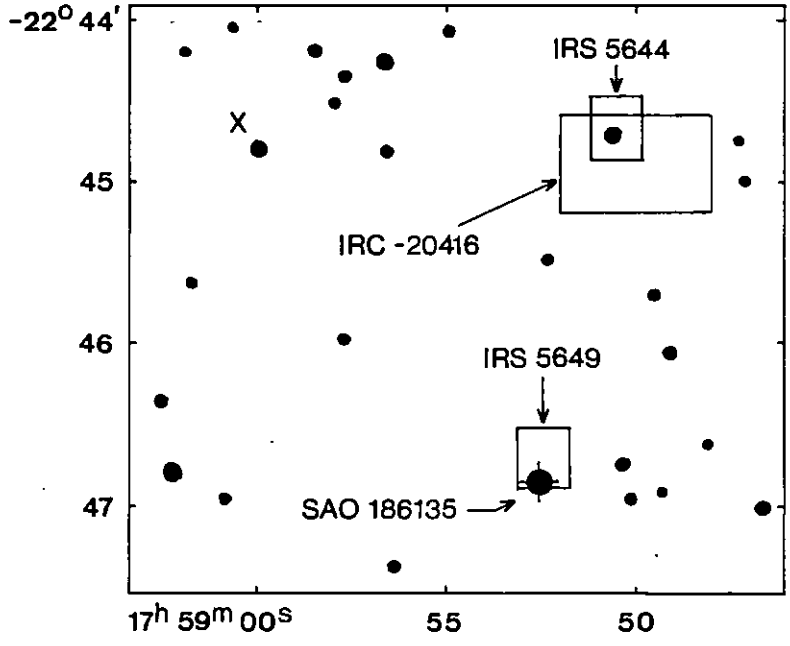

Figure 4.9 - Identification of IRC -20416

This chart is adapted from the AAT poster of the Trifid Nebula. Star X is as bright as the IRC star on I plates, and is likely to be an equally strong 2.2 μm source.

4.7.3 IRC -20416

Curiously, the IRC identifies this source with GC 24526 (SAO 186135), a type BO star of V = 5.73 even though the star is >2' from the infrared source and far outside the error box (see Figure 4.9).

I believe this identification is incorrect. Another bright source (our IRS 5649) lies close to the position of this star, with H = 6.1, K = 6.0. This does seem to be the star, even though V-K = -0.3 ±0.2, rather more than the -0.9 expected for a BO star (Johnson 1966). There is certainly no other candidate.

But there is no doubt about IRC -20416. Our IRS 5644 (K = 2.5) must be the same object, since the position and magnitude agree closely. Moreover, IRS 5644 coincides with a star of B ∿ 16 and R ∿ 13 on the POSS plates, which is much brighter on I plates of the area (I have no calibration for these). A detailed comparison is in Table 4.4. I have so far been unable to deredden this source to a simple stellar spectrum.

(Readers with the AAT poster of the Trifid Nebula can see this source for themselves. The bright star at top right of the poster is SAO 186135. Just above it are two red stars; the one on the right is IRC -20416, our IRS 5644. The one on the left is equally bright on the I plate and should also be a strong 2.2 μm source, though it is just outside the survey area.)

4.7.4 IRC -20427 / AFGL 2062

These sources are linked in the AFGL catalogue but otherwise there is no identification. Both of the catalogue positions, and the entire IRC error box, are outside the present survey area. The AFGL error box partly overlaps Block 70, including 5 sources. None of these is as bright as K = 2.58, the IRC magnitude.

4.8 Have we detected the 5 kpc ring?

As we saw in Chapter 1, there is good evidence for a ring of dusty, luminous Population I sources at R ∿ 5 kpc. Type M supergiants are the most likely candidates, and will appear with K < 6; near the saturation limit of the survey (Table 1.2). Figure 4.1 hints at a

change of slope in the n(m) plots near K ∿ 6.5 and H ∿ 7-7.5 with a surplus of bright objects. Can these be the 5 kpc supergiants?

Okuda (1981) says that the required density of type M supergiants in the ring is 3×10^{-5} pc^{-3}. If the width of the ring is 300 pc (Section 1.2.2) then there should be about 12 of these stars in our survey catalogue. In fact, there are 24 sources for which K < 6.5, which is at least consistent with the supergiant hypothesis.*

We need more information about these sources, in particular multiband photometry. However, we can make some progress by noting that there is only one SAO star in the area covered, and that has been identified with one of these bright sources (Section 4.7.3). Therefore, since the SAO catalogue lists stars to V ≃ 9.5, the remaining 23 sources with K < 6.5 must have V-K > 3.0, or more likely, V-K > 3.5. This constraint rules out two possibilities:

(1) The bright sources cannot be unreddened foreground objects. If they were, they would have to be late K or M stars. Of these, main sequence dwarfs would be too faint, and giants too far away to be unreddened. (1-2 kpc).

(2) They cannot be reddened, early-type stars, (with intrinsic V-K < 0). The observed V-K would put them further than 2 kpc, whereas their apparent magnitudes would require them to be much closer.

Only giants and supergiants remain plausible candidates. If giants, they are within 2 kpc and cannot be associated with the 5 kpc ring. Giants in the ring would have K ∿ 9, but there is no sign of a discontinuity in n(K) in Figures 4.1 or 4.2. If supergiants, they can certainly be at 5 kpc. Type Ia would have K ∿ 3.5, V ∿ 16-17, and Type Ib would have K ∿ 6, V ∿ 18-21. The optical images will be faint.

In conclusion, the present observations are consistent with a population of supergiants in the 5 kpc ring, but are not conclusive. More photometry is required.

4.9 Further work on optical identifications

An obvious next move is to correlate the positions of the infrared sources with objects on photographic plates. With this intent

* Elias (1978, Astrophys. J. 223, 859) measured N(K=6·5) = 16±3 deg^{-2} in a field near ℓ = 95°, b = -5°, equivalent to about 3 stars in the present survey area.

we have obtained three V/I plate pairs from the UK Schmidt Telescope (Job T57). These plates each $6^{o} \times 6^{o}$, cover the entire survey area from $\ell = 0^{o}$ to $\ell = 10^{o}$. The plate numbers are V5890/I6378, V2187/I3229 and V5878/I6382.

In February 1981 parts of these plates were scanned with the COSMOS plate measuring machine at the Royal Observatory, Edinburgh, and the data stored on magnetic tapes (Job 427). Mercedes Prieto has undertaken to reduce these tapes at IAC. The big problem is calibration. We have found four open star clusters with suitable V sequences (NGC 6456, NGC 6531, Collinder 347 and Bochum 14), but I standards are non-existent in this area. Our experience so far is that COSMOS is not nearly as convenient to use as is commonly supposed.

4.10 Benefits of hindsight

It is clear to me that this project would have been much more productive if we had not made several errors of judgement in the early stages. Most of these failings led directly to inefficient use of telescope time.

4.10.1 The need for clear objectives

At the start of the project we had no clear aims in view, other than to detect as many stars as possible and as faint as possible. The results of the survey are relevant to the previous work outlined in Chapter 1, but this is more through luck than judgement. I think our main error was to try to do too much.

In any survey it is necessary to draw a compromise between area and depth of coverage. One either covers a small area, with high resolution and high sensitivity, or a big area with low resolution and low sensitivity. The survey would have been more valuable if we had forsaken sensitivity for area, and so avoided source confusion and concomitant loss of information. For example, if we had decided to search to K = 8, we could have covered ~ 2 deg^{2} (10 times the area achieved) and detected about the same number of sources, with negligible confusion. It is ironic that in our quest for very faint stars, the putative supergiants in the 5 kpc ring have been too bright for the magnitude range of the survey.

4.10.2 Recommendations

The following suggestions may assist observers contemplating similar projects.

(1) A small pilot survey, conducted in advance of the main project, would provide a chance to try out and refine alternative strategies.

(2) Survey blocks should be placed near to convenient guide stars which are bright enough to be usable no matter how much moonlight. We did not do this, and lost many hours trying to find faint stars that happened to be close to our blocks.

(3) Big blocks are more efficient than small blocks. The widths of our blocks were chosen to be the same as that of the guiding eyepiece, and the lengths were then fixed by the need for the total survey area to be about 1 deg^2. This was a needless restriction.

(4) An unbiased, non-selective survey, such as this one, can be of great value. But there is a good case for being more selective, and placing blocks where they are likely to yield information of special interest. Examples of such places are the tangential direction to the 5 kpc ring ($\ell = 30^\circ$), and the intriguing hump at $\ell = 355^\circ$.

(5) Drift-scanning in RA is a better way to survey an area than declination scanning. The scan speed is precise and invariable (being the sidereal rate) and so allows accurate and direct determination of equatorial coordinates. The faster speed (15 cos δ arcsec s^{-1}) would complement a larger aperture ($\sim$ 1 arcmin) and lower sensitivity.

(6) Flux calibration deserves more attention than it often gets. For a large-scale survey it would be prudent to use a few nights to set up a sequence of secondary standards in the sky close to the survey area. This way it should be possible to eliminate systematic errors due to atmospheric extinction.

(7) Data reduction could be simplified. It took over a year to process our survey data by computer. This could have been done with a ruler if we had not tried to detect sources down to the limits of the photometry system.

(8) It is not worth skimping on equipment. We lost many, good clear nights trying to repair faulty cryostats. Given eight weeks of telescope time, an investment in a purpose-built cryostat, designed for reliability and ease of maintenance, would have been cheap at the price.

(9) Much time can be saved by using a photometer with two or more parallel channels to simultaneously measure sources in several bands.

(10) The 1.5 m telescope is ideal for survey work, but would be greatly enhanced by a moderately accurate pointing system (say to within an arcminute). Although it has been operating for ten years, this telescope has yet to realise its full potential in advancing infrared astronomy.

4.11 Conclusions

In this Chapter I have reviewed the principal results to emerge from the survey. First, there are four conclusions about the survey itself:

(1) It is complete to H = 10.5 and K = 9.5. This is equivalent to detecting M giants at 6–7 kpc.

(2) The limiting factor is source confusion rather than sensitivity or noise.

(3) Survey catalogues contain about 800 sources brighter than these limits in 0.18 deg^2.

(4) Block 1 is probably wrongly calibrated.

Regarding the two objectives set in Chapter 1:

(5) The integrated surface brightness of the 2.2 μm survey sources is 40–50% of the 2.4 μm disk brightness measured from balloons. The bulge has not been detected.

(6) Our observations are consistent with the presence of supergiants in the 5 kpc ring, but are not conclusive.

There are three more conclusions of astrophysical interest:

(7) There is evidence for a population of highly reddened objects, which are probably supergiants within 0.4° (70 pc) of the

galactic centre. Their number density is $\sim$ 1000 deg^{-2}.

(8) Otherwise, the distributions of survey sources do not depend strongly on longitude.

(9) The optical counterpart to IRC -20416 is not SAO 186135, as published in the Infrared Catalogue, but a faint red star 2' to the north.

CHAPTER 5

INFRARED BURSTS FROM THE X-RAY RAPID BURSTER

The Rapid Burster MXB1730-335, is one of about 30 X-ray burst sources clustered around the central bulge of the Galaxy, and is unique in producing $\sim 10^3$ Type II bursts a day in its active state, as well as the more usual Type I bursts. It is seated in the core of the globular cluster Liller 1 and is probably a neutron star in a close binary system. In 1979, bright infrared bursts were detected at Kavalur and Tenerife, but it is not clear if they are connected with the X-ray bursts. They are notable for their great brightness ($K \sim 6$), accompanying flashes, and improbable brightness temperatures (10^{10} to 10^{18} K). Present models of the Rapid Burster do not predict observable infrared emission. A concerted international campaign failed to detect any further X-ray or infrared activity from the Rapid Burster during 1980, but identified several phenomena which could be mistaken for infrared bursts.

5.1 Characteristics of X-ray bursters

Sources emitting bursts of X-rays were discovered around 1975 using the new generation of X-ray astronomy satellites (e.g. SAS 3, OSO 8, Ariel 5 and ANS). Most of the work on these sources has been done by Walter Lewin's group at MIT, and he has written at least five reviews in the last few years (Lewin and Joss 1981, Lewin 1980, Lewin 1979, Lewin and Joss 1977, and Lewin 1977). The information in this section is largely compiled from these reviews.

First, what is an X-ray burster? Lewin and Joss (1977) propose the following operational definition:

1. Bursts have rise times of less than a few seconds.
2. Their durations vary from a few seconds to a few minutes.
3. They are seen to recur from the same source.

This is a list of the more important characteristics of the X-ray bursters:

1. There are about 30 known burst sources. About 20 of these conform with the operational definition of a burster (the others fail on the third point).

2. The sources are concentrated towards the galactic equator, and most of them lie within 30° of the galactic centre. This suggests they belong to the bulge population and have a mean distance of 10 kpc.

3. At least 5 of the bursters have been identified with globular clusters. This is significantly more than would be expected if the bursters were randomly distributed, though there now seems to be no general association between bursters and globular clusters as was once suspected. Another 5 sources correspond to faint blue stars ($m_v \sim 18$).

4. A typical burst rises from the background in < 1s and lasts from several seconds to minutes. In general, each source produces a characteristic shape of burst.

5. The peak X-ray flux received at the Earth is $\sim 10^{-11}$ to 10^{-12} W m^{-2}, corresponding to a luminosity of 10^{31} to 10^{32} W at a distance of 10 kpc. The energy in each burst may vary from 10^{31} to 10^{33} J (2.5×10^{32} J is enough to disperse the Earth (AQ p.113)).

6. The burst spectra soften during decay. The best fit is a black body of peak temperature $\simeq 3 \times 10^{7}$ K and radius ~ 10 km.

7. Bursts recur at approximately regular intervals of 10^{4} to 10^{5} s (Joss 1977). Recurrence intervals often change over a few days.

8. Most sources have periods when they do not burst at all, though no definite periodicities have been detected.

9. At least 8 sources are known to emit a persistent X-ray flux as well as bursts.

10. Faint optical bursts ($m_v \sim 17$) have been detected from at least 3 sources coincidentally with X-ray bursts. There is evidence that the optical bursts are delayed 2-3 s with respect to the X-ray ones (McClintock et al. 1979, Pedersen et al., IAUC 3399).

5.2 The Rapid Burster

The Rapid Burster was discovered by Lewin et al. (1976) and designated MXB1730-335 (MXB stands for "MIT X-ray Burster"). It is unique in producing bursts at intervals of a few seconds, rather than hours. These are some of its properties:

1. Unlike other bursters, MXB1730-335 can produce up to 4000 bursts a day (Hoffman et al. 1978). Hence the name "Rapid Burster".

2. It is active for 2 to 6 weeks every six months or so.

3. The bursts do not soften during decay. They are best fitted a black body spectrum of temperature $\simeq 2 \times 10^7$ K and inferred radius $\sim$ 15 km (Marshall et al. 1979).

4. Energies are in the range 10^{31} to 10^{33} J, and seem to be related to the intervals between the bursts. Except for the very small and very big bursts, the energy in a given burst is proportional to the interval to the next one (Lewin et al. 1976). This is known as the E-Δt relationship.

5. Ulmer et al. (1977) reported the discovery of "anomalous" bursts that violate the E-Δt relation. They tend to have longer rise times ($\sim$ 3 s) and lower peak intensities ($\sim$ 30%) than the normal bursts. Lewin suspects they are "hiccups" in the accretion flow (1980 personal communication; see Section 5.4.2).

In 1978 Hoffmann et al. showed that the Rapid Burster also produces bursts similar to those of normal burst sources. What is more, the two kinds of burst seem to be produced independently of each other, with the "special" (i.e. normal) bursts not disturbing the E-Δt relationship of the rapid ones. This led to a classification of all bursts into two types: Type I for the normal bursts and Type II for the rapid ones. Table 5.1 contrasts the two types, and there are examples in Figure 5.4c.

Table 5.1 - Comparison of Type I and Type II X-ray Bursts

Characteristic	Type I	Type II
Rise time (s)	1 (smooth)	1 (50 ms structure)
Decay time (s)	3 - 30	1 - 30
Intervals	Hours or days (perhaps more)	Seconds or minutes
Spectral behaviour	Softening during decay	No softening
Peak luminosity (W)	$\sim 10^{31}$	$\sim 10^{31}$
Energy (J)	$\sim 10^{32}$	$10^{31} - 10^{33}$
Best fit spectrum	Black body	Black body
T_{max} (K)	3×10^7 cooling	2×10^7 constant
R (km)	10 constant	15 decreasing
Energy source	Nuclear (helium flash)	Gravitational (accretion)

Adapted from Lewin (1979) and Lewin and Joss (1981).

5.3 Optical identification - Liller 1

We now know that the Rapid Burster is seated in a highly reddened globular cluster about 10 kpc away. Liller (1977) searched for an optical counterpart to the burster on a set of plates taken with the 4 m Cerro Tololo telescope. On the R and I plates he found a faint smudge with integrated magnitudes $m_R \simeq 21$ and $m_I \simeq 19$, and suggested it was a globular cluster. Kleinmann et al. (1977) confirmed this by observations in the 1-5 μm infrared bands. They found it to be considerably extended (> 1 arcmin diameter) and the relationship between beam diameter and total flux was consistent with that of a highly condensed globular cluster. They derived a core diameter of 13" and a visual extinction $A_V = 11 \pm 1$ mag. In

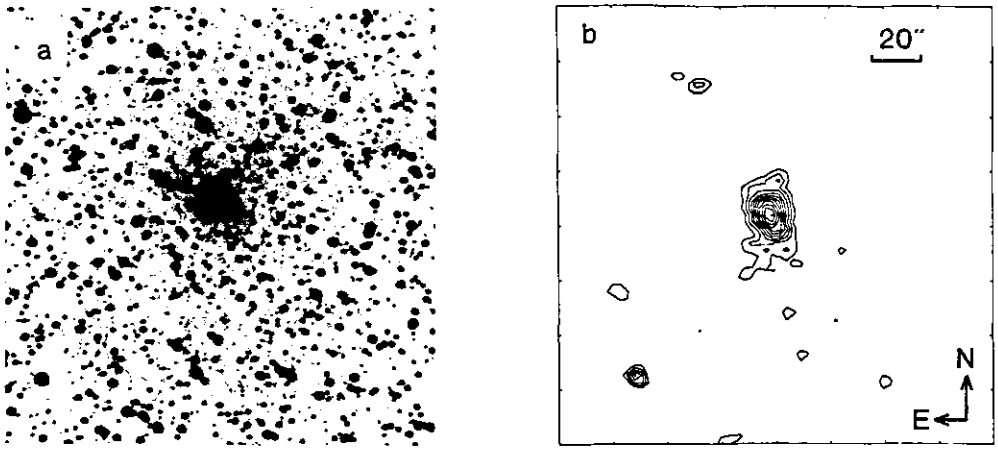

Figure 5.1 - The globular cluster Liller 1

a Photograph taken at 0.83 μm.

b Map of the same area made at 2.2 μm with a 6.5" beam.

(Adapted from Malkan et al. 1980)

the hour they spent watching the source there were no flux variations greater than 10%.

Malkan et al. (1980) mapped the cluster, now called Liller 1, at 2.2 μm with a 6.5" beam. Their map is shown in Figure 5.1 together with a 0.83 μm photograph of the same area. From JHK photometry they estimated the visual extinction to be A_V = 10.3 mag (assuming metal-poor stars), or 8.6 mag (metal-rich). Recently, Malkan has confirmed that the stars of Liller 1 are metal-rich with A_V = 9-10 mag. High metallicity appears to be a property of all globular clusters containing X-ray bursters (personal communication, 1982).

A finding chart for Liller 1 is presented in Figure 5.2.

5.4 Theoretical models

There is now good evidence that X-ray burst sources contain either a neutron star or a black hole of a few solar masses. This conclusion hinges entirely on the observation that bursts (both types) have black body spectra consistent with an emitting radius of about 10 km (see Section 5.1). Van Paradijs (1978) has proposed that the Type I bursts can be considered as "standard candles" at maximum

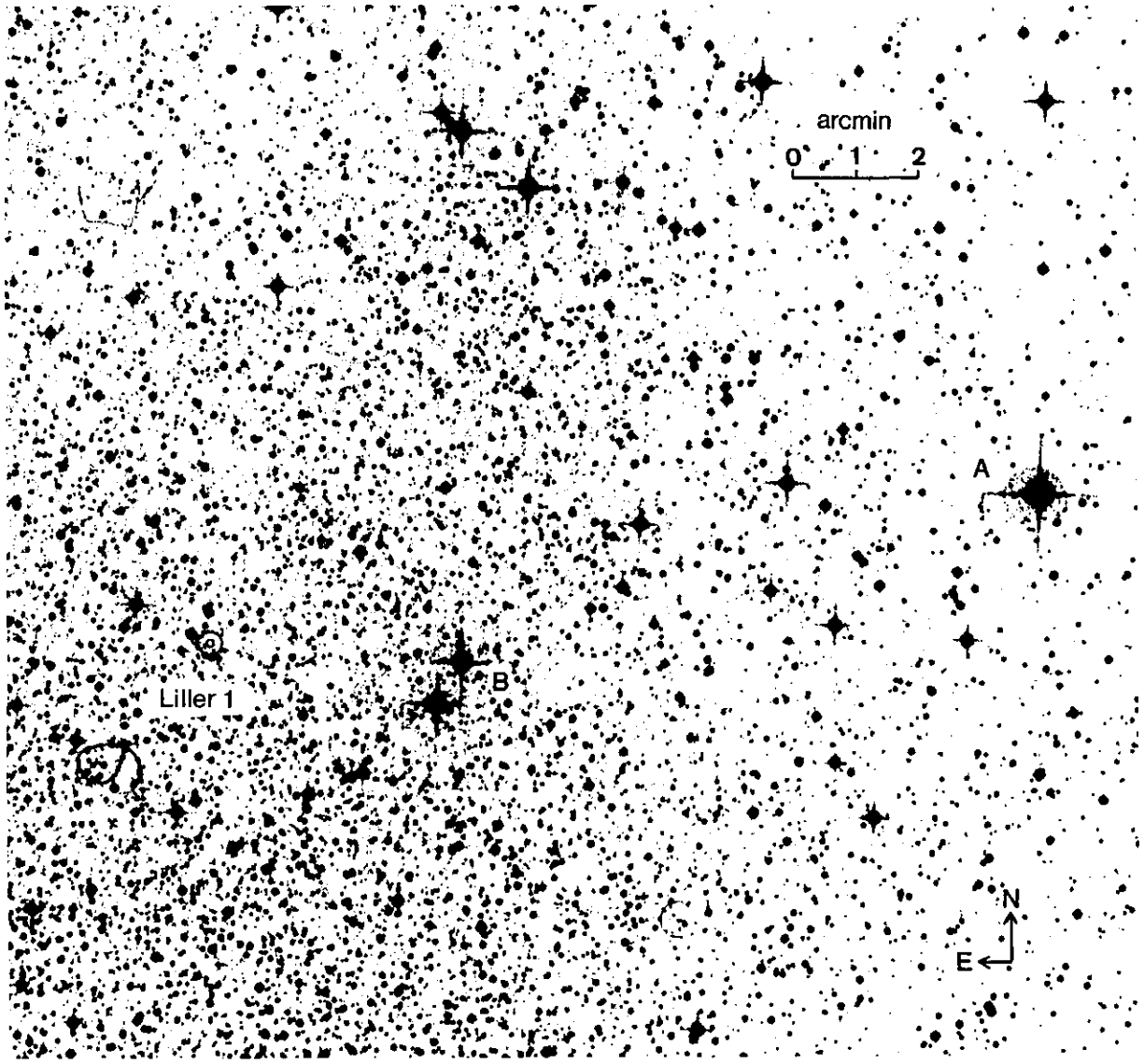

Figure 5.2 - Finding chart for Liller 1

This 18 × 17' IIIa-J print is from field 393 of the SERC Southern Sky Survey. Liller 1, which is obscured at visible wavelengths, is marked by the double circle near centre left. Its position is (1950):

Liller 1 RA $17^h\ 30^m\ 07^s.0 \pm 0.1$

Dec $-33^\circ\ 21'\ 17'' \pm 1$

(ref. Liller 1977). For telescopes without accurate setting (such as the 1.5 m IRFC), the safest procedure is to locate star A, SAO 208933, V = 9.6, and then offset to the pair B.

Star A RA $17^h\ 29^m\ 03^s.3$

Dec $-33^\circ\ 18'\ 16''$

Then with the northern star of the pair in the aperture, offset in RA until the infrared source appears. It is bright ($K \sim 6$), extended ($> 1'$) and difficult to miss. The conspicuous parallelogram to the NE confirms the identification of Liller 1.

luminosity, corresponding to the Eddington limit of 1.8×10^{31} W for 1.4 solar masses. Assuming this luminosity, he derived the distances and radii of 10 bursters, and showed that the radii were all about 6.5 ± 1.3 km. In Lewin's words (1979): "The conclusion that burst sources are neutron stars (or perhaps black holes of a few solar masses) becomes almost inescapable".

All the major theories take as their starting point the existence of a neutron star, or black hole, in a close binary system. It should be said, though, that there is no evidence at all for a binary system. No-one has observed periodicities or eclipses in the X-ray emission from any burster (Cominsky et al. 1980).

There are two main models - the thermonuclear flash model and the accretion instability model.

5.4.1 Thermonuclear flash

Paul Joss of MIT has championed the cause of thermonuclear flashes on the surface of a neutron star as a source of X-ray bursts (e.g. Joss, 1979). He has produced numerical models which reproduce many of the features of X-ray bursts, including luminosity, energy, rise and decay times, recurrence time, black-body spectrum and spectral evolution

The neutron star is in a close binary system and accretes matter from its companion star. Stellar material (mainly hydrogen and helium) splashes on to the surface of the neutron star in a steady stream producing a "steady" X-ray flux. As the accreted layer builds up, hydrogen is transmuted to helium, though not fast enough to start a thermonuclear runaway. However, as the pressure and temperature rise, helium fusion begins and leads to a thermonuclear flash on a time scale < 1 s. The gamma radiation released is thermalised as it pushes its way to the surface of the accreted layer.

5.4.2 Accretion instability

As soon as the E-Δt relationship for Type II bursts became clear, a plausible explanation suggested itself. In their paper announcing the discovery of MXB 1730-335 (Lewin et al. 1976) the MIT group proposed that the bursts were caused by instabilities in the

accretion flow on to a magnetised neutron star. This was not a new model; F.K. Lamb had done some early work on it as a possible model for other burst phenomena (personal communication, cited in Lewin et al. 1976).

Once again, a neutron star is in a close binary system, accreting material from a stellar companion (the published models, e.g. Lamb et al. (1977) assume radial accretion). When it encounters the magnetosphere, the infalling matter is decelerated and builds up in a reservoir behind a shock front. It piles up until the magnetosphere can no longer support it, and the reservoir springs a leak (Rayleigh-Taylor instability), releasing a blob of material which splashes on to the neutron star in a burst of thermal X-rays. Continuedinflow fills up the reservoir once again, and the process repeats itself. This has been described as a "relaxation oscillator" model (Lewin et al. 1976). However, the physics is complex and no-one has yet produced a satisfactory numerical model.

With the realisation that there were two types of burst, both these theories could be accommodated. The present consensus is that Type I bursts are thermonuclear flashes and Type II bursts are the result of accretion instabilities. So far, only the Rapid Burster is known to produce both types, so presumably both mechanisms are operating there. Neither predicts an observable infrared flux.

5.5 The discovery of infrared bursts

On April 4 1979, P.V. Kulkarni and N.M. Ashok of the Physical Research Laboratory (PRL), Ahmedabad, discovered infrared bursts from the Rapid Burster. In $2\frac{1}{2}$ hours they detected six bright bursts at 1.6 μm using the 1.0 m telescope at Kavalur. This was a result of theoretical speculations by K.M.V. Apparao and S.M. Chitre at the Tata Institute of Fundamental Research (TIFR), Bombay. Kulkarni's discovery was reported in the IAU Circulars (IAUC 3344) and a full account appeared in Nature (Kulkarni et al. 1979). No X-ray astronomy satellite was observing MXB1730-335 at the time (although it was believed to be active) so we do not know if the infrared bursts corresponded to X-ray ones.

5.6 Detection of infrared bursts at Tenerife

The next period of X-ray activity began earlier than expected,

on August 8, 1979, when the X-ray satellite Hakucho detected a train of Type II bursts from the region of MXB1730-335 (IAUC 3392). Kulkarni's group was not able to observe the burster again because of monsoon weather at Kavalur.

At my request, Mattias Mountain, Carlos Sánchez and Mercedes Prieto monitored the Rapid Burster with the 1.5 m Tenerife telescope on September 5. Fifteen minutes into the observation they detected two bright bursts at 2.2 μm. When, about an hour later, the burster became too low to follow, the observers calibrated their signals on φ Ophiuchi, and performed several tests to ensure that the burst signals were not caused by a radiation leak in the photometer or by transients on the electrical supply.

Further monitoring, on the nights of September 6, 11 and 12, failed to reveal any more bursts. Table 5.2a gives details of the observing times. The only operational X-ray satellites were Einstein, Hakucho, Ariel 5 and Ariel 6, but none of these was observing the Rapid Burster at the time (personal communications).

These infrared bursts were reported in Nature in February 1980 (Jones et al. 1980). Chapter 6 contains a critical assessment of these and other observations.

5.6.1 The observations

The photometry system was that described in Chapter 2 (details in Table 5.2b). Observations were recorded on the chart recorder, and also on the printer, as digitised samples at 1 s intervals. Figure 5.3a shows a photograph of the original chart trace, and Figure 5.3b shows the corresponding digitised record.

5.6.2 Calibration

Before useful information can be gleaned from these detections, the observations must be calibrated. All measurements for these calibrations were made from a 3.4X photographic enlargement of the chart trace. Two calibrations are required: time and flux.

Unfortunately, the observers did not record time pulses in parallel with the signal. Instead they set the dome clock to within 0.5 s of UT by means of BBC Greenwich time signals, and occasionally

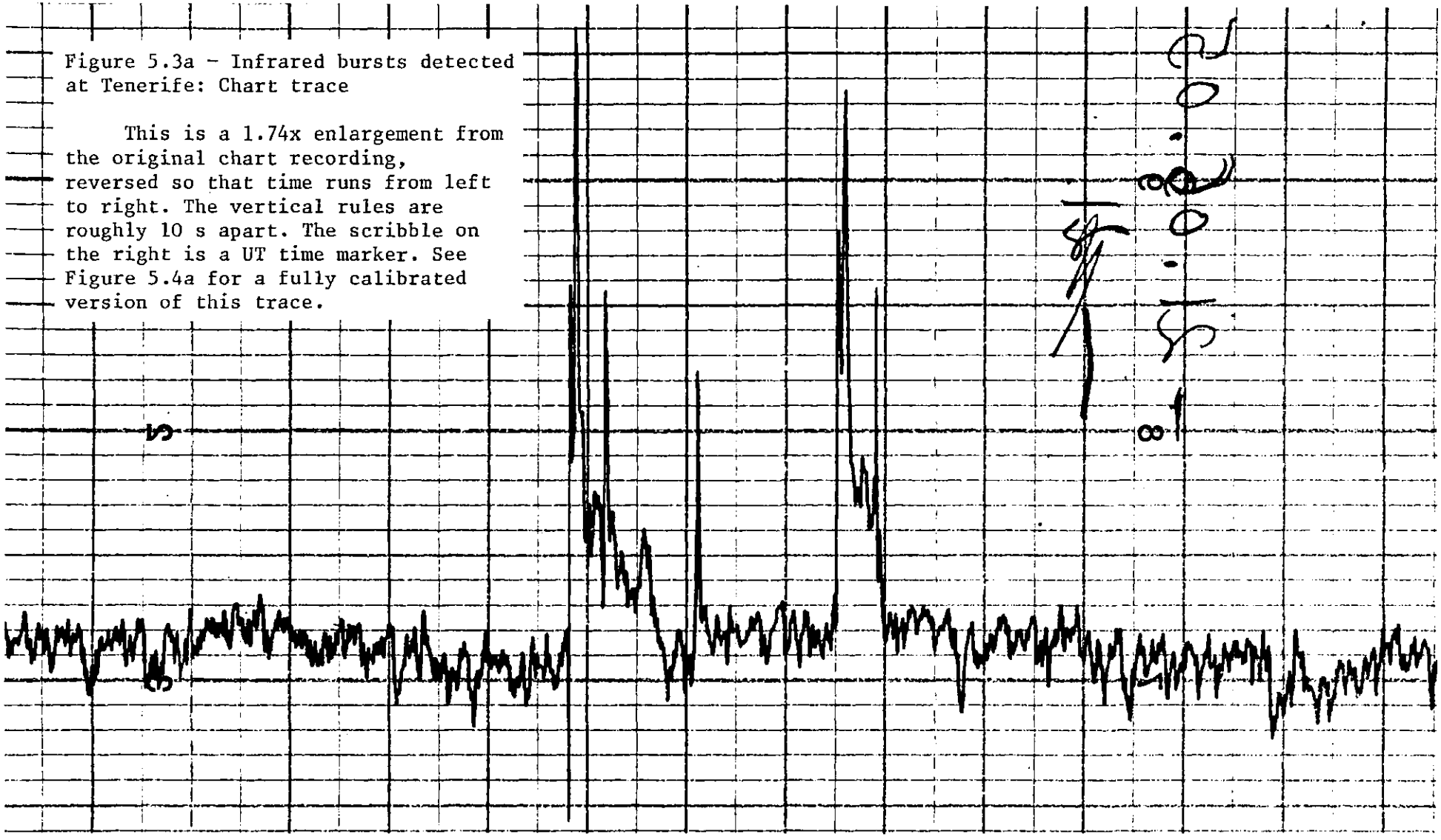

Figure 5.3a – Infrared bursts detected at Tenerife: Chart trace

This is a 1.74x enlargement from the original chart recording, reversed so that time runs from left to right. The vertical rules are roughly 10 s apart. The scribble on the right is a UT time marker. See Figure 5.4a for a fully calibrated version of this trace.

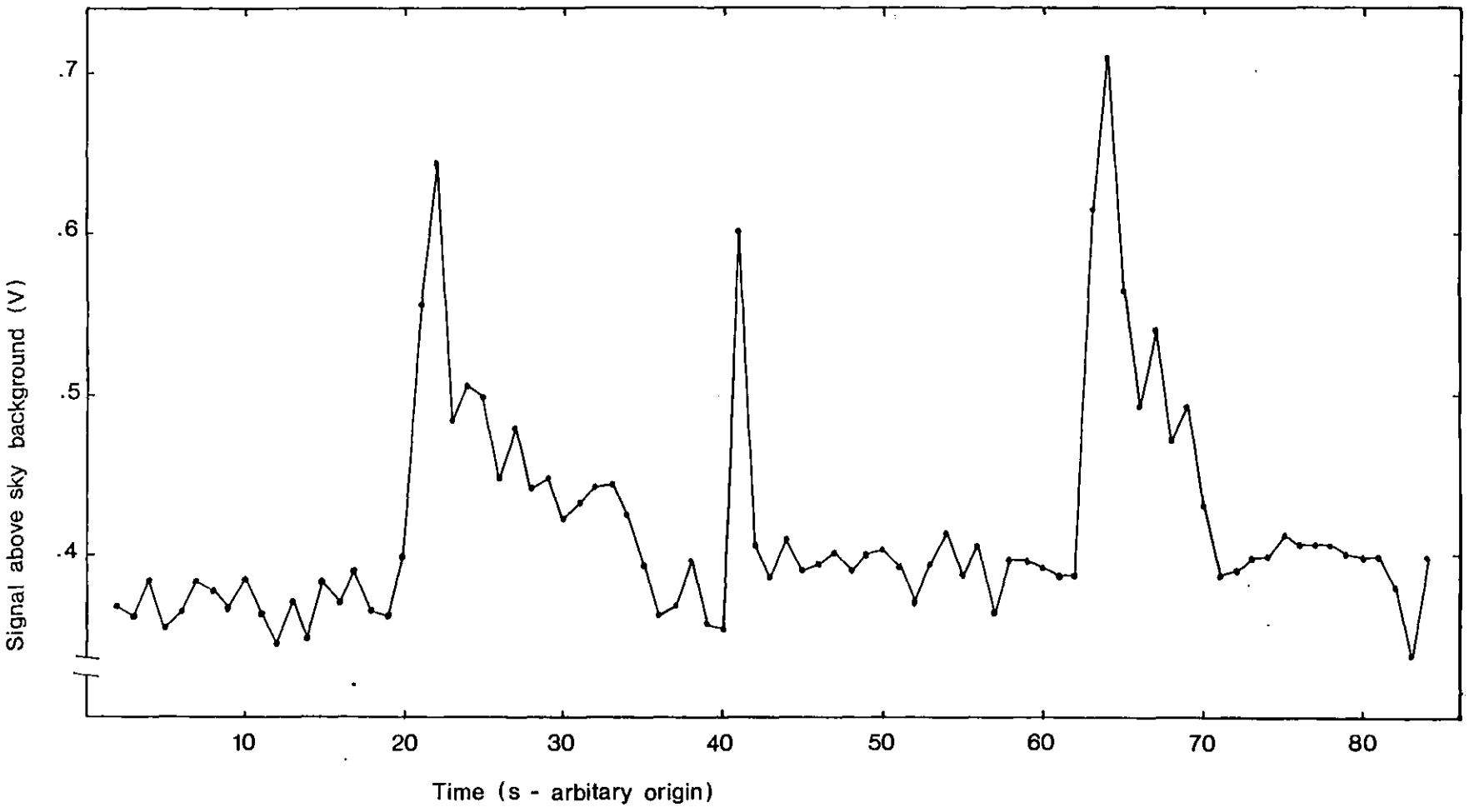

Figure 5.3b – Infrared bursts detected at Tenerife: Digitised recording

This plot shows the signal voltage at approximately 1 s intervals throughout the burst activity. Note that although the very brief flash between the bursts has been caught, the two initial flashes in each burst have not been resolved (see Figure 5.3a).

Table 5.2 - Infrared Observations of the Rapid Burster in September 1979

5.2a - Observing times

Date (Sep. 1979)	Start (UT)	Finish (UT)	Duration (min)	Bursts
5	20.50	22.09	79	2
6	20.22	22.05	103	0
11	21.09	21.45	36	0
12	20.05	21.40	95	0

Total observing time = 313 min = 5 h 13 min.

5.2b - Auxiliary data

Cryostat: Oxford Instruments (OI)
Aperture 20 arcsec
Filter: $\lambda = 2.2\ \mu m$, $\Delta\lambda = 0.4\ \mu m$

Chopper:
Throw 20 arcsec (reference beam to north)
Frequency 20 Hz

Calibration star: ϕ Ophiuchi
K = 2.27
$F_\lambda = 4.8 \times 10^{-11}$ W m^{-2} μm^{-1}

marked the time on the chart paper. The time scale on the chart was 2 s mm^{-1}, and 0.6 s mm^{-1} on the working print. Absolute timings should be accurate to better than 2 s (see Table 5.3).

Flux calibration is derived from the measurement of ϕ Oph (m_K = 2.27, see Table 2.1) and Johnson's (1966) absolute flux of 3.9×10^{-10} W m^{-2} μm^{-1} for m_K = 0.0. A correction is included for the difference in air mass between the two observations (2.33 for the bursts, 2.85 for ϕ Oph). There was no measure of the atmospheric extinction on that night, so I assumed a typical K extinction of 0.1 mag am^{-1} or 0.05 mag between ϕ Oph and the burster.

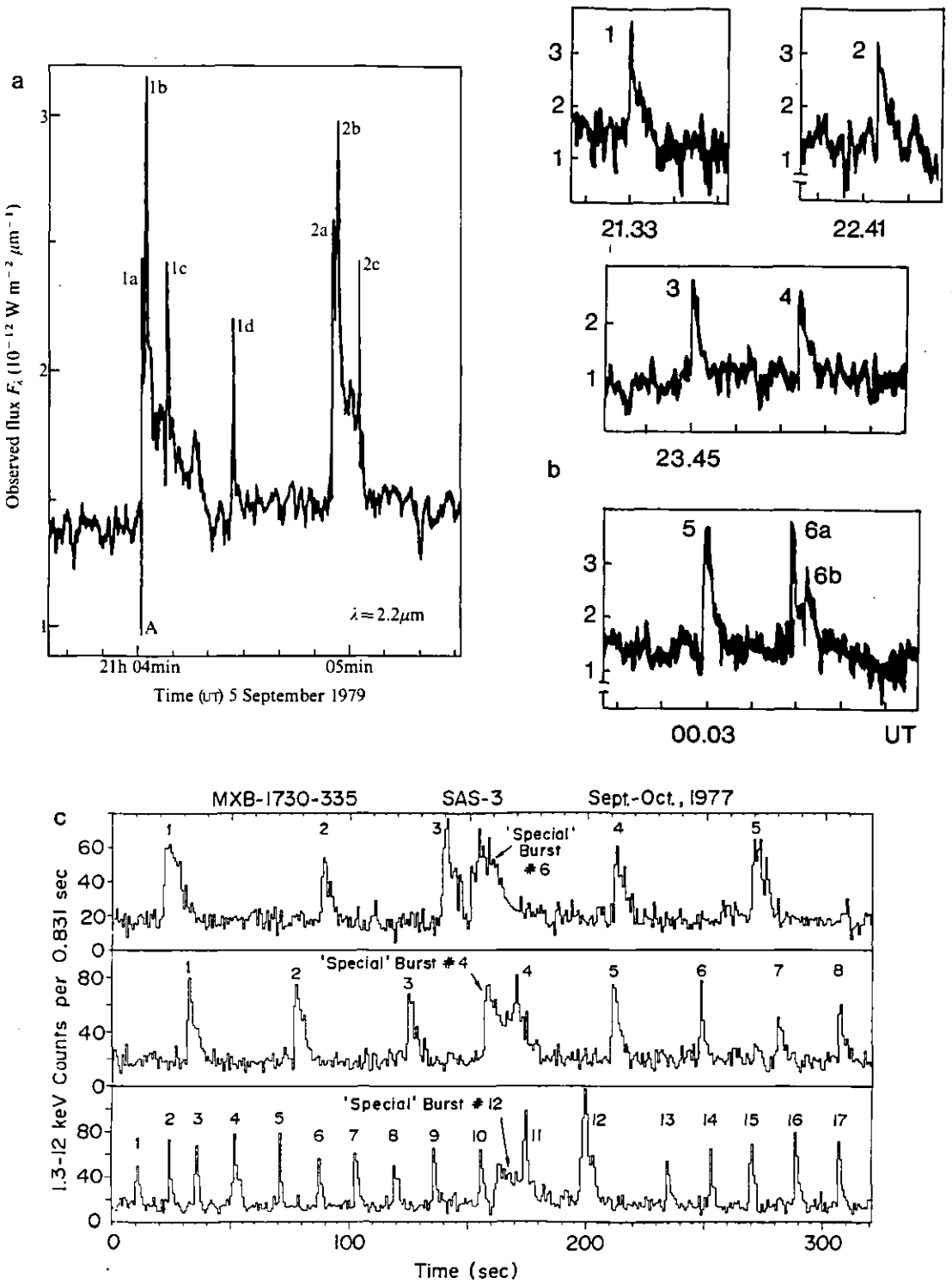

Figure 5.4 - Comparison of infrared and X-ray bursts from Liller 1

a Tenerife infrared bursts, detected at 2.2 μm, September 5 1979 (from Jones et al. 1980).

b Kavalur infrared bursts, detected at 1.6 μm, April 4/5 1979. Time intervals are minutes, flux units are as Figure 5.4a (adapted from Kulkarni et al. 1979).

c Trains of Type II X-ray bursts with examples of the less frequent Type I ('special') bursts (from Lewin and Joss 1981).

Figure 5.4a shows a fully calibrated diagram of the two bursts. The flux scale is probably accurate to about 10%.

5.7 Properties of the bursts

5.7.1 Luminosity and energy

According to Kleinmann et al. (1976; see Section 5.3) the interstellar extinction towards Liller 1 is 1.1 mag at 2.2 μm, or a factor of 2.75. Let this factor be f_e. Then, if the observed burst flux is F_λ W m^{-2} μm^{-1}, the luminosity, assumed isotropic, is given by:

$$L_{IR} = f_e \, 4\pi d^2 \, F_\lambda \Delta\lambda \quad \text{Watts in bandwidth } \Delta\lambda \qquad (5.1)$$

where d is the distance to the source (10 kpc = 3×10^{20} m).

The total energy in each burst is obtained by integrating L_{IR} with respect to time (in practice, by tracing the burst profiles on to millimetre graph paper and counting the squares).

Values of the energies ($\sim 10^{31}$ J) and luminosities ($\sim 10^{30}$ W) are listed in Table 5.3.

5.7.2 Flashes

The most remarkable feature of these bursts is the seven spikes accompanying them. Each burst begins with a sharp peak, another spike follows a second or so later, and there is another in the tail 6 s after that. The seventh spike comes in the interval between the bursts. This close association with the structure of the bursts is convincing evidence that they have a common origin. If the bursts come from the Rapid Burster then so do the spikes, and they can properly be described as "flashes".

A first glance at Figure 5.4a is enough to see that there is a pattern in the occurrence of the flashes. Indeed, if the first burst were cut off after flash 1c, the two bursts would be nearly identical. This pattern is borne out by careful measurements of the time of each flash (see Table 5.4).

I have also measured the half-peak width of each flash, but in at least two cases (flashes 1d and 2c) these durations are close to the

Table 5.3 - Observed and Inferred Properties of the Infrared Bursts

Burst	UT of onset (h m s)	Duration (s)	Energy (10^{30} J)	L_{max} (10^{30} W)	L_{mean} (10^{30} W)
1	21 04 01	20	9.1	2.2	0.45
2	21 04 55	10	6.4	1.9	0.64

Energies and luminosities are in a bandwidth of 0.4 μm and assume a distance of 10 kpc, isotropic radiation, and a 2.2 μm extinction of 1.1 magnitudes.

Table 5.4 - Observed and Inferred Properties of the Infrared Flashes

Flash	Time of peak (s)	Half-peak width (s)	Observed peak flux (10^{-12} W m^{-2} μm^{-1})	Peak luminosity (10^{30} W)	Energy (10^{30} J)
1a	0.0	0.5	1.03	1.3	0.6
1b	1.2	0.9	1.73	2.2	1.9
1c	7.0	0.8	1.01	1.3	1.0
1d	25.7	0.3	0.79	1.0	0.3
2a	54.2	0.6	1.10	1.4	0.8
2b	55.6	1.5	1.51	1.9	2.8
2c	61.7	0.2	0.94	1.2	0.2

See notes to Table 5.3

time constant (0.3 s) of the output filter on our PSD. Their actual half-peak widths may well be smaller than this. We should also note the feature at A in Figure 5.4a, which is the characteristic response of a PSD to a sharply rising signal i.e. when the signal changes appreciably in a time comparable to the chop period (0.05 s). We reproduced this with a laboratory PSD.

5.7.3 Brightness temperature

If we see transient events from astrophysical sources with a time scale Δt, we can reasonably assume that the emitting region has a radius $R < c\Delta t$. Using $\Delta t = 0.3$ s, from the flashes, gives $R < 10^8$ m (the radius of the sun is 7×10^8 m).

We can now say something about the temperature of the emitting region. The brightness temperature of a source is the temperature of a black body subtending the same solid angle as the source and producing the same observed F_λ. On the Rayleigh-Jeans tail of a black body ($T > 10^4$ K at 2 μm) it is given by:

$$T_B = \frac{F_\lambda}{2\pi kc} \lambda^4 \alpha^{-2} \qquad (\alpha = \text{angular semi-diameter})$$

$$= \frac{F_\lambda}{2\pi kc} \lambda^4 \left(\frac{d}{R}\right)^2 \qquad (R = \text{radius of source}) \qquad (5.2)$$

Putting $R = 10^8$ m gives $T_B = 4 \times 10^{10}$ K. This value of R is a lower limit set only by the time resolution of our PSD, so T_B must be at least 4×10^{10} K and probably more. We know that the X-ray bursts come from a region of $R \simeq 10$ km (neutron star size, see Section 5.2). If the infrared bursts come from the same place then T_B rises to 4×10^{18} K. Whatever the true size of the infrared emitting region, its brightness temperature lies in the range 10^{10} to 10^{18} K, compared with the 2×10^7 K of the X-rays (Marshall et al. 1979).

This is very hot. In fact, a 10 km object at 10^{12} K would already be 10^2 times as luminous as all the stars in the universe put together (assuming 10^{11} galaxies of 10^{11} suns each). Clearly, the source cannot be a black body or any kind of thermal emitter.

5.7.4 Comparison with X-ray bursts

It is not possible to compare the infrared bursts directly with X-ray bursts, because there were no simultaneous X-ray observations. But by comparing the energies in Tables 5.1 and 5.3 we can see that

$$10^{-2} < E_{IR}/E_X < 1 \qquad (5.3)$$

The infrared energy is a considerable fraction of the X-ray energy, yet the improbably high brightness temperatures imply that these infrared bursts are not merely the tails of the X-ray ones. Another way of looking at this is to ask what infrared emission we would expect from the X-ray bursts. We know they have black body spectra with $T = 2 \times 10^7$ K and R = 10 km. The predicted 2.2 μm flux is then

$$F_\lambda = \frac{2\pi ckT}{\lambda^4} \left(\frac{R}{d}\right)^2 \sim 10^{-23} \text{ W m}^{-2} \text{ μm}^{-1} \qquad (5.4)$$

This is a factor of 10^{11} below the observed values and undetectable.

5.7.5 Comparison with the Kavalur bursts

How do the Tenerife bursts compare with those detected by Kulkarni et al at Kavalur? We must bear in mind that the two sets of observations are not directly comparable:

(a) Kulkarni was working in the H band (1.6 μm) whereas the Tenerife bursts were detected at K (2.2 μm).

(b) The S/N ratio of the Tenerife bursts is some 2-3 times that of the Kavalur events, as is plain from Figure 5.4.

(c) Kulkarni used a 0.6 s smoothing time constant compared with 0.3 son Tenerife.

On the other hand, both detections were made with similar equipment: InSb detectors, a 20" aperture and a focal-plane chopper of 20" throw working at 20 Hz.

In Figure 5.4 I show the Kavalur bursts with the Tenerife ones for comparison, and in Table 5.5 I have collected the important characteristics of both detections. The following points emerge:

(a) The energies and luminosities are of the same order of magnitude, but the Kavalur values are consistently higher than the Tenerife ones.

(b) The Kavalur bursts are also longer than the Tenerife events, but only by a factor of 3 or so, and not long enough to account for the energy differences.

(c) Kulkarni et al. report rise times of 2-3 s, whereas our bursts rose in ≈ 0.5 s (but see note to Table 5.5).

(d) The general shape of the bursts - sharp rise followed by a gradual decay over many seconds - is similar.

(e) No flashes came with the Kavalur bursts, but the question arises - would they have been recognised if they had? Kulkarni's inferior time resolution and noisy signals may have obscured any flashes, but looking at figure 5.4b I find it difficult to believe there are flashes there.

(f) Although the Tenerife observers watched for over 5 hours, they saw only two bursts and those appeared within a minute. Do bursts appear in pairs? There certainly seem to be groupings among the Kavalur bursts, obviously 6a and 6b (together with 5) and perhaps 3 and 4. But Bracewell (1965, p.307) notes that randomly occurring events often give the illusion of coming in pairs or groups. Unfortunately, we do not have enough observations of these bursts to make a significant test of randomness.

Taken together, these considerations suggest that the Kavalur and Tenerife detections are observations of the same phenomenon. The differences in mean luminosity could plausibly be attributed to a gradient in the emission spectrum, (the ratio $L_{2.2}/L_{1.6}$ is 0.60 ± 0.15 corresponding to a colour temperature in the range 2000 to 3500 K). The flashes are a puzzle.

5.8 Coordinated observations of the Rapid Burster at several wavelengths

For the past few years, Walter Lewin's group at MIT have been

Table 5.5 - Comparison of the Tenerife and Kavalur Bursts

Characteristic	Tenerife	Kavalur
Number of bursts	2	7[a]
Wavelength (μm)	2.2	1.6
Bandwidth (μm)	0.4	0.3
Rise time (s)	0.5	2-3[b]
Duration (s)	20, 10	30 ± 8
Energy (10^{31} J μm^{-1})	2.3, 1.6	6.8 ± 2.3
Peak luminosity (10^{30} W μm^{-1})	5.5	7.7
Average luminosity (10^{30} W μm^{-1})	1.1, 1.6	2.2 ± 0.4

a Although Kulkarni et al. (1979) write of 6 bursts, one of these is double and deserves to be counted as 2.

b A photocopy of the original chart trace shows the line thickness to be 0.5 mm, equivalent to 3 s. It is doubtful whether rise times much less than this could be resolved.

organising "world wide coordinated burst watches" in the hope of catching simultaneous X-ray and optical bursts. An X-ray satellite monitors a chosen source while optical astronomers keep watch from the ground. Following the discovery of infrared bursts from Liller 1, the most urgent question was whether these bursts were the infrared counterparts of X-ray events, or else something separate. The watch which had already been planned for 1980 (IAUC 3420) was therefore broadened to include infrared observers as well (IAUC 3428).

During 1980 the participating satellite was Hakucho and ground-based observers were encouraged to arrange their monitoring to coincide with the satellite's observation "windows". The IC group's main contribution was in April and May, when Carlos Martinez and myself watched the Rapid Burster for several weeks with the 50 cm telescope on Tenerife. Other observations were made by Mike Selby in Hawaii in April and by myself with the 1.5 m Tenerife telescope in August and September.

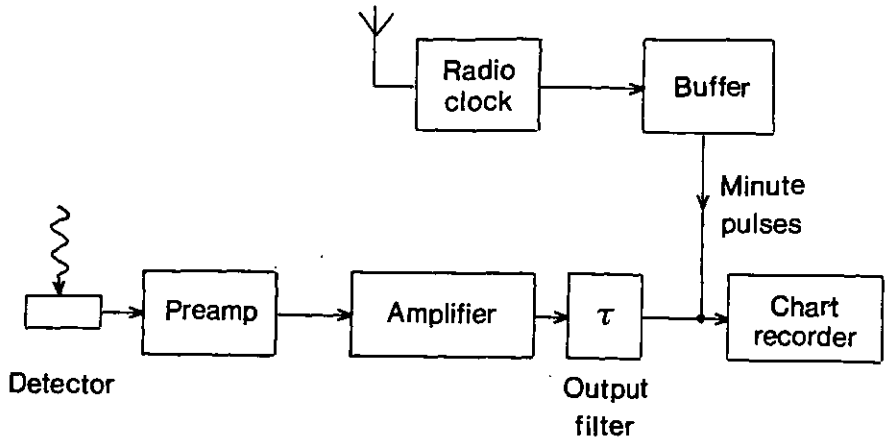

Figure 5.5 - Electronics for the IAC photometer (DC mode).

5.9 Infrared monitoring from Tenerife, Spring 1980

In April and May 1980 the only telescope available was the 50 cm reflector set up on Tenerife by the University of Mons. It is far from ideal, having no slow motions, an erratic drive, and a potential difference of 58 V (rms) between earth points on opposite sides of the dome. The photometer, designed and built at IAC, is similar to the IC photometer described in Chapter 2, and was used with the OI cryostat.

The electronics and recording equipment were very simple (see Figure 5.5), mainly because we were restricted to DC operation because of a faulty chopper. The radio clock, whose rate is stable to a few parts in 10^{11}, provided a pulse every minute which we mixed with the signal to the single-channel chart recorder. This way, events could be timed to within a second of UT.

5.10 Results of the coordinated observations

Throughout 1980 not one X-ray burst was seen to come from the Rapid Burster, and no infrared activity was reported. Hakucho was monitoring the source from April 14 to 21, and from July 14 to August 15, with occasional looks up to September 26 - a total of 324 hours. The satellite may have missed the expected spring turn-on, but there was certainly no activity in the summer up to the end of September.

Table 5.6 – 2.2 μm Observations of the Rapid Burster Made by the IC/IAC Group as Part of the MIT Burst Watch, 1980

Date (1980)	Start (UT)	End (UT)	Duration (min)	Effective[a] duration (min)	Flux limits[b] (10^{-12} W m^{-2} μm^{-1})
Hawaii: 3.8 m UKIRT, 15" aperture					
April 7	13.54	15.55	121	-	0.09
8	15.07	16.20	73	-	0.09
Tenerife: 50 cm, 25" aperture					
April 18	05.58	06.23	25	21	0.22
19	04.20	04.38	18	17	0.20
	04.46	06.16	90	81	0.20
20	04.37	06.15	98	89	0.18
21	03.37	06.13	133	122	0.22
23	03.32	04.53	81	73	0.22
	05.07	05.53	46	44	0.22
27	04.50	06.10	80	73	0.26
May 1	02.14	06.06	232	197	0.26
12	02.20	03.40	80	77	0.35
	03.40	04.20	40	37	0.23
16	02.26	03.40	74	60	0.42
	04.03	04.25	22	21	0.42
18	01.21	02.21	60	60	0.32
Tenerife: 1.5 m IRFC, 15" aperture					
Aug 22	22.05	22.43	38	32	0.16
23	21.34	22.34	60	54	0.11
29	21.12	22.34	82	74	0.06
Sep 4	21.11	22.10	59	58	0.13

Total observing time = 1512 min = 25.2 h

a Effective duration is the time that the source was in the aperture during the watch.

b Flux limit is the range of variation on either side of the mean background flux. It is the upper limit on any burst flux.

Over 180 hours of infrared monitoring were reported by observers at Mount Wilson (60 cm), Mauna Kea (3.8 m and 60 cm), Sutherland (75 cm), Siding Springs (3.9 m) as well as Tenerife. In Table 5.6 I list all the observations by the IC group, amounting to some 25 hours. The flux limits are the upper limit on the intensity of any burst emission, judged by eye and measured from the chart records. The bursts seen in September 1979 were, at worst four times these flux limits. If bursts like those had occurred, we would have detected them.

The results of the coordinated observations will be published by MIT in 1982 (A. Lawrence, personal communication).

5.11 Related infrared phenomena

We spent over 20 hours monitoring the Rapid Burster (and the sky) in April and May, and in that time detected several interesting phenomena. I mention them here not so much for their own value but in preparation for the discussion on the origin and detection of infrared bursts in Chapter 6.

5.11.1 Spurious phenomena

It has been argued that infrared bursts could not be caused by aircraft, or satellites or meteors because of the improbability of one passing through the telescope beam. In fact, an aircraft did pass through our 25" beam on April 23 at 03.40 UT (see Figure 5.6a). It produced a single sharp spike, lasting about a second, with a peak flux of 1.2×10^{-12} W m^{-2} μm^{-1}. This is close to the flux from the infrared bursts, but it is difficult to see how bursts of several tens of seconds could be produced in this way (unless the aircraft were moving almost radially with respect to the observer).

Another spurious event occurred on April 20, which was important because we did not finally reject it as spurious until August. At 06.11 UT we saw an infrared burst that happened to coincide with Carlos Martinez lighting a cigarette (see Figure 5.6b). Ordinarily we would have rejected it outright but for two things. First, we could not repeat it, and second it looked remarkably similar to our second burst seen onSeptember 5 1979 (see the detailed comparison in Table 5.7). On Tenerife again in August, I set up the 50 cm telescope just as it had been in April and succeeded in

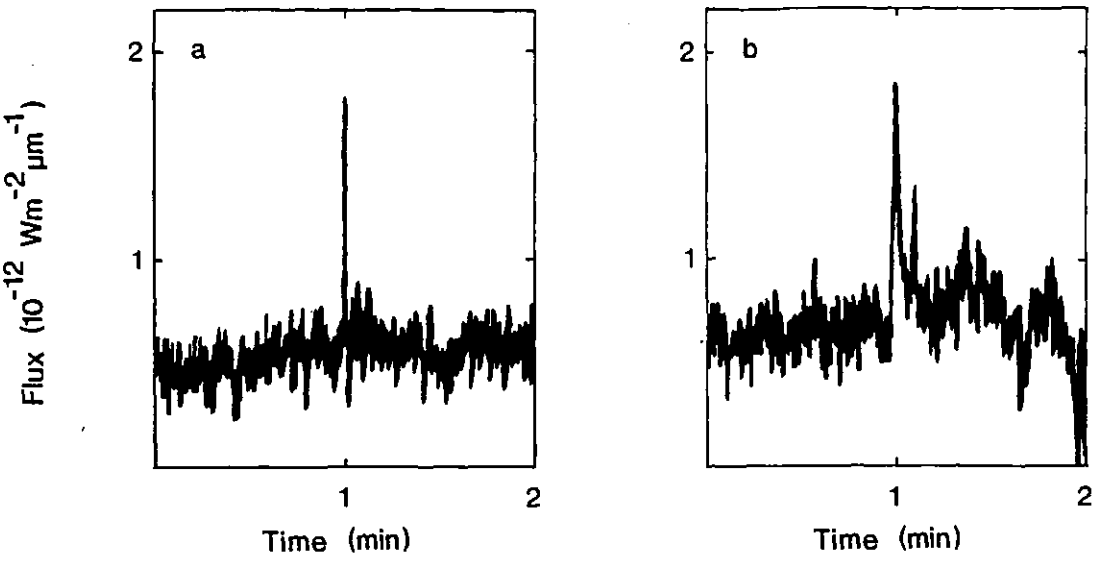

Figure 5.6 - Examples of spurious phenomena

a An aircraft passing through the 25" beam at 03.39.57 UT, April 23, 1980. The spike lasts about 1 s.

b A convincing "burst" (06.10.45 UT, April 20, 1980) which was traced to a match being struck in the dome.

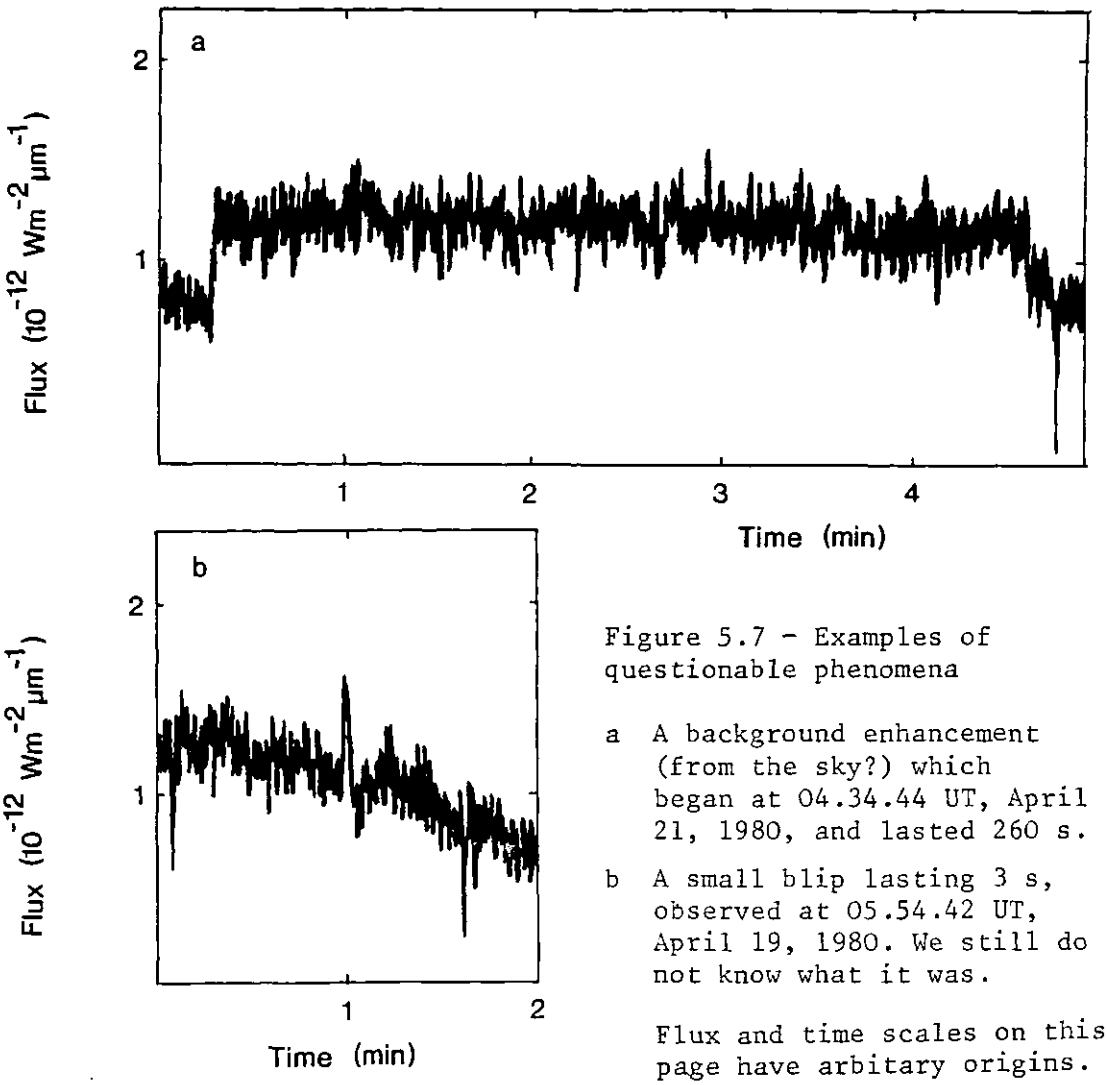

Figure 5.7 - Examples of questionable phenomena

a A background enhancement (from the sky?) which began at 04.34.44 UT, April 21, 1980, and lasted 260 s.

b A small blip lasting 3 s, observed at 05.54.42 UT, April 19, 1980. We still do not know what it was.

Flux and time scales on this page have arbitary origins.

producing "infrared bursts" similar in form and flux to the April one by striking a match near the position of the chart recorder. The radiation was being reflected around the inside of the metallic dome and entering the photometer through the main eyepiece which was pointing upwards (this could not happen with the 1.5 m telescope). A red torch produced a similar effect but a white torch did not (presumably the red filter was reradiating absorbed light as infrared). I still do not know why we could not reproduce the April burst at the time (perhaps positioning was critical) but this experiment casts more than enough doubt on the detection to reject it.

5.11.2 Questionable phenomena

Spurious phenomena are not dangerous as long as they can be recognised as such. More worrying are phenomena which cannot be positively identified as coming from the Rapid Burster, but cannot be eliminated either.

On many occasions we saw sudden enhancements of the signal of about 4×10^{-13} W m^{-2} μm^{-1} (about one third of the burst flux), which rose in 1–2 s and persisted for several seconds or even minutes. Some of them tailed off gradually, but others had flat tops and cut off as suddenly as they arose. (See Figure 5.7a). During one long-lasting enhancement we moved the telescope off Liller 1 and on to the sky and found that the sky background had risen by a similar amount. Did these enhancements come from the sky? From time to time we spent several minutes monitoring the empty sky next to the burster, but saw no enhancements under these conditions (if they were from the sky they would have been eliminated by chopping).

Sometimes events occur only once, and are so brief that there is no time to test them while they are in progress (e.g. by moving the telescope off the source). One such event occurred on April 19 at 05.55 UT and is shown in Figure 5.7b. It had a duration of 3–4 s and a peak flux of 5×10^{-13} W m^{-2} μm^{-1}. Was it an infrared burst?

5.11.3 Sky bursts

The most fascinating discovery we made in the spring of 1980

Table 5.7 - Comparison of Tenerife Burst 2 with a Known Spurious Burst

Characteristic	Tenerife burst 2	Spurious burst
Peak flux (2.2 μm) (10^{-12} W m^{-2} μm^{-1})	1.5	1.2
Duration (s)	10	12
Timings (s):		
Initial rise	0.0	0
First peak	0.6	2
Second peak	2.0	
Flash in tail	8.1	8

The spurious burst was traced to a lighted match.

Table 5.8 - Zenith Angle and Azimuth of the Sky Bursts and the Sun

		Sky bursts			Sun	
Date (1980)	Time (UT)	Air mass	z (o)	A (o)	z (o)	A (o)
April 18	06.28	2.44	65.8	202.3	87.2	76.1
19	06.35	2.54	66.8	204.6	91.2	76.6

In this table z is the zenith distance, and A the azimuth (reckoned from north through east).

was not infrared bursts from the Rapid Burster, but infrared bursts from the sky itself. At that time of year the burster is a morning object and we were observing it in the few hours before dawn and, on occasion, through sunrise. About 20 minutes before sunrise the 2.2 μm sky suddenly begins to brighten, the change being noticable in about a minute. On three mornings, within a few minutes of sunrise, we observed violent changes in this background flux on scales of a second, lasting from 1 to 3 minutes. During the first event we were pointed at Liller 1, but the others occurred when the telescope was on a patch of empty sky a few arcminutes away. On each occasion the signal went off the range of the chart recorder, and the only reliable measure we have of the flux is on April 19, when there was a burst at least 40 times brighter than those from the Rapid Burster ($> 4 \times 10^{-11}$ W m^{-2} μm^{-1} in a 25" beam). Figure 5.8 shows bursts observed on April 18 and 19, and Table 5.8 lists the times of the bursts and the positions of the telescope and the sun. The first burst, on April 15, came as a complete surprise and we do not have accurate timings or a useful chart trace. On two other mornings, April 20 and 21, we observed through sunrise but did not see any bursts.

I do not know what these bursts are, or why they did not occur on every morning, but they seem to be connected with the brightening of the sky as sunrise approaches. They may be the effect of sunlight on something high in the atmosphere, perhaps to do with the air-glow.

5.12 Conclusions

1. There have been two, independent detections of infrared bursts from the globular cluster Liller 1, which contains the X-ray source MXB1730-335 known as the Rapid Burster.

2. The high brightness temperatures and intense infrared emission are not predicted by the favoured models of X-ray bursts. A powerful, non-thermal emission mechanism is required.

3. There were no simultaneous X-ray observations at the time of the bursts, and an extensive international campaign has failed to secure any further X-ray or infrared events. We still do not know if the infrared bursts correspond to the X-ray bursts. This problem is discussed in the next chapter.

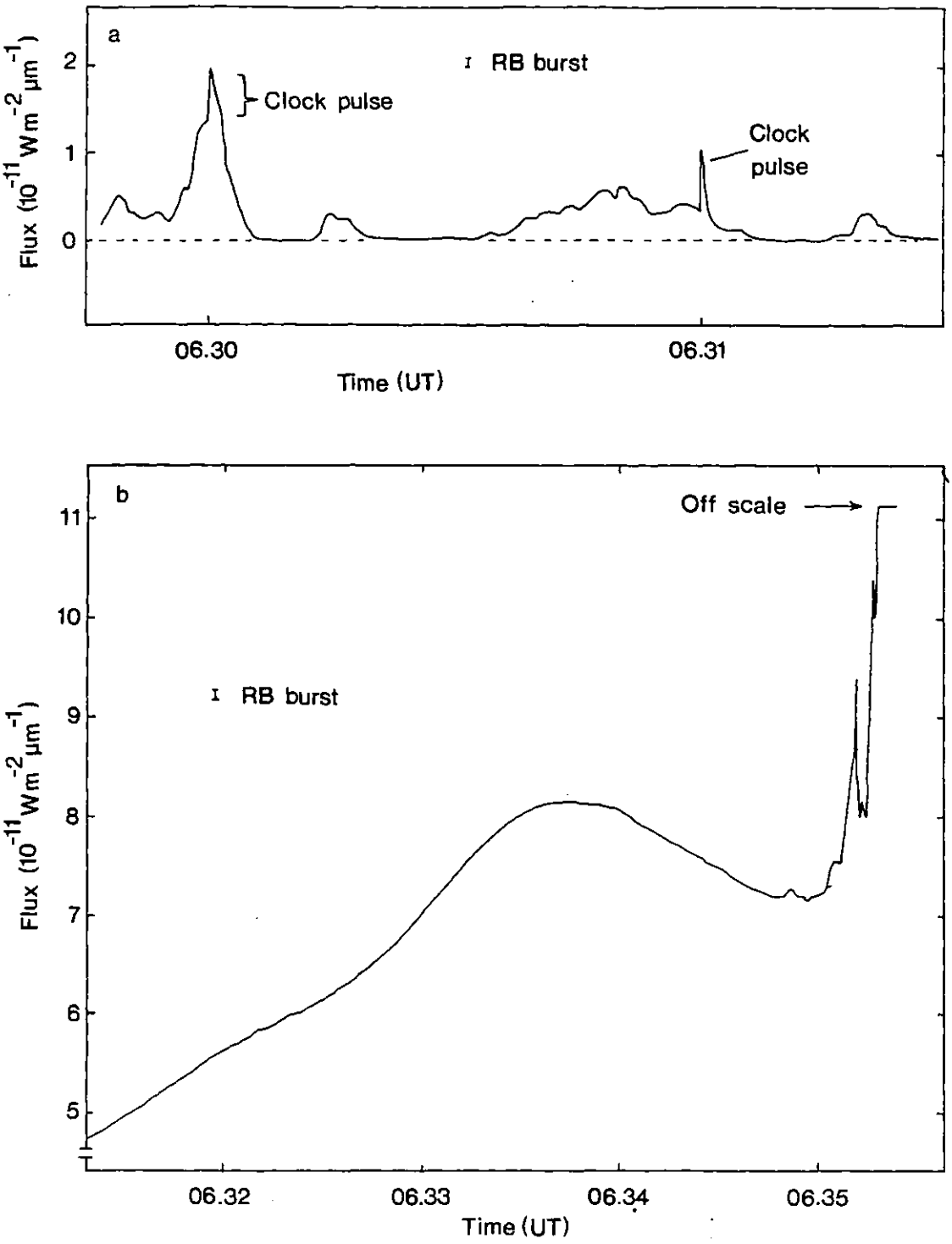

Figure 5.8 - Infrared bursts from the sky

These diagrams show 2.2 μm bursting activity from the sky near Liller 1, observed in DC mode with a 25" aperture. On each occasion the bursts appeared near sunrise. The bars marked 'RB burst' represent the flux of the infrared bursts from the Rapid Burster.

a April 18, 1980. The final part of the burst sequence. The flux scale is measured with respect to the sky background when the bursts had stopped.

b April 19, 1980. The start of the burst sequence. Note the steeply rising background, followed by a hump and then the bursts proper. The origin of the flux scale is the sky background at 06.18 UT, before the sky began to brighten.

APPENDIX C

~~CHAPTER 6~~

WHAT ARE THE INFRARED BURSTS?

What little evidence there is points to the infrared bursts being most probably associated with the Type II X-ray bursts from MXB 1730-335. It is too early to propose detailed models, but the energy source is almost certainly either gravitational or nuclear, requiring material to be processed at rates greater than 10^{13} to 10^{15} kg s^{-1}. The recent reports of radio bursts from the same source have not been substantiated, but if the events are real they may be relevant to the origin of infrared bursts. It is essential to obtain reliable, independent confirmation of the infrared bursts before further progress can be made.

6.1 Evidence for infrared bursts

Most of this chapter will be a critical evaluation of the evidence for infrared bursts, but I begin with a summary of the evidence itself. There are two kinds: positive and negative.

6.1.1 Positive

There have been two observations of infrared bursts from the Rapid Burster:

1. On April 4 1979, Kulkarni et al.(1979) detected 6 or 7 bursts at 1.6 μm in 2.5 hours, with fluxes around 2.0×10^{-12} W m^{-2} μm^{-1}.

2. On September 5 1979 Jones et al.(1980) detected two bursts at 2.2 μm in 1.3 hours, and none for a further 3.9 hours over 3 nights. The fluxes were about 1.5×10^{-12} W m^{-2} μm^{-1}.

There were no simultaneous X-ray observations. See Chapter 5 for a full account.

6.1.2 Negative

1. In June 1977 Alistair Walker and Bruce Robertson at SAAO monitored the X-ray burster Ser X-1 (MXB 1837+05) at 2.2 μm for a continuous 5.8 h period. In this time SAS-3 detected a Type I X-ray

burst (such as those which come from the R.B.) but no infrared activity was seen down to a 3σ limit of K = 7 (6×10^{-13} W m^{-2} μm^{-1}) (Lewin et al. 1980).

2. Soon after the R.B. turned on in August 1979 Sato et al. (1980) observed it for 6.2 h over 3 nights at I, H, K and L with the 61 cm telescope on Mauna Kea. At the time, the R.B. was producing Type II bursts every 20-30 minutes, but Hakucho's observing windows overlapped with the ground observers long enough for only one Type II burst to occur. There was no sign of infrared activity down to 7×10^{-13} W m^{-2} μm^{-1} at H and 2×10^{-13} W m^{-2} μm^{-1} at K (rms limits).

6.2 Analysis of the evidence

With so few observations, any conclusions as to the nature of the bursts must remain tentative. In this section I will argue that:

1. The bursts probably do come from Liller 1.

2. They are likely to be associated with Type II X-ray bursts, but in a selective fashion.

3. If they are not from Liller 1 they are probably caused by a local disturbance.

In Figure 6.1 I have mapped out the possible causes of the bursts in a logical manner. The diagram has two main branches representing the origin of the bursts; "From Liller 1" and "From elsewhere".

"From elsewhere" contains the sources that may give rise to mistakes, subdivided into "Distant" and "Local" sources. There is a compelling argument that practically eliminates the "Distant" branch.

The infrared detections (Section 6.1.1) were all made with a chopper. The 20" aperture was switched between the object beam and the reference beam 20 times a second, spending half its time in each.

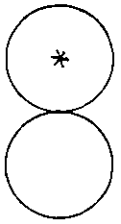

The fact that bursts can be detected with a chopping system implies that the emitting region is smaller than the aperture and remains within it for 10-40 s. Emission over areas much

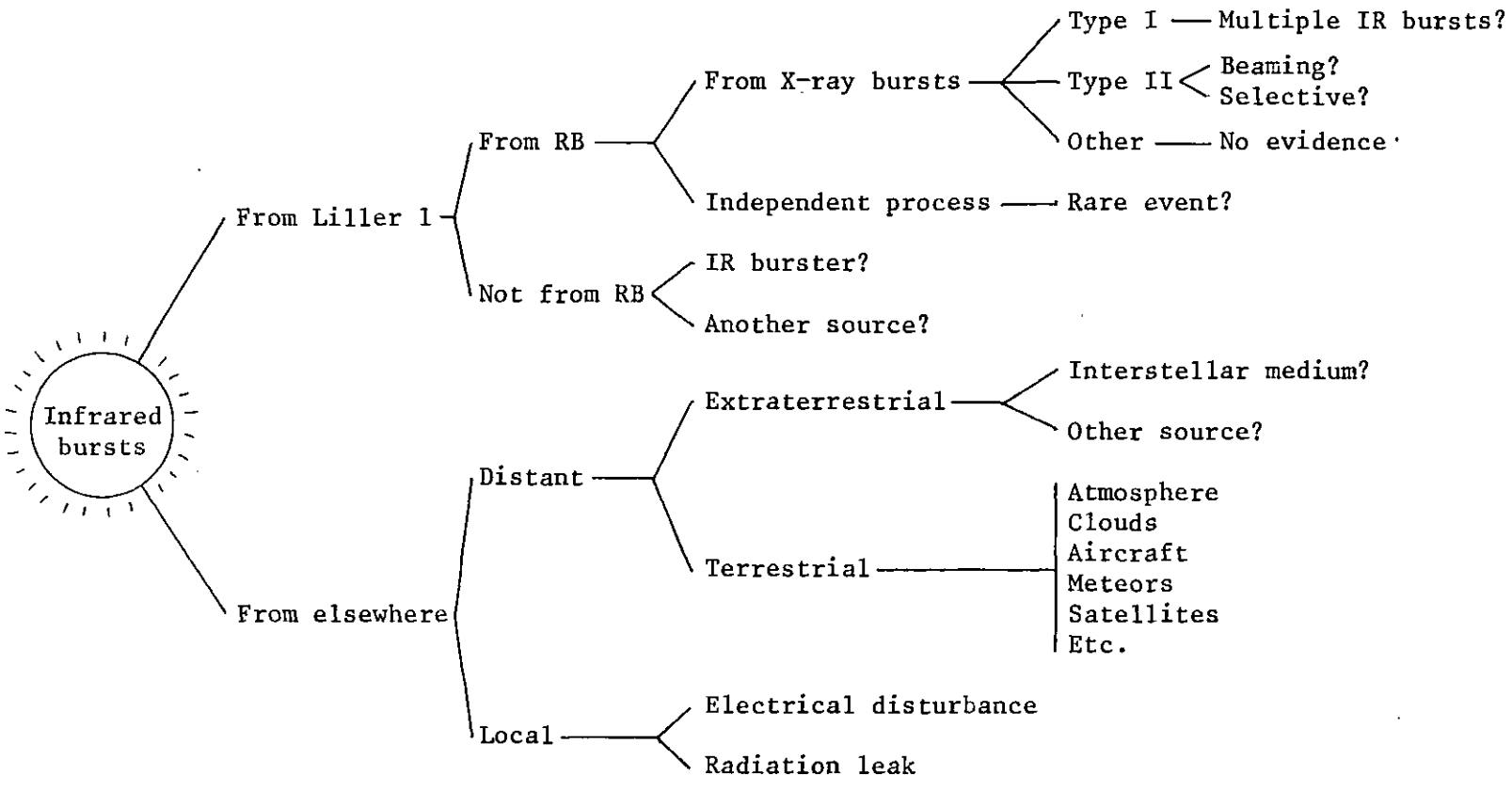

Figure 6.1 - Possible origins for the infrared bursts

bigger than the aperture (e.g. from the atmosphere) would not be detected.

Note that the two beams are symmetrical. We can choose either one to be the object beam. If the bursts are caused by objects passing through, or appearing in, the aperture, there is no reason for them to prefer one beam to the other. Yet all 9 bursts appeared in the object beam (i.e. the same beam as Liller 1); there were no negative bursts from the reference beam. The probability of 9 spurious objects, of whatever nature, appearing by chance in the same beam as Liller 1 is 1 in 512 (2^9; like tossing 9 heads in a row).

This effectively eliminates localised emission from the atmosphere, clouds, aircraft, meteors, satellites and other spurious sources not yet thought of (i.e. the "Terrestrial" branch of the diagram).

The "Extraterrestrial" branch does not look promising either. If the bursts occur by some mysterious process in the interstellar medium, then they are localised to a region $< 10^8$ m across (Section 5.7.3), and so can be eliminated along with the "Terrestrial" sources. Or we could say that there is some other, unknown, unseen, object in the direction of Liller 1, but this is an unnecessary contrivance (Occam's razor!).

We pass to the "local" branch. Could the bursts originate from a disturbance near the telescope? We have already seen how a radiation leak can produce a convincing "burst" (Section 5.11.1), though this kind of leak was not possible with the 1.5 m telescope and photometer used for the detections in Chapter 5. Nevertheless, I think the possibility of some kind of local disturbance must be left open. Although radiation leaks can be tested for and eliminated, electrical interference, for example, is much more difficult to suppress.

So at this point I conclude (1) that the bursts probably do come from Liller 1, and (3) if not, they are probably caused by a local disturbance.

We move on to consider the branch labelled "From Liller 1". The bursts may or may not come from the Rapid Burster itself. A globular cluster contains upward of 10^5 stars (AQ p.280) and we have no way of telling which is the X-ray source or which is the infrared

source. It may well be that we have here a new and separate object; an "infrared burster" in its own right. Although such a hypothesis is a firm candidate for Occam's razor again, we should not forget that a strong selection effect is operating here. Suppose there were purely infrared bursters. How would we know? No-one is going to spend many hours of valuable telescope time looking at a globular cluster unless he expects to see something. If pure infrared bursters exist they will be discovered by someone looking for something else; like infrared emission from an X-ray burster. But we will leave that to the Razor for now.

So the bursts are "From the R.B.", but are they associated with X-ray bursts? Unfortunately there were no simultaneous X-ray observations for the detections in Section 6.1.1, so we do not know if there were X-ray bursts. Let us suppose the two kinds of bursts are not connected. That is, there is some "thing" which sometimes throws out X-ray bursts and sometimes infrared ones, but by different processes. It seems unlikely to me that the two processes would be completely separate. More plausibly, the infrared bursts are characteristic of some phase in the life of a rapid X-ray burster, and so may be rare events. After all, there is only one known rapid burster in our Galaxy and we don't know how long they live. In Chapter 5 I reported that the R.B. was not seen to make its two expected appearances in 1980. Our observations in September 1979 may have been the last anyone saw of it. Are infrared bursts the death throes of a rapid burster?

Most investigators like to think that there is some connection between the X-ray bursts and the infrared ones, if only because this is the simplest hypothesis. There is a vague (though plausible) idea that the infrared bursts are some kind of secondary emission triggered by the X-rays. This view is prevalent in the case of optical bursts from other X-ray sources (van Paradijs 1981). If this is so, the infrared bursts must be associated with either Type I or Type II X-ray bursts (or both?) or some as yet undiscovered third category.

We can dispose of this last possibility. All bursts from the Rapid Burster have been classified as either Type I or Type II, by the way their spectra change as they fade (W.H.G. Lewin, 1980, personal communication). Nothing deserving a third category has been seen, although Type II bursts can take several forms (see below).

Type I bursts have been seen from all burst sources. Although each source has its own characteristic burst profile, Type I bursts are all believed to be thermonuclear helium flashes (Section 5.4.1). They occur at intervals of hours or even days. No Type I bursts from MXB 1730-335 have ever been seen to occur as closely spaced as the infrared bursts (W.H.G. Lewin 1980, personal communication). Moreover, we have to accommodate the observations of Lewin et al. (1980) who saw a Type I burst from Ser X-1 without accompanying infrared emission (Section 6.1.2.) These facts can only be reconciled if either (a) Type I bursts can give rise to multiple infrared bursts, or (b) they were occurring at an unprecedented rate. Even then we have to admit that if Type I bursts can produce infrared ones, then they do not do so every time.

Finally, we consider the Type II "rapid" bursts that are peculiar to MXB 1730-335. These occur at intervals of seconds or minutes, in a pattern determined by the E-Δt relationship (Section 5.2) which is regarded as evidence that these bursts are the result of accretion instabilities (Section 5.4.2). These short intervals are consistent with the intervals between infrared bursts, but there cannot be a simple one-to-one correspondence between Type II bursts and infrared ones, or else infrared bursts would be as common as the Type II's. Then we have the observations of Sato et al. (1980; see Section 6.1.2) who saw a Type II X-ray burst with no infrared counterpart. I cannot agree with their claim that "this conflicts with previous results by Kulkarni et al. and Jones et al." There is no conflict. It just tells us that if Type II bursts produce infrared bursts, then they do not do so all the time, and that is something we already knew.

Why should we see infrared bursts from some X-ray bursts but not from others? I can see two possible explanations.

1. Only some Type II's produce infrared bursts. But why? Can we distinguish different kinds of Type II bursts, only one of which leads to infrared activity? This leads us to ponder the "anomalous" bursts discovered soon after the Rapid Burster itself (Section 5.2) or the recently discovered "trapezoidal" bursts (Inoue et al. 1980). On the other hand, the infrared bursts may only be produced through favourable external circumstances (orientation of an accretion disk?).

2. All Type II's produce infrared bursts, but we only see some of them. I am imagining some kind of "window" (either spatial or temporal) which opens up to let us see the infrared bursts for a while and then closes again. While the window is open the bursts would have a Type II recurrence pattern. An example of this could be a beaming mechanism, which would also help explain the improbable brightness temperatures (10^{10} to 10^{18} K) deduced from the flashes in the bursts (Section 5.7.2).

I am being deliberately vague. I am not considering detailed models here, but trying to circumscribe the area where any proposed models must lie. Of all the possibilities discussed in this section, the most likely appears to be that the infrared bursts are "selective Type II". Hence conclusion (2), that they are likely to be associated with Type II X-ray bursts, but in a selective fashion. That is the best we can say at present.

6.3 Sources of energy

Although there is, at present, little justification for pursuing detailed models of infrared burst emission, it is still worthconsidering the available sources of energy that a model will have to draw on. Two sources of potential energy are important on the astrophysical scale: gravitational energy and nuclear energy.

6.3.1 Gravitational energy

Assume that the Rapid Burster contains a neutron star of radius R = 10 km and mass M = 1.4 M_o. The energy released by material falling in from infinity will be:

$$\frac{dE}{dm} = \frac{GM}{R} \sim 2 \times 10^{16} \text{ J kg}^{-1} \quad \text{or} \quad 200 \text{ MeV nucleon}^{-1} \tag{6.1}$$

6.3.2 Nuclear energy

The most efficient conversion of rest mass to free energy (other than matter-antimatter annihilation) is the fusion of hydrogen to helium, with an efficiency of 0.7% (Harwit 1973, p.308). Thus, the energy released is:

$$\frac{dE}{dm} = 0.007\ c^2 \sim 6 \times 10^{14} \text{ J kg}^{-1} \quad \text{or} \quad 6 \text{ MeV nucleon}^{-1} \tag{6.2}$$

Other reactions (such as the helium fusion model for X-ray bursts) are less efficient, usually below 0.1%.

6.3.3 Implications for possible models

Any proposed models must conform to the scheme shown in Figure 6.2. Gravitational potential energy (which appears as kinetic energy) or nuclear binding energy (which appears as gamma ray photons) must ultimately be converted into infrared photons. We also note:

1. In this case, a given mass of hydrogen can release 30 times more gravitational than nuclear energy.

2. A typical infrared burst of 10^{31} J would require 5×10^{14} kg of infalling material or 2×10^{16} kg of fusing hydrogen.

3. To produce a mean luminosity of about 10^{30} W (Table 5.3) material would have to be processed at 5×10^{13} kg s^{-1} (infalling) or 2×10^{15} kg s^{-1} (fusion).

4. These large masses (comparable to those of large asteroids (AQ p.152)) are strictly lower limits which assume complete conversion of potential energy to infrared radiation. A more realistic estimate could be orders of magnitude higher.

5. The infrared generating mechanism would have to reach full intensity in times $\sim$ 0.1 s to account for the structure observed in the bursts.

6. The large consumption of mass may be avoided if the infrared radiation is not isotropic.

7. The energy released per nucleon (which effectively means a hydrogen atom) is midway between the rest masses of the electron (0.5 MeV) and the proton (938 MeV). Relativistic effects may be important.

8. Neutron stars can be expected to have very strong magnetic fields of up to $\sim 10^{8}$ T (Harwit 1973, p.364).

Two groups, to my knowledge, have models for infrared bursts: Apparao and Chitre (1980) propose a "cyclotron maser" and Prasanna (preprint 1980) produces infrared bursts from an accretion disk around a black hole. Both models use infalling material to release gravitational energy.

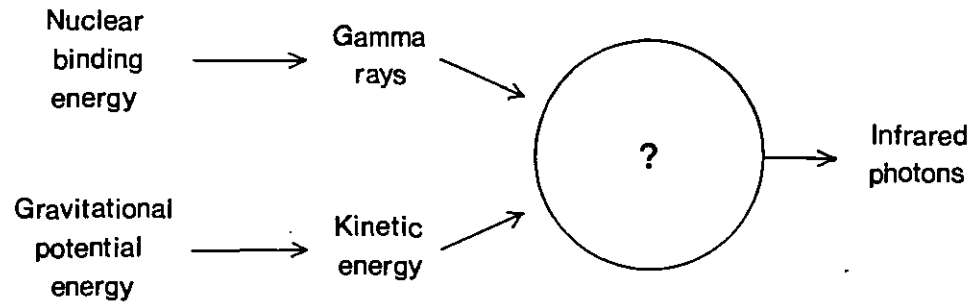

Figure 6.2 – Energy sources for infrared bursts

Two sources of energy are important on astrophysical scales: gravitational and nuclear. Models for the infrared bursts will have to convert either one to infrared photons.

6.4 Reports of radio bursts

Soon after the first detections of infrared bursts in April 1979, a group led by O.P.N. Calla at the Space Applications Centre (SAC), Ahmedabad, began to report radio bursts from the Rapid Burster.

The circumstances of these reports leave much to be desired. Although the SAC group claimed to have detected bursts on at least nine different dates between April 1979 and April 1980, they have published no more than brief announcements in the IAU Circulars. Almost three years after the first detection there is no account published in a primary journal available to the astronomical community. Moreover, there were at least eight independent attempts to detect radio bursts in 1980, but nothing was seen (A. Lawrence, personal communication, and e.g. Pramesh Rao and Venugopal, preprint 1979).

6.4.1. Assessment

If these bursts are real, then they are clearly of great importance. In this section I summarise and weigh up the available evidence.

1. The first report came on April 18 1979 in IAUC 3347. Calla and colleagues detected bursts on April 14 and 16 using a 14 m parabolic aerial at 4.1 GHz (7.3 cm). They gave no absolute flux measurement of the burst intensities. Their first burst was followed by a "series of six very narrow spikes", which is suggestive of the flashes that accompanied the Tenerife infrared bursts.

2. In response to an inquiry via P.V. Kulkarni, Dr. M. R. Deshpande (PRL) sent me a photocopy of radio bursts observed at SAC on April 21 (this date does not appear in the IAUC reports). According to Deshpande, "the bursts ... have Gaussian structure and usually appear in pairs". This is apparent from Figure 6.3 where there is clearly a repetitive pattern, though bearing little resemblance to either the X-ray or infrared bursts. The brightest bursts have fluxes of 200 to 300 Jy.

3. In IAUC 3458 (1980 March 13) Calla reports further detections made in August and September 1979. These differ from the earlier ones, having "a long-duration (9 min) flat-top profile and a relatively shorter and more irregular decay". Calla comments that they appear similar to the trapezoidal X-ray bursts detected by Inoue et al. (1980).

4. The first detections of 1980 came in IAUC 3467 (1980 April 10) in which Calla announced bursts detected on March 21, again trapezoidal.

5. At this time we were monitoring the Rapid Burster from Tenerife (Chapter 5). A telex from MIT received on April 21 reported that Calla had seen radio bursts on March 21, March 30, April 9 and April 10 with durations from 30 to 360 s at 3.95 GHz.

6. These long, flat, "trapezoidal" bursts are reminiscent of the sudden infrared enhancements seen in April 1979 (Section 5.11.2). I mentioned this in a letter to Calla, asking if I could see his results. He replied in a telex on July 9 saying "our data is being mailed to you". Unfortunately, I heard nothing more.

7. The SAC group have not reported bursts since April 10, 1980, and according to a circular from MIT sent to all observers on December 5, 1980; "to this day we have not yet received a clear report from them of exactly when and how bright activity was."

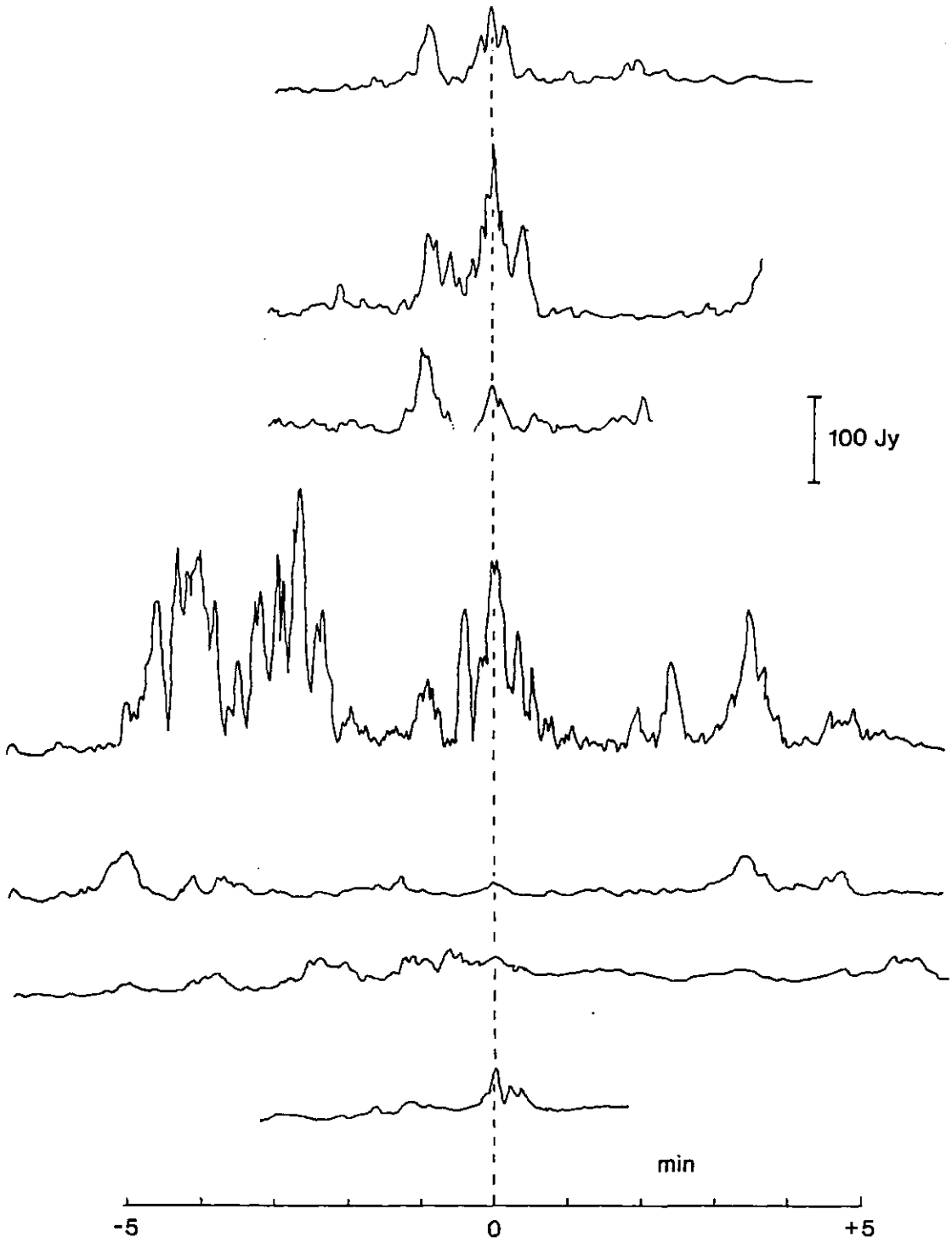

Figure 6.3 - Radio bursts reported from Liller 1

This is a series of radio bursts observed on April 21, 1979, at Ahmedabad. The telescope was a 14 m dish operating at 4.12 GHz (73 mm). In this figure the burst sequences have been aligned to highlight a possible repetitive pattern, though there is no apparent periodicity (adapted from M.R. Deshpande 1979; personal communication).

We must conclude that the present evidence for radio bursts is, at best, inconclusive. This does not mean that there are no radio bursts, but it is unsatisfactory that the details of such an important alleged discovery are still not available to the scientific community.

6.4.2 Tests of origin

There are two methods which could settle the question of whether these bursts are real.

1. A simultaneous detection at two or more independent stations would be a very strong piece of evidence that these bursts are not locally generated (this is discussed more fully in Section 6.6).

2. If the bursts do come from Liller 1, they will have traversed about 10 kpc of interstellar medium, largely ionised hydrogen. The dispersion of two different frequencies should lead to a measurable time delay.

Lang (1974) gives the differential time delay as

$$\Delta t \simeq 4.3 \times 10^{15} \, (\nu_1^{-2} - \nu_2^{-2}) D \text{ s} \qquad (6.3)$$

where D is the dispersion measure along a path of length ℓ such that

$$D = \int_o^{\ell} N_e \, d\ell \qquad \text{pc cm}^{-3} \qquad (6.4)$$

AQ (p.265) gives a mean N_e of 0.04 cm^{-3} near the galactic plane. Hence $D \sim 0.04 \times 10$ kpc = 400 pc cm^{-3} (it is probably higher, since the density of interstellar material increases towards the galactic centre). Now put ν_1 = 4 GHz (Calla's frequency) and ν_2 = 0.4 GHz. Then $\Delta t \simeq 10$ s.

If Calla could equip his telescope with two receivers, one operating at 4 GHz and the other at 400 MHz, he could test for a galactic origin for his bursts by looking for delays of order 10 s between the two channels (I am grateful to Dr. Peter Meikle for suggesting this to me).

6.5 A speculative burst spectrum

For the purposes of this speculation I will assume that both the infrared bursts and the microwave bursts do come from the Rapid Burster. Figure 6.4 shows spectral information consisting of four parts:

1. A black body spectrum of an object at $T = 2 \times 10^7$ K with a radius of 10 km and a distance of 3×10^{20} m (10 kpc). In the X-ray region this is characteristic of X-ray bursts.

2. The mean fluxes of the infrared bursts observed at Kavalur (1.6 μm) and Tenerife (2.2 μm), corrected for interstellar extinction.

3. A flux of 200 Jy representative of the microwave bursts (M.R. Deshpande, personal communication).

4. The mean fluxes of optical Type I bursts from MXB 1837+05 and MXB 1735-44 (both around 10 kpc distant) not corrected for extinction (Hackwell et al. 1979).

I have drawn a straight line through the infrared and microwave observations, presuming that they have a common origin. The slope of this line is -0.44, which puts it well outside the thermal region of +2.0 (optically thick, Rayleigh-Jeans tail) to -0.1 (optically thin thermal bremsstrahlung). According to Harwit (1973, p.238) non-thermal cosmic sources typically have spectral indices in the range -0.2 to -1.2, so -0.44 is by no means unusual.

Note also that the optical bursts are a factor of 10^4 (10 mag) below this line, a figure which is consistent with the extinction to the sources.

However, the line passes above the X-ray peak by two orders of magnitude, something which is not observed. Presumably, this extrapolation is not valid in the X-ray region.

6.6 What to do next

In these chapters I have described the detection of infrared bursts and shown that they are most plausibly associated with Type II X-ray bursts. This conclusion is based on slender evidence and is by no means generally accepted. Indeed, the very existence of infrared bursts is treated with scepticism (as it should be) and so the immediate

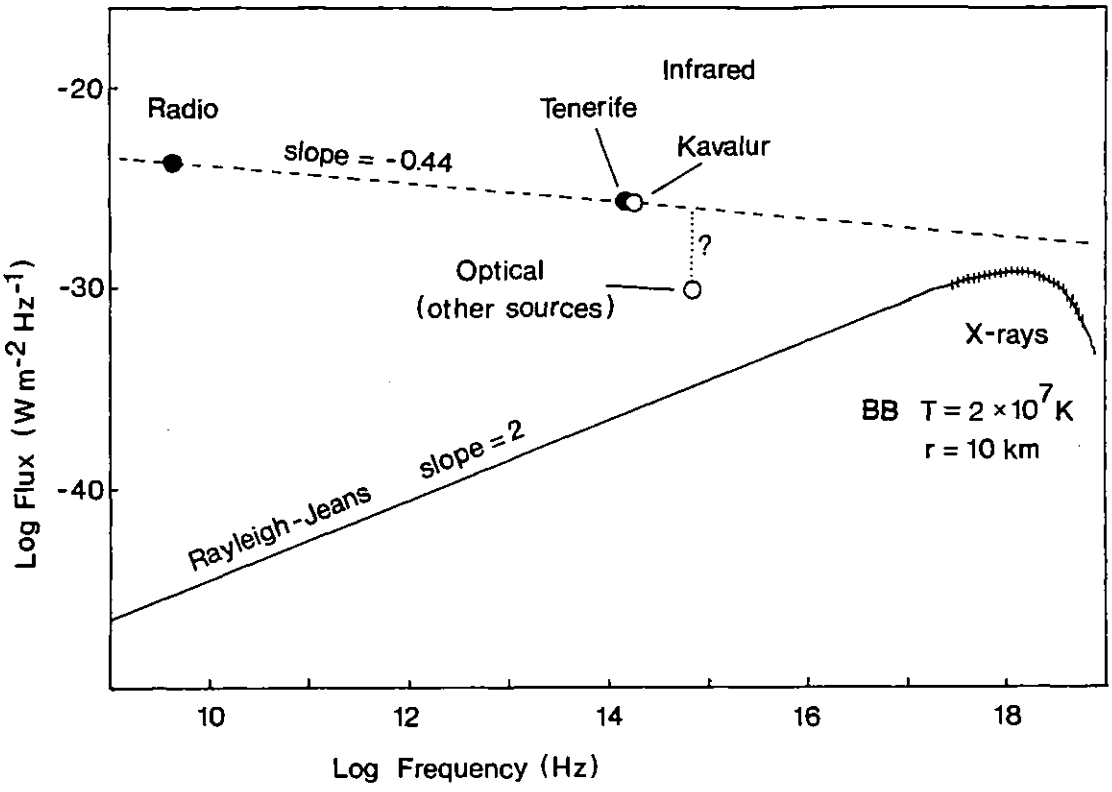

Figure 6.4 - A speculative burst spectrum

The dashed line connects the infrared bursts observed at Tenerife and Kavalur with the reported radio bursts. An extinction correction of about 10 mags would bring the optical fluxes from other bursters (all near 10 kpc) up to this line. The black-body curve is an extrapolation from the X-ray spectrum (shown hatched).

priority must be to settle whether they exist or not.

6.6.1 Problems of verification

The verification of transient events is inherently difficult, the more so when there is little or no pattern in their occurrence. If we see a burst, or other unusual activity, how do we know it is "real"? One of the biggest problems, but often overlooked, is the psychological aspect; that is, prejudice on the part of the investigator.

For example, the spurious burst of April 20, 1980 turned out to be scattered radiation from a lighted match (Section 5.11.1). But it looked so similar to the bursts of September 5, 1979 that we thought it must be real, despite the plausibility of the match hypothesis.

On the other hand, on the previous night we saw a small "burst" (see Section 5.11.2), that was not accompanied by any known stimulus, yet was not given the credibility of the April 20 burst. Likewise, the many background enhancements seen at that time were never seriously considered as coming from the burster.

Why is this? Why do we want to believe observations that match our expectations and disregard those that do not? After all, the very fact that infrared bursts have been detected from the Rapid Burster tells us that we do not know what to expect from this object. It is worth asking if we would have published our observations of September 1979 if Kulkarni had not published his first. Or what would we have done if our bursts had looked completely different?

I think a clear principle is emerging here. We should not accept or reject observations because of conformity with our expectations. Ideally, observations should stand alone, independent of any hypothesis they are designed to test. For that to be so, we need complete confidence in our equipment and observing procedure. If we see a deflection on the chart recorder we want to be able to say, "this is radiation from Liller 1", because it could not be anything else.

6.6.2 Requirements for further observations

With this in mind, the requirements for further observations are as follows:

1. First-rate telescope, photometer and recording equipment. The telescope need not be big (0.5 m is adequate), but the whole system should be tried and tested, sealed against radiation leaks and isolated from electrical disturbances.

2. Chopping is essential for three reasons:

a. It removes sky emission (such as the enhancements) leaving only the signal from Liller 1.

b. It allows a statistical test of a non-random hypothesis (the beam-preference argument in Section 6.2).

c. Recording the chopped signal and phase reference separately provides a further test of origin. If the burst signal is found to be chopped, then it is almost certainly caused by radiation coming down the telescope tube.

The disadvantage of chopping is that it distorts time variations of the order of the chop period, and so could not be used to obtain reliable measurements of the bursts' flashes.

3. Other considerations:

a. The core of the cluster is 13" across and the burster could be anywhere in that diameter. It is judicious to use a biggish sky aperture (say 20") to ensure that the burster is always in view.

b. Likewise, the telescope must track well enough to keep the burster in the aperture. If guide stars are visible, poor tracking can be corrected manually.

c. If possible the observations should be timed to within a second of UT (or better) to facilitate comparison with parallel observations.

These, and similar precautions, which a prudent observer would ensure, should be enough to convince the investigator of the reality of any detections. However, they will not necessarily convince the scientific community as a whole. In any normal astronomical investigation other observers can repeat measurements at their convenience. Transient events can never be repeated, so the standard of evidence required is much higher, and ideally we want incontestable evidence. There are two ways of doing this:

1. Simultaneous detection by independent stations. Such a detection would be as near incontestable as possible provided that:

a. Each detection were simultaneous within calibration errors and uncertainties in the shape of the burst.

b. The form of the activity recorded were consistent between stations.

This is a very powerful test (though difficult to put into practice). For example, the energetic gamma-ray burst of March 5 1979 was detected by nine different spacecraft spread across the inner solar system (Cline et al. 1980). Analysis of the arrival times at each spacecraft located the direction of the source to within 2'. It is inconceivable that this could have been anything other than a burst of gamma-rays passing through the solar system.

Meikle (1973) describes a search for radio pulses from supernova explosions, by simultaneous monitoring from five sites. In this case the requirements of simultaneity and consistency eliminated many spurious events that could not otherwise have been rejected. On two occasions, there were near-simultaneous events at three out of the four or five stations then operating, although the pulses had different shapes. These events could have been rejected because of the inconsistency in shape, even if all the stations had recorded them.

2. More detections by other, independent observers. This comes a poor second (other people may see spurious events too, especially if they are looking for them, e.g. N-rays (Klotz 1980)) but it is better than nothing. X-ray bursts themselves are a good example of this. Sources observed by more than one satellite can be considered confirmed.

The alleged gravitational waves provide another example. While Weber continued to detect waves, other investigators did not, despite using more sensitive detectors (Tyson and Giffard 1978). For this reason, further detections of infrared bursts by ourselves or Kulkarni would not carry so much weight.

6.7 Conclusions

1. On the limited evidence available at present, the infrared bursts from Liller 1 are most probably associated with Type II X-ray bursts from MXB 1730-335.

2. The energy source for the bursts is almost certainly either gravitational potential energy or nuclear binding energy. Unless the infrared radiation is non-isotropic, the burst luminosity requires material to be processed at minimum rates of 10^{13} to 10^{15} kg s^{-1}.

3. Reports of radio bursts from the same source have not been verified and are doubtful. However, if they turn out to be real, they may have an origin in common with the infrared bursts.

4. The most urgent priority is to obtain further, independent observations of infrared bursts. Although bursts have now been seen by two groups, their existence will not be generally accepted until more evidence is forthcoming. Until that time there is little value in pursuing detailed models. A simultaneous detection from two observatories would settle the question for good.

APPENDIX A

A CATALOGUE OF INFRARED SOURCES IN THE GALACTIC PLANE

These tables list 826 sources for which H ≤ 10.5 and K ≤ 9.5 (Block 1 has H ≤ 11.5 and K ≤ 10.5: see Chapter 4). Observations at both H and K were reduced for Blocks 1, 2, 3, 4, 23, 32, 42, 52, 56, 59 and 62. Block 72 was partly covered at H and K. Blocks 16, 31, 40 and 70 were only covered at K.

Of these sources, 314 were detected at both wavelengths. Such pairs are defined as H and K peaks less than 15" apart. Many sources are not paired, even in blocks covered at both H and K. There are several possible reasons:

(1) The H and K peaks may be more than 15" apart. If so, the two peaks will be listed separately.

(2) The areas of coverage for H and K do not coincide exactly. Sources near the edges may not have a match (see Table 4.3).

(3) A source listed at one wavelength may be too faint at the other.

(4) The source may be spurious.

Each block has its own table containing the following information for each source:

(1) Infrared source number (IRS). The first one or two digits are the block number, and the last two are the source number in that block, in order of increasing right ascension.

(2) Right ascension and declination for equinox 1950.0. Where there are both H and K detections, the positions are the mean of the two. Errors vary systematically from block to block (see Section 3.3.6), but should not be more than ± 1 s in RA and ± 15" in declination.

(3) H and K magnitudes. The symbol < means that the source was too bright to measure. There are 17 of these sources, which usually saturate in the range 6.0 to 6.5. A few bright magnitudes were measured from chart traces. Errors are within ± 0.2 mag.

(4) SEP is the separation in arcseconds between the H and K source positions.

CATALOGUE OF H AND K SOURCES IN BLOCK 1

IRS	H	M	S	°	′	″	H	K	SEP
101	17	42	20.5	-28	59	44	8.9	7.2	1
102	17	42	20.5	-28	56	43		10.3	
103	17	42	20.5	-28	54	11	10.5	8.9	0
104	17	42	21.0	-29	3	12		9.6	
105	17	42	21.0	-29	1	36		9.9	
106	17	42	21.2	-28	58	48	10.6	9.3	6
107	17	42	21.5	-28	57	3		10.3	
108	17	42	21.9	-28	57	47	10.8		
109	17	42	22.4	-28	55	15		10.3	
110	17	42	22.8	-29	1	16		10.2	
111	17	42	22.8	-28	57	55		9.6	
112	17	42	23.8	-29	1	59		10.1	
113	17	42	24.7	-28	54	59		10.2	
114	17	42	24.9	-28	56	32	11.3	10.2	6
115	17	42	25.1	-29	4	13	10.3	8.6	9
116	17	42	25.1	-29	1	10	11.4		
117	17	42	25.1	-29	0	57	11.5	10.3	2
118	17	42	25.1	-28	57	31		10.1	
119	17	42	25.6	-28	59	4	10.2	8.6	0
120	17	42	26.0	-29	2	34	9.7	7.9	4
121	17	42	26.0	-28	55	4	11.1		
122	17	42	26.5	-29	0	13	11.0		
123	17	42	26.5	-28	57	49	10.7	9.3	13
124	17	42	26.9	-28	58	48	10.7		
125	17	42	26.9	-28	55	15		10.2	
126	17	42	27.2	-29	0	28	11.4	9.3	11
127	17	42	28.1	-29	2	19	9.7	7.9	6
128	17	42	28.3	-28	57	14	11.0		
129	17	42	28.8	-28	56	19		10.3	
130	17	42	28.8	-29	1	5	10.3	8.6	2
131	17	42	29.2	-28	57	31	10.8	9.4	7
132	17	42	29.3	-29	4	20		9.6	
133	17	42	29.3	-29	3	8	11.3		
134	17	42	29.7	-28	59	12	9.1	7.4	1
135	17	42	30.1	-28	55	12	10.6	9.4	7
136	17	42	31.3	-28	57	0	10.7	9.5	8
137	17	42	31.3	-29	2	25	11.3	10.3	7
138	17	42	32.0	-28	58	35	10.5	8.8	14
139	17	42	32.4	-28	56	11		9.8	
140	17	42	32.9	-28	57	47	10.7		
141	17	42	33.1	-28	55	9	11.5	10.2	13
142	17	42	33.4	-29	3	40		9.8	
143	17	42	33.4	-28	57	3	11.0	9.1	1
144	17	42	33.8	-29	2	56		9.8	
145	17	42	33.8	-28	57	59		8.8	
146	17	42	35.2	-28	58	29	11.2	9.3	4
147	17	42	35.6	-28	57	31		10.1	
148	17	42	35.6	-28	53	59	10.2		
149	17	42	36.3	-28	55	4	11.1	9.6	9
150	17	42	36.6	-29	3	28	11.3		
151	17	42	37.0	-29	2	9	8.0	6.4	5

CATALOGUE OF H AND K SOURCES IN BLOCK 2

IRS	H	M	S	°	′	″	H	K	SEP
201	17	42	38.6	-28	57	28		8.6	
202	17	42	38.6	-28	56	28		9.3	
203	17	42	38.6	-28	52	39		8.7	
204	17	42	38.7	-28	55	31	9.1	8.0	2
205	17	42	38.8	-28	51	4	9.9	7.8	7
206	17	42	39.2	-28	57	12		9.1	
207	17	42	39.5	-28	56	20		9.1	
208	17	42	39.7	-28	48	3	8.5	7.1	7
209	17	42	40.1	-28	52	59		9.3	
210	17	42	40.1	-28	51	24	8.4	8.0	6
211	17	42	40.7	-28	50	19	10.0	8.4	7
212	17	42	40.7	-28	50	59		9.1	
213	17	42	40.9	-28	56	41	9.8	8.4	7
214	17	42	41.0	-28	51	51	10.3	8.5	6
215	17	42	41.3	-28	58	8		9.4	
216	17	42	41.3	-28	52	43		8.7	
217	17	42	41.4	-28	54	0	8.8	8.0	6
218	17	42	41.6	-28	54	53	9.5	7.9	3
219	17	42	42.3	-28	55	43		9.4	
220	17	42	42.3	-28	49	6		9.2	
221	17	42	42.5	-28	50	34		9.4	
222	17	42	42.5	-28	49	54		9.5	
223	17	42	42.6	-28	58	12	9.8	9.2	6
224	17	42	42.9	-28	47	38		9.4	
225	17	42	43.2	-28	53	47		9.4	
226	17	42	43.2	-28	48	30		8.4	
227	17	42	43.5	-28	56	16		9.3	
228	17	42	43.5	-28	54	35		8.7	
229	17	42	43.5	-28	52	31		9.3	
230	17	42	43.5	-28	50	18	9.8	7.9	6
231	17	42	43.8	-28	55	18	6.8	<6.2	2
232	17	42	43.8	-28	52	59		9.2	
233	17	42	43.8	-28	51	47		9.1	
234	17	42	43.8	-28	48	6		9.0	
235	17	42	44.1	-28	54	12	9.7	8.3	9
236	17	42	44.7	-28	48	59	10.0	8.2	1
237	17	42	44.7	-28	47	34		8.9	
238	17	42	45.0	-28	55	35		8.8	
239	17	42	45.0	-28	53	27		9.5	
240	17	42	45.2	-28	51	26	9.1	7.8	3
241	17	42	45.3	-28	52	3		9.1	
242	17	42	45.4	-28	49	49	10.3	8.3	6
243	17	42	46.3	-28	48	9	9.8	8.5	5
244	17	42	46.5	-28	53	31		9.3	
245	17	42	46.7	-28	49	19	10.5	9.3	4
246	17	42	47.1	-28	54	39		8.2	
247	17	42	47.1	-28	50	47		8.8	
248	17	42	47.2	-28	57	57	6.9	<6.1	7
249	17	42	47.7	-28	52	23		9.0	
250	17	42	47.9	-28	53	6	9.9	8.9	13
251	17	42	48.0	-28	52	10	9.7	8.4	3
252	17	42	48.0	-28	56	7	10.3	9.4	8
253	17	42	48.0	-28	49	47		8.6	
254	17	42	48.6	-28	55	3		8.9	
255	17	42	48.6	-28	53	55		9.0	
256	17	42	48.6	-28	53	23		9.2	
257	17	42	48.9	-28	47	49	9.0	8.0	8
258	17	42	49.0	-28	55	35		9.0	
259	17	42	49.2	-28	50	55		8.3	
260	17	42	49.3	-28	54	23		8.9	
261	17	42	49.9	-28	55	20		8.4	
262	17	42	49.9	-28	53	35		9.0	
263	17	42	49.9	-28	52	43		9.4	
264	17	42	49.9	-28	52	7		8.0	
265	17	42	50.2	-28	56	44		9.4	
266	17	42	50.7	-28	50	38	9.3	9.0	3
267	17	42	50.8	-28	47	54		8.8	
268	17	42	50.8	-28	51	11		8.3	
269	17	42	50.8	-28	53	46	10.3	8.5	11
270	17	42	51.1	-28	48	39	8.9	7.7	6
271	17	42	51.7	-28	56	3		8.3	
272	17	42	51.7	-28	53	7		9.1	
273	17	42	52.0	-28	50	34		8.8	
274	17	42	52.0	-28	58	20		<6.2	
275	17	42	52.0	-28	51	55		8.8	
276	17	42	52.4	-28	56	59	10.4	9.1	2
277	17	42	52.5	-28	51	41	10.1		
278	17	42	52.6	-28	54	11		9.5	
279	17	42	52.6	-28	47	38		6.8	
280	17	42	52.9	-28	48	18		8.7	
281	17	42	52.9	-28	53	31		8.3	
282	17	42	52.9	-28	52	29	10.1		
283	17	42	53.2	-28	51	15		9.3	
284	17	42	53.2	-28	50	19		8.7	
285	17	42	53.2	-28	48	30		9.5	
286	17	42	53.6	-28	55	33	7.9	7.4	8
287	17	42	53.6	-28	51	26	9.9	7.7	6
288	17	42	53.8	-28	56	59		9.3	
289	17	42	53.8	-28	56	21	9.7	7.4	3
290	17	42	54.1	-28	53	11		9.4	
291	17	42	55.0	-28	50	11	8.0	6.4	6
292	17	42	55.1	-28	57	53	10.0	8.0	9
293	17	42	55.1	-28	52	12	10.0	8.8	3
294	17	42	55.3	-28	54	30	10.3	9.1	10

CATALOGUE OF H AND K SOURCES IN BLOCK 3

IRS	H	M	S	o	'	"	H	K	SEP
301	17	42	57.5	-28	48	39		7.5	
302	17	42	57.5	-28	47	34		7.2	
303	17	42	57.5	-28	46	21		9.2	
304	17	42	57.5	-28	45	1		8.9	
305	17	42	57.8	-28	42	19	8.5	7.4	6
306	17	42	58.0	-28	41	19		8.4	
307	17	42	58.5	-28	49	43		8.9	
308	17	42	58.5	-28	46	30		8.9	
309	17	42	58.9	-28	51	23	10.3	8.3	2
310	17	43	0.0	-28	50	24	9.6	9.3	9
311	17	43	0.3	-28	45	25		9.4	
312	17	43	0.7	-28	48	44	10.3	8.3	12
313	17	43	0.7	-28	46	6	9.9	9.1	6
314	17	43	0.7	-28	43	8		9.5	
315	17	43	1.2	-28	47	42		9.2	
316	17	43	1.2	-28	45	17		9.1	
317	17	43	1.7	-28	46	53	8.3	6.5	2
318	17	43	1.7	-28	51	37	8.8	7.1	2
319	17	43	2.1	-28	44	25		8.2	
320	17	43	2.1	-28	48	45	10.0		
321	17	43	3.2	-28	43	35	8.7	8.4	6
322	17	43	3.5	-28	47	17	10.4	8.3	12
323	17	43	3.5	-28	45	32	8.5	9.0	6
324	17	43	3.5	-28	51	33	9.6	8.5	12
325	17	43	3.9	-28	50	8	9.2	7.4	2
326	17	43	3.9	-28	44	12		9.2	
327	17	43	3.9	-28	42	56		8.4	
328	17	43	4.4	-28	48	21	8.5	<6.0	13
329	17	43	4.6	-28	46	6	9.6	8.4	6
330	17	43	5.8	-28	49	39		8.9	
331	17	43	5.8	-28	44	57		9.2	
332	17	43	6.0	-28	43	3	9.0	7.7	9
333	17	43	6.2	-28	51	15		9.1	
334	17	43	6.4	-28	41	45	10.0	8.5	6
335	17	43	6.7	-28	48	49	9.6	7.3	2
336	17	43	7.1	-28	50	24	9.4	7.5	2
337	17	43	7.1	-28	47	15	8.9	6.8	2
338	17	43	7.6	-28	45	17		8.5	
339	17	43	7.8	-28	43	17	9.8	7.5	6
340	17	43	9.9	-28	45	53		8.9	
341	17	43	10.6	-28	47	37	10.3	8.4	9
342	17	43	10.8	-28	42	1	10.0	8.0	12
343	17	43	11.0	-28	48	45	9.7	7.9	9
344	17	43	11.2	-28	50	34	8.9	7.3	2
345	17	43	11.9	-28	43	24	6.8	<6.1	9
346	17	43	12.6	-28	45	45		8.4	
347	17	43	13.1	-28	41	11		9.0	
348	17	43	13.3	-28	49	22	9.8	8.0	8
349	17	43	13.5	-28	42	32		9.2	
350	17	43	13.5	-28	47	22		7.8	
351	17	43	14.0	-28	50	51		8.8	
352	17	43	14.0	-28	49	35		8.4	
353	17	43	14.0	-28	49	9	10.4		

CATALOGUE OF H AND K SOURCES IN BLOCK 4

IRS	H	M	S	o	'	"	H	K	SEP
401	17	43	15.6	-28	35	18		8.2	
402	17	43	16.3	-28	38	6	10.1	8.5	7
403	17	43	16.5	-28	41	50	10.3		
404	17	43	16.5	-28	36	51	10.3		
405	17	43	17.0	-28	44	55	9.8		
406	17	43	17.0	-28	43	27	10.2	8.5	1
407	17	43	17.2	-28	36	39	9.8	8.3	9
408	17	43	18.2	-28	35	2	10.0	9.2	6
409	17	43	18.4	-28	41	46	9.8	7.8	14
410	17	43	18.4	-28	39	2	10.4	8.2	4
411	17	43	18.8	-28	43	57	9.1	7.5	12
412	17	43	19.3	-28	40	41	9.7	7.7	12
413	17	43	19.3	-28	35	31	10.4		
414	17	43	19.7	-28	36	6		9.4	
415	17	43	20.9	-28	40	17	7.7	7.3	6
416	17	43	21.1	-28	38	34	9.7	8.9	13
417	17	43	21.1	-28	34	32	7.7	7.1	3
418	17	43	21.6	-28	42	34	9.8		
419	17	43	21.6	-28	36	31	10.1		
420	17	43	22.0	-28	43	35		9.0	
421	17	43	22.5	-28	38	2	10.0	8.3	4
422	17	43	22.5	-28	37	15		9.3	
423	17	43	22.5	-28	36	6		8.3	
424	17	43	23.2	-28	34	34	10.1	8.5	6
425	17	43	23.4	-28	42	24	8.5	7.4	5
426	17	43	23.4	-28	39	12		9.1	
427	17	43	24.5	-28	41	18	9.9	8.3	6
428	17	43	24.8	-28	38	56	10.4		
429	17	43	24.8	-28	37	59	9.9		
430	17	43	24.8	-28	35	18	10.3	8.5	1
431	17	43	25.7	-28	37	51		8.4	
432	17	43	26.1	-28	39	28		8.7	
433	17	43	26.1	-28	35	40	9.9	8.1	12
434	17	43	26.6	-28	43	17	10.3	9.4	5
435	17	43	26.6	-28	37	3		7.9	
436	17	43	26.6	-28	36	47	10.0	7.9	7
437	17	43	26.6	-28	35	54		8.3	
438	17	43	27.0	-28	44	10	10.2		
439	17	43	27.0	-28	43	31		9.2	
440	17	43	27.0	-28	38	24	9.6	7.5	8
441	17	43	27.5	-28	42	39		8.8	
442	17	43	27.5	-28	42	27		8.9	
443	17	43	27.5	-28	40	21		9.1	
444	17	43	27.5	-28	36	46		9.1	
445	17	43	27.5	-28	35	42		8.2	
446	17	43	28.0	-28	40	9		8.9	
447	17	43	28.4	-28	44	16		9.3	
448	17	43	28.4	-28	37	48	9.1		
449	17	43	28.6	-28	37	35	9.0	7.3	6
450	17	43	29.3	-28	39	41		9.1	
451	17	43	29.8	-28	41	58		8.8	
452	17	43	29.8	-28	36	39		9.2	
453	17	43	30.2	-28	41	10		9.4	
454	17	43	30.4	-28	34	34	9.7	8.3	6
455	17	43	30.9	-28	40	15	9.5	9.4	7
456	17	43	31.4	-28	35	30	7.2	<6.3	6
457	17	43	31.6	-28	42	39		9.4	
458	17	43	31.6	-28	41	34		9.1	
459	17	43	31.6	-28	37	13	9.7	7.8	5

CATALOGUE OF K SOURCES IN BLOCK 16

IRS	H	M	S	°	′	″	K
1601	17	46	53.3	-27	24	25	9.5
1602	17	46	53.6	-27	17	14	8.7
1603	17	46	53.9	-27	25	13	9.4
1604	17	46	54.5	-27	23	2	9.1
1605	17	46	55.1	-27	26	35	9.2
1606	17	46	55.4	-27	25	39	9.4
1607	17	46	55.4	-27	25	8	9.3
1608	17	46	55.4	-27	24	3	9.2
1609	17	46	55.4	-27	18	45	9.1
1610	17	46	55.4	-27	17	27	6.4
1611	17	46	56.0	-27	14	51	9.4
1612	17	46	56.3	-27	15	43	8.9
1613	17	46	56.3	-27	23	33	9.0
1614	17	46	56.3	-27	22	58	9.2
1615	17	46	56.3	-27	17	45	8.7
1616	17	46	56.9	-27	26	9	9.4
1617	17	46	57.5	-27	25	13	8.6
1618	17	46	58.4	-27	20	25	9.4
1619	17	46	59.0	-27	17	10	9.5
1620	17	46	59.3	-27	17	53	9.3
1621	17	46	59.3	-27	20	38	9.5
1622	17	46	59.6	-27	24	46	9.2
1623	17	46	59.9	-27	25	47	9.1
1624	17	47	0.2	-27	15	30	8.9
1625	17	47	0.5	-27	17	27	8.4
1626	17	47	0.5	-27	21	5	7.6
1627	17	47	0.8	-27	21	48	9.2
1628	17	47	0.8	-27	20	4	9.3
1629	17	47	1.4	-27	24	21	8.2
1630	17	47	2.3	-27	17	49	9.1
1631	17	47	2.3	-27	22	49	8.5
1632	17	47	2.3	-27	21	18	9.5
1633	17	47	3.2	-27	18	41	9.0
1634	17	47	3.2	-27	21	53	8.5
1635	17	47	3.5	-27	23	46	8.9
1636	17	47	3.8	-27	24	33	9.0
1637	17	47	3.8	-27	22	18	8.6
1638	17	47	3.8	-27	21	26	9.1
1639	17	47	4.1	-27	16	22	8.8
1640	17	47	4.4	-27	20	25	8.9
1641	17	47	4.4	-27	18	19	9.3
1642	17	47	4.4	-27	21	9	9.3
1643	17	47	5.0	-27	23	2	9.1
1644	17	47	5.3	-27	19	59	7.5
1645	17	47	5.6	-27	22	45	8.9
1646	17	47	5.6	-27	24	46	9.2
1647	17	47	5.9	-27	22	10	9.2
1648	17	47	6.2	-27	25	13	8.3
1649	17	47	6.5	-27	19	20	8.6
1650	17	47	6.5	-27	18	28	9.2
1651	17	47	6.5	-27	23	11	8.1
1652	17	47	6.8	-27	17	49	8.9
1653	17	47	7.1	-27	23	50	9.3
1654	17	47	8.0	-27	23	24	7.0
1655	17	47	9.2	-27	14	59	6.0
1656	17	47	9.2	-27	23	50	8.6
1657	17	47	9.5	-27	17	36	9.1

CATALOGUE OF K SOURCES IN BLOCK 31

IRS	H	M	S	°	′	″	K
3101	17	51	25.5	-25	39	13	8.8
3102	17	51	25.5	-25	35	57	7.6
3103	17	51	26.4	-25	42	16	8.9
3104	17	51	26.4	-25	40	49	8.4
3105	17	51	26.4	-25	36	50	9.0
3106	17	51	27.0	-25	39	44	8.8
3107	17	51	27.3	-25	39	9	9.2
3108	17	51	27.6	-25	40	1	7.9
3109	17	51	27.6	-25	34	39	8.6
3110	17	51	28.5	-25	38	21	8.8
3111	17	51	29.3	-25	34	48	9.3
3112	17	51	29.3	-25	45	49	9.1
3113	17	51	29.3	-25	42	42	8.6
3114	17	51	29.6	-25	40	31	7.8
3115	17	51	30.2	-25	41	41	9.0
3116	17	51	30.8	-25	45	40	6.1
3117	17	51	30.8	-25	41	37	8.9
3118	17	51	31.7	-25	38	30	9.3
3119	17	51	32.3	-25	46	2	8.3
3120	17	51	32.3	-25	44	35	9.2
3121	17	51	32.3	-25	41	46	9.3
3122	17	51	33.5	-25	35	32	8.8
3123	17	51	33.5	-25	39	31	9.2
3124	17	51	34.6	-25	36	32	8.5
3125	17	51	34.6	-25	34	48	9.2
3126	17	51	34.7	-25	42	46	9.4
3127	17	51	34.7	-25	41	19	9.2
3128	17	51	35.9	-25	40	40	9.2
3129	17	51	36.1	-25	36	2	9.0
3130	17	51	36.1	-25	42	16	8.8
3131	17	51	36.5	-25	39	18	8.8
3132	17	51	36.5	-25	44	31	8.6
3133	17	51	37.6	-25	37	7	7.0
3134	17	51	37.9	-25	43	47	9.4

CATALOGUE OF H AND K SOURCES IN BLOCK 23

IRS	H	M	S	°	′	″	H	K	SEP
2301	17	49	2.8	-26	38	52	10.2		
2302	17	49	2.9	-26	30	2		9.3	
2303	17	49	3.2	-26	36	27		9.2	
2304	17	49	3.5	-26	32	25		9.4	
2305	17	49	3.7	-26	36	31	8.6	8.2	2
2306	17	49	3.8	-26	36	43		8.2	
2307	17	49	4.1	-26	32	9		9.2	
2308	17	49	4.4	-26	40	7	9.4	9.3	9
2309	17	49	4.4	-26	35	30	10.1	9.3	10
2310	17	49	5.0	-26	38	5	10.0	9.3	3
2311	17	49	5.5	-26	37	8	10.2	9.4	4
2312	17	49	5.9	-26	39	45	9.5		
2313	17	49	5.9	-26	31	6	9.0	9.0	1
2314	17	49	6.8	-26	31	42	10.1	7.9	1
2315	17	49	6.8	-26	34	24		9.2	
2316	17	49	7.7	-26	33	32		9.0	
2317	17	49	7.7	-26	32	35	10.5		
2318	17	49	8.0	-26	40	21	7.6	6.5	2
2319	17	49	8.2	-26	34	24	9.1	8.8	9
2320	17	49	8.3	-26	36	51		9.4	
2321	17	49	8.6	-26	31	15	9.9	9.2	3
2322	17	49	9.6	-26	37	31	10.2	9.4	4
2323	17	49	10.0	-26	34	24		8.3	
2324	17	49	10.9	-26	32	26	7.8	7.6	3
2325	17	49	10.9	-26	40	11	9.7	8.7	4
2326	17	49	11.0	-26	38	43	9.8	9.5	6
2327	17	49	11.4	-26	35	16	9.9	8.9	4
2328	17	49	11.8	-26	34	10	8.7	8.2	5
2329	17	49	12.1	-26	37	11	10.0		
2330	17	49	12.4	-26	32	21		9.0	
2331	17	49	12.7	-26	31	21		8.9	
2332	17	49	13.0	-26	35	34	9.4	9.3	6
2333	17	49	13.3	-26	40	33		9.1	
2334	17	49	13.7	-26	31	26	9.3	8.0	6
2335	17	49	14.1	-26	39	21	10.1	8.8	4
2336	17	49	14.2	-26	36	15		9.0	
2337	17	49	14.8	-26	31	45		9.3	
2338	17	49	15.1	-26	37	58		9.2	
2339	17	49	15.7	-26	38	48	10.2		
2340	17	49	16.0	-26	40	37		9.2	
2341	17	49	16.1	-26	33	46	9.4	8.5	4
2342	17	49	16.3	-26	33	56		9.1	
2343	17	49	16.5	-26	33	6	10.4	8.8	5
2344	17	49	17.7	-26	31	29	<6.4	<6.0	6
2345	17	49	18.6	-26	38	31	10.0	9.2	7
2346	17	49	18.9	-26	36	46	9.6	8.5	2
2347	17	49	19.0	-26	35	3		7.9	

CATALOGUE OF H AND K SOURCES IN BLOCK 32

IRS	H	M	S	°	′	″	H	K	SEP
3201	17	51	39.2	-25	37	38	9.5		
3202	17	51	39.2	-25	37	25	9.7		
3203	17	51	39.2	-25	30	2		8.1	
3204	17	51	39.2	-25	29	37	10.0		
3205	17	51	39.2	-25	28	47	10.0		
3206	17	51	39.7	-25	34	38		9.1	
3207	17	51	39.7	-25	33	18	9.7		
3208	17	51	39.7	-25	31	9		8.1	
3209	17	51	39.7	-25	30	48	8.4		
3210	17	51	41.0	-25	34	0		7.4	
3211	17	51	41.0	-25	33	50	8.3	7.2	4
3212	17	51	41.4	-25	34	48	9.4	8.1	4
3213	17	51	41.4	-25	29	24		9.4	
3214	17	51	41.7	-25	32	5	8.9	8.0	8
3215	17	51	41.9	-25	34	59		8.5	
3216	17	51	41.9	-25	33	39	9.0		
3217	17	51	41.9	-25	32	20		8.1	
3218	17	51	42.8	-25	33	31		8.4	
3219	17	51	43.2	-25	37	50		8.9	
3220	17	51	43.2	-25	30	21	9.5	8.7	13
3221	17	51	44.1	-25	39	10	9.3		
3222	17	51	44.1	-25	29	39	8.8	9.3	13
3223	17	51	44.3	-25	37	48	10.1	9.2	14
3224	17	51	44.6	-25	34	25	10.0		
3225	17	51	44.6	-25	31	21		7.1	
3226	17	51	44.6	-25	29	55	8.8	8.5	4
3227	17	51	44.8	-25	34	42	9.8	9.3	6
3228	17	51	45.7	-25	31	17	7.9	6.5	6
3229	17	51	46.6	-25	38	34	10.2	8.7	7
3230	17	51	46.8	-25	34	57	9.5	9.0	4
3231	17	51	47.0	-25	32	59	10.2	9.5	14
3232	17	51	47.0	-25	36	1	10.1	8.9	10
3233	17	51	47.2	-25	33	18		9.3	
3234	17	51	47.2	-25	28	34		8.4	
3235	17	51	47.2	-25	28	21		8.5	
3236	17	51	48.5	-25	35	53	10.2		
3237	17	51	49.4	-25	35	38	10.4	9.3	13
3238	17	51	49.4	-25	34	25		9.3	
3239	17	51	49.4	-25	31	23	9.3	8.2	13
3240	17	51	49.9	-25	32	32	10.0		
3241	17	51	49.9	-25	32	20	10.0		
3242	17	51	50.8	-25	35	11		9.4	
3243	17	51	50.8	-25	30	52	9.9	8.5	8
3244	17	51	51.2	-25	29	14	10.1	9.4	13
3245	17	51	52.1	-25	37	2	9.5	8.5	4
3246	17	51	52.3	-25	29	47	10.4	9.1	8
3247	17	51	52.3	-25	31	44	8.9	7.3	7
3248	17	51	52.5	-25	29	33	10.5		
3249	17	51	52.5	-25	28	51		9.1	
3250	17	51	52.6	-25	37	59		9.4	
3251	17	51	53.0	-25	30	21	10.0	7.9	4
3252	17	51	53.4	-25	35	28	10.2		
3253	17	51	53.4	-25	38	49	8.1	7.5	0
3254	17	51	53.9	-25	30	2	10.3		
3255	17	51	53.9	-25	32	5	10.0	9.2	13
3256	17	51	53.9	-25	36	14		8.6	
3257	17	51	53.9	-25	32	49	10.0	9.4	8
3258	17	51	54.3	-25	35	38	10.3	9.1	4
3259	17	51	54.7	-25	33	23	9.5	8.7	0
3260	17	51	54.7	-25	30	18	10.0		
3261	17	51	54.7	-25	29	33	9.1	7.5	0
3262	17	51	55.2	-25	35	20		9.4	

CATALOGUE OF K SOURCES IN BLOCK 40

IRS	H	M	S	°	′	″	K
4001	17	54	0.9	-24	44	53	9.3
4002	17	54	0.9	-24	36	35	9.3
4003	17	54	1.3	-24	40	11	8.4
4004	17	54	1.3	-24	34	5	4.6
4005	17	54	1.7	-24	42	54	8.3
4006	17	54	1.7	-24	37	15	8.9
4007	17	54	3.1	-24	34	5	9.3
4008	17	54	3.1	-24	39	49	8.9
4009	17	54	3.5	-24	41	43	9.1
4010	17	54	4.4	-24	33	39	9.3
4011	17	54	4.4	-24	44	39	9.0
4012	17	54	4.4	-24	43	29	9.1
4013	17	54	4.4	-24	35	11	7.6
4014	17	54	5.3	-24	40	51	7.3
4015	17	54	5.3	-24	39	22	9.1
4016	17	54	5.7	-24	34	53	9.4
4017	17	54	7.5	-24	41	39	8.9
4018	17	54	8.8	-24	40	46	7.9
4019	17	54	8.8	-24	39	27	9.0
4020	17	54	9.2	-24	36	57	9.0
4021	17	54	10.1	-24	35	24	9.2
4022	17	54	10.6	-24	34	9	8.1
4023	17	54	10.6	-24	39	14	8.5
4024	17	54	10.6	-24	44	39	9.4
4025	17	54	12.3	-24	36	35	8.6
4026	17	54	13.2	-24	38	16	8.3
4027	17	54	13.2	-24	40	37	9.4
4028	17	54	14.1	-24	34	9	8.5
4029	17	54	14.5	-24	36	53	9.0
4030	17	54	15.4	-24	35	20	8.5
4031	17	54	16.3	-24	36	44	8.7

CATALOGUE OF H AND K SOURCES IN BLOCK 42

IRS	H	M	S	°	′	″	H	K	SEP
4201	17	54	36.1	-24	28	4	8.7	7.6	6
4202	17	54	36.1	-24	25	4	10.3	9.1	0
4203	17	54	36.8	-24	26	0	9.5	9.0	6
4204	17	54	37.0	-24	29	3	9.9	8.7	3
4205	17	54	37.0	-24	22	19	9.6	8.5	3
4206	17	54	37.5	-24	30	14		9.4	
4207	17	54	37.5	-24	24	15	10.4		
4208	17	54	37.9	-24	27	11	10.3	9.2	3
4209	17	54	37.9	-24	25	7	10.3		
4210	17	54	39.2	-24	28	20	9.1	8.0	6
4211	17	54	39.2	-24	22	45		9.3	
4212	17	54	39.2	-24	21	37	10.4	9.2	6
4213	17	54	39.4	-24	30	50	10.3	8.6	10
4214	17	54	40.5	-24	22	14	10.2		
4215	17	54	40.8	-24	27	42	9.7	8.8	6
4216	17	54	41.2	-24	28	47	10.1	9.3	7
4217	17	54	41.4	-24	23	59	9.6	8.9	0
4218	17	54	41.8	-24	30	4	< 6.2	< 6.0	13
4219	17	54	41.8	-24	28	25	8.9		
4220	17	54	41.8	-24	24	55		9.4	
4221	17	54	43.2	-24	24	25	9.5	8.2	4
4222	17	54	43.4	-24	30	58	6.6	< 6.1	6
4223	17	54	44.3	-24	29	51	9.8	9.0	7
4224	17	54	44.7	-24	28	8	9.3	8.6	6
4225	17	54	45.1	-24	26	37	10.1	9.4	6
4226	17	54	45.1	-24	21	37	9.1	8.3	6
4227	17	54	45.4	-24	29	9		9.4	
4228	17	54	45.8	-24	22	46	10.0	9.4	1
4229	17	54	46.2	-24	24	55	7.1	< 6.3	0
4230	17	54	46.2	-24	24	6	7.2	6.8	0
4231	17	54	46.9	-24	31	27	6.8	< 5.9	6
4232	17	54	47.1	-24	27	7	9.6	8.6	2
4233	17	54	47.8	-24	23	6	9.5	9.0	6
4234	17	54	48.0	-24	28	26	9.6	8.3	3
4235	17	54	48.6	-24	23	56	10.1	8.8	8
4236	17	54	48.9	-24	29	37	8.3	6.9	1
4237	17	54	49.7	-24	25	32	10.1		
4238	17	54	50.2	-24	22	8		8.6	
4239	17	54	50.2	-24	20	59		9.4	
4240	17	54	50.2	-24	27	54	9.1	8.1	6
4241	17	54	51.3	-24	21	57	9.0	9.0	6
4242	17	54	51.5	-24	24	55	10.0	8.5	0
4243	17	54	51.5	-24	20	59		8.7	
4244	17	54	51.5	-24	27	30	9.3	9.3	6
4245	17	54	52.0	-24	30	14	6.7	6.6	0

CATALOGUE OF H AND K SOURCES IN BLOCK 52

IRS	H	M	S	o	'	"	H	K	SEP
5201	17	57	30.3	-23	13	13		8.1	
5202	17	57	30.8	-23	17	21	9.4		
5203	17	57	30.8	-23	11	54	9.8		
5204	17	57	31.4	-23	19	30	9.5	7.4	10
5205	17	57	31.6	-23	22	0	9.1	8.1	1
5206	17	57	31.8	-23	15	59	10.0	9.0	6
5207	17	57	32.7	-23	13	29	9.7	8.6	6
5208	17	57	33.0	-23	20	59	10.2	9.2	10
5209	17	57	33.0	-23	14	29	9.1	8.2	1
5210	17	57	33.4	-23	19	55	10.0	9.5	2
5211	17	57	33.4	-23	17	54	10.0	8.8	3
5212	17	57	33.8	-23	14	51	10.3		
5213	17	57	34.2	-23	16	35	9.9	9.2	7
5214	17	57	34.7	-23	22	13	8.6	7.8	2
5215	17	57	35.6	-23	19	36	9.5	8.3	5
5216	17	57	36.0	-23	22	0		7.4	
5217	17	57	36.6	-23	14	42	9.6	8.5	6
5218	17	57	36.9	-23	20	31	9.5		
5219	17	57	36.9	-23	18	40	9.0	7.9	3
5220	17	57	37.3	-23	21	53	9.4		
5221	17	57	37.3	-23	16	39	9.1	9.3	1
5222	17	57	37.3	-23	13	7	10.0		
5223	17	57	37.5	-23	17	31	9.1	7.9	6
5224	17	57	37.7	-23	11	24	10.1		
5225	17	57	37.7	-23	19	26	10.0		
5226	17	57	37.9	-23	14	9	9.0	8.4	9
5227	17	57	38.2	-23	15	51	10.4		
5228	17	57	38.6	-23	21	2	9.7	8.0	13
5229	17	57	38.6	-23	15	4	10.3		
5230	17	57	39.3	-23	21	58	9.8	9.1	7
5231	17	57	39.5	-23	17	32		9.5	
5232	17	57	39.7	-23	16	6	10.0	7.9	7
5233	17	57	40.3	-23	12	12		8.1	
5234	17	57	40.6	-23	18	46	10.0	9.3	9
5235	17	57	42.7	-23	19	24	9.6	8.4	7
5236	17	57	42.7	-23	18	0	10.1	8.8	6
5237	17	57	43.0	-23	21	23	8.2	7.3	1
5238	17	57	43.0	-23	17	9	10.0	8.3	0
5239	17	57	43.2	-23	12	47	8.8	7.8	7
5240	17	57	43.4	-23	11	24	9.1		
5241	17	57	44.3	-23	13	7	10.3		
5242	17	57	45.4	-23	18	59	9.8	8.9	7
5243	17	57	45.5	-23	12	20		9.3	
5244	17	57	45.6	-23	15	49	10.0	8.7	5
5245	17	57	46.0	-23	13	45		8.1	

CATALOGUE OF H AND K SOURCES IN BLOCK 56

IRS	H	M	S	o	'	"	H	K	SEP
5601	17	58	40.8	-22	48	36	9.1	8.1	5
5602	17	58	40.9	-22	49	41	8.2	7.3	2
5603	17	58	41.2	-22	54	40	10.1		
5604	17	58	41.2	-22	43	43	10.1	9.3	4
5605	17	58	41.8	-22	52	22	10.2		
5606	17	58	41.8	-22	51	13	10.4		
5607	17	58	42.1	-22	44	17	9.1	8.0	4
5608	17	58	42.4	-22	55	5	10.1	8.9	0
5609	17	58	42.5	-22	52	56	8.1	7.6	4
5610	17	58	42.7	-22	47	49	10.3	8.8	2
5611	17	58	43.0	-22	49	20	10.1	8.8	7
5612	17	58	43.0	-22	46	27	9.8	9.1	6
5613	17	58	43.6	-22	47	40	9.3	8.1	3
5614	17	58	43.6	-22	45	10	10.3		
5615	17	58	43.7	-22	54	13	9.0	8.0	4
5616	17	58	43.8	-22	43	58	9.3	8.4	1
5617	17	58	44.0	-22	54	57	9.5	8.4	4
5618	17	58	44.1	-22	52	42		9.5	
5619	17	58	44.1	-22	48	9		9.2	
5620	17	58	44.3	-22	48	45	8.7	7.5	5
5621	17	58	44.4	-22	47	19	7.5	7.1	3
5622	17	58	44.7	-22	50	8	10.4		
5623	17	58	44.7	-22	46	25	9.0	8.2	8
5624	17	58	45.0	-22	43	36	10.5		
5625	17	58	45.3	-22	44	54	7.8	6.6	1
5626	17	58	45.6	-22	46	9	8.3	7.4	10
5627	17	58	45.6	-22	43	31	10.5		
5628	17	58	45.9	-22	44	30	9.4	8.3	4
5629	17	58	46.2	-22	49	4	9.6	8.8	8
5630	17	58	46.3	-22	51	44	9.7	8.4	5
5631	17	58	46.7	-22	46	58	10.3		
5632	17	58	47.0	-22	51	26	10.5		
5633	17	58	47.0	-22	45	32	10.3		
5634	17	58	47.6	-22	48	23	10.5	9.2	6
5635	17	58	47.6	-22	43	31	10.4		
5636	17	58	47.7	-22	52	26	9.7	8.3	9
5637	17	58	48.8	-22	51	10	10.3	8.8	6
5638	17	58	49.6	-22	53	40		9.0	
5639	17	58	49.6	-22	49	42	10.1		
5640	17	58	50.2	-22	53	36		9.2	
5641	17	58	50.2	-22	52	41	9.3	8.0	5
5642	17	58	50.5	-22	50	0	9.8	8.0	1
5643	17	58	50.5	-22	46	41	9.5		
5644	17	58	50.5	-22	44	41	<6.0	2.5	8
5645	17	58	50.5	-22	43	27	10.4		
5646	17	58	51.1	-22	49	21	9.6	9.3	1
5647	17	58	51.4	-22	47	23		9.3	
5648	17	58	52.2	-22	53	18	10.3		
5649	17	58	52.4	-22	46	40	6.1	6.0	4
5650	17	58	52.4	-22	53	57	9.9	8.4	4
5651	17	58	52.8	-22	49	39		9.5	
5652	17	58	53.5	-22	52	40	9.5	9.2	5
5653	17	58	53.8	-22	44	26	9.4	8.5	6
5654	17	58	54.3	-22	51	58	9.9	8.8	1
5655	17	58	54.8	-22	52	7	9.9		
5656	17	58	55.0	-22	49	26	9.1	8.8	4
5657	17	58	55.4	-22	46	42	8.3	7.1	5
5658	17	58	55.7	-22	50	10		8.1	
5659	17	58	55.8	-22	51	19	9.9	8.7	10
5660	17	58	56.0	-22	45	12		9.2	

CATALOGUE OF H AND K SOURCES IN BLOCK 59

IRS	H	M	S	o	'	"	H	K	SEP
5901	17	59	32.2	-22	25	12	9.3		
5902	17	59	32.7	-22	31	48	9.7	8.8	0
5903	17	59	32.7	-22	27	11	8.5	7.1	4
5904	17	59	32.7	-22	23	59	10.1		
5905	17	59	33.5	-22	25	44		9.4	
5906	17	59	34.4	-22	33	23	8.4	7.4	4
5907	17	59	34.4	-22	30	47	9.8	8.8	0
5908	17	59	34.4	-22	29	14	8.6	8.0	0
5909	17	59	34.4	-22	27	33	9.7		
5910	17	59	34.6	-22	32	28	9.8	9.1	6
5911	17	59	34.8	-22	24	19	9.2	7.6	0
5912	17	59	35.3	-22	26	20		9.5	
5913	17	59	36.1	-22	25	12		9.0	
5914	17	59	37.4	-22	32	55	10.3	9.1	4
5915	17	59	37.4	-22	31	52		9.2	
5916	17	59	37.8	-22	24	11	10.0		
5917	17	59	38.3	-22	24	59		9.2	
5918	17	59	38.3	-22	30	19	10.4		
5919	17	59	39.2	-22	27	37		9.3	
5920	17	59	39.6	-22	30	7	9.5	8.2	0
5921	17	59	39.6	-22	29	14	9.4		
5922	17	59	40.9	-22	29	22	10.1	8.9	0
5923	17	59	40.9	-22	29	10		8.7	
5924	17	59	41.1	-22	33	45	10.1	9.3	6
5925	17	59	41.3	-22	32	19	8.6	7.6	4
5926	17	59	41.3	-22	26	34	9.7	8.2	12
5927	17	59	43.1	-22	29	30	10.5		
5928	17	59	43.7	-22	31	30	6.8	<6.0	7
5929	17	59	44.4	-22	23	59	8.4		
5930	17	59	44.4	-22	23	45	8.3	7.8	4
5931	17	59	44.6	-22	24	45	10.1	8.7	14
5932	17	59	44.8	-22	33	39	10.2	9.3	4
5933	17	59	45.4	-22	32	22	8.4	7.8	7
5934	17	59	45.6	-22	31	24	10.3		
5935	17	59	45.6	-22	26	12	10.1	8.9	0
5936	17	59	46.5	-22	27	31	10.3	8.1	4
5937	17	59	46.7	-22	30	43	10.4	8.9	6
5938	17	59	46.9	-22	28	26		9.4	
5939	17	59	47.4	-22	33	5	10.3		

CATALOGUE OF H AND K SOURCES IN BLOCK 62

IRS	H	M	S	o	'	"	H	K	SEP
6201	18	0	24.2	-22	2	42	10.1		
6202	18	0	24.7	-22	12	14	6.7	<6.2	4
6203	18	0	24.7	-22	9	9	10.4		
6204	18	0	25.1	-22	4	44		9.0	
6205	18	0	25.1	-22	2	52	10.3	8.3	3
6206	18	0	25.5	-22	8	41	10.3		
6207	18	0	25.5	-22	6	37	10.2		
6208	18	0	26.4	-22	9	45	10.0		
6209	18	0	26.4	-22	5	28		9.2	
6210	18	0	26.4	-22	4	3	8.9	7.7	10
6211	18	0	26.8	-22	11	28	10.2		
6212	18	0	27.5	-22	2	32	10.0	8.7	7
6213	18	0	27.9	-22	6	13	10.3	9.0	6
6214	18	0	27.9	-22	9	20	9.6	8.1	7
6215	18	0	28.1	-22	4	29	8.8	8.8	2
6216	18	0	28.3	-22	7	39	9.7	8.8	7
6217	18	0	28.6	-22	12	12	8.6	7.7	0
6218	18	0	29.0	-22	10	42	8.8	8.2	12
6219	18	0	29.2	-22	6	41	7.3	6.8	6
6220	18	0	29.4	-22	10	57	9.9		
6221	18	0	29.8	-22	5	14	10.2		
6222	18	0	29.9	-22	9	53	10.5		
6223	18	0	30.3	-22	4	26	10.1		
6224	18	0	30.9	-22	5	45	9.2	9.1	11
6225	18	0	31.1	-22	8	37	9.1	7.8	7
6226	18	0	31.1	-22	3	24	10.3	9.4	11
6227	18	0	32.0	-22	8	54		9.0	
6228	18	0	32.0	-22	12	8	<6.3	<6.1	0
6229	18	0	32.0	-22	10	44	10.2		
6230	18	0	32.4	-22	2	23		7.3	
6231	18	0	32.8	-22	7	37	10.2		
6232	18	0	32.8	-22	6	13	7.1	<6.1	1
6233	18	0	33.7	-22	3	26	10.4		
6234	18	0	34.1	-22	9	59	8.5	8.6	2
6235	18	0	34.1	-22	8	5	10.3		
6236	18	0	35.0	-22	7	3	10.0	8.7	4
6237	18	0	35.0	-22	4	6	10.2		
6238	18	0	35.3	-22	11	34	9.7	8.6	7
6239	18	0	35.5	-22	12	32	10.1		
6240	18	0	36.3	-22	4	59	9.3	8.0	12
6241	18	0	36.5	-22	9	33	9.9	8.8	9
6242	18	0	36.5	-22	7	43	8.9	8.1	7
6243	18	0	36.7	-22	10	40	9.4		
6244	18	0	36.7	-22	5	47	9.1	8.4	5
6245	18	0	36.7	-22	3	39	10.3	9.2	6
6246	18	0	37.6	-22	8	19	9.9	8.7	5
6247	18	0	38.0	-22	10	22	10.0	8.7	3
6248	18	0	38.0	-22	10	9	10.0		
6249	18	0	38.5	-22	7	15	8.8	8.8	4
6250	18	0	38.7	-22	5	19	7.8	7.2	8
6251	18	0	39.3	-22	11	36		9.5	
6252	18	0	39.3	-22	9	50	9.6	9.0	2
6253	18	0	39.8	-22	8	9	10.4		
6254	18	0	39.8	-22	6	17	10.4		
6255	18	0	39.8	-22	5	4		8.3	
6256	18	0	39.8	-22	3	37	10.4	9.3	3

CATALOGUE OF H AND K SOURCES IN BLOCK 72

IRS	H	M	S	o	'	"	H	K	SEP
7201	18	3	15.7	-20	53	27	9.5		
7202	18	3	16.0	-21	1	6	9.9		
7203	18	3	16.2	-20	55	44	10.5		
7204	18	3	16.5	-20	56	48	10.5		
7205	18	3	16.5	-20	54	3	10.4		
7206	18	3	16.8	-21	0	42	10.3		
7207	18	3	17.1	-20	58	57	10.4		
7208	18	3	17.1	-20	58	13	9.8		
7209	18	3	17.4	-20	52	10	7.6		
7210	18	3	17.7	-20	59	54	7.9		
7211	18	3	18.0	-21	1	50	10.2		
7212	18	3	19.7	-20	58	29	10.2		
7213	18	3	19.7	-20	57	45	10.5		
7214	18	3	20.0	-20	54	55	10.1		
7215	18	3	20.5	-21	1	42	9.5		
7216	18	3	20.5	-21	0	54	10.4		
7217	18	3	21.1	-21	0	1	9.3		
7218	18	3	21.1	-20	57	12	10.3		
7219	18	3	21.7	-21	2	2	10.5		
7220	18	3	21.7	-20	56	20	10.4		
7221	18	3	21.7	-20	55	28	10.5		
7222	18	3	22.5	-20	54	35	10.3		
7223	18	3	23.1	-20	58	35	9.0	8.1	4
7224	18	3	23.3	-21	0	39	10.2	9.2	4
7225	18	3	23.6	-20	52	43	10.3	8.7	6
7226	18	3	24.0	-21	1	33	9.7	9.3	4
7227	18	3	24.3	-20	55	8	9.3	7.9	3
7228	18	3	24.8	-20	59	37	10.3		
7229	18	3	25.0	-21	2	17	8.7	8.5	6
7230	18	3	25.1	-20	57	7	10.4	9.3	9
7231	18	3	26.2	-21	1	6		7.6	
7232	18	3	26.2	-20	58	32		8.8	
7233	18	3	26.5	-20	54	19	10.4	7.5	14
7234	18	3	27.0	-20	52	45		9.5	
7235	18	3	29.2	-20	59	59		9.3	
7236	18	3	29.2	-20	57	1		7.6	
7237	18	3	29.6	-20	59	5		8.9	
7238	18	3	30.0	-20	55	43		9.2	
7239	18	3	30.4	-20	58	45		7.3	

CATALOGUE OF K SOURCES IN BLOCK 70

IRS	H	M	S	o	'	"	K
7001	18	2	42.3	-21	15	30	8.6
7002	18	2	42.3	-21	12	1	8.3
7003	18	2	42.3	-21	11	30	8.2
7004	18	2	42.3	-21	7	21	8.6
7005	18	2	42.8	-21	10	34	8.1
7006	18	2	43.1	-21	13	15	8.9
7007	18	2	43.7	-21	12	53	9.1
7008	18	2	43.7	-21	8	44	6.7
7009	18	2	44.5	-21	10	29	9.1
7010	18	2	44.6	-21	16	53	9.3
7011	18	2	44.6	-21	13	45	7.6
7012	18	2	44.6	-21	12	9	9.0
7013	18	2	45.1	-21	9	54	7.8
7014	18	2	45.7	-21	11	30	<5.7
7015	18	2	46.0	-21	6	24	9.1
7016	18	2	46.6	-21	15	39	8.1
7017	18	2	46.6	-21	14	38	9.1
7018	18	2	46.8	-21	5	41	8.2
7019	18	2	46.8	-21	13	37	8.5
7020	18	2	46.8	-21	12	18	8.2
7021	18	2	46.8	-21	9	41	8.7
7022	18	2	47.1	-21	6	55	8.6
7023	18	2	47.7	-21	8	48	8.7
7024	18	2	47.7	-21	6	38	9.2
7025	18	2	48.3	-21	5	15	7.8
7026	18	2	48.5	-21	7	21	8.3
7027	18	2	49.4	-21	16	14	8.9
7028	18	2	49.7	-21	9	6	8.8
7029	18	2	50.3	-21	11	21	8.6
7030	18	2	50.3	-21	14	59	9.2
7031	18	2	51.1	-21	12	18	8.7
7032	18	2	51.4	-21	9	41	8.8
7033	18	2	51.4	-21	7	8	9.1
7034	18	2	51.4	-21	11	43	9.4
7035	18	2	51.7	-21	15	39	8.5
7036	18	2	51.7	-21	10	59	8.6
7037	18	2	52.6	-21	12	18	9.3
7038	18	2	52.8	-21	5	19	7.7
7039	18	2	53.1	-21	7	48	8.9
7040	18	2	53.7	-21	16	49	9.0
7041	18	2	53.7	-21	15	13	7.7
7042	18	2	54.0	-21	7	4	8.7
7043	18	2	54.6	-21	9	32	7.6
7044	18	2	54.6	-21	8	57	8.6
7045	18	2	55.1	-21	8	40	9.5
7046	18	2	55.4	-21	12	1	7.6
7047	18	2	56.0	-21	14	25	9.1
7048	18	2	56.6	-21	9	45	8.9
7049	18	2	56.9	-21	16	14	9.2
7050	18	2	57.1	-21	10	20	8.2
7051	18	2	57.1	-21	9	28	8.8
7052	18	2	57.1	-21	15	4	8.5
7053	18	2	57.4	-21	14	20	8.7
7054	18	2	58.0	-21	10	47	9.3

APPENDIX B

PUBLICATIONS

I have contributed to the following research papers. Copies of numbers (1) and (6) are attached below.

(1) 'IR flashes from the X-ray Rapid Burster'
A W Jones, M J Selby, C M Mountain, R Wade, C Sánchez Magro and M Prieto Muñoz.
Nature, 283, 550-551 (1980).

(2) 'Infrared bursts from the X-ray Rapid Burster'
A W Jones, M J Selby, C Martinez Roger, C Sánchez Magro, P V Kulkarni and N M Ashok.
Paper read by C Sánchez at the Fifth European Regional Meeting on Astronomy (Variability in Stars and Galaxies), Liege, July 1980.

(3) 'Observaciones en el infrarrojo de fuentes eruptivas de rayos X'
C Martinez Roger, C Sánchez Magro, A W Jones and M J Selby.
Paper read by C Martinez at the III Asamblea Nacional de Astronomia y Astrofisica, Almeria, September 1980.

(4) 'Destellos en el infrarrojo de MXB 1730-335'
C Martinez Roger.
Dissertation, Universidad de La Laguna, June 1981.

(5) 'X-ray, radio and infrared observations of the Rapid Burster (MXB 1730-335) during 1979 and 1980'
A Lawrence et 51 al, including A W Jones, M J Selby, C Martinez Roger and C Sánchez Magro.
To be submitted to the Astrophysical Journal, Spring 1982.

(6) 'Quasars near companion galaxies: a reappraisal'
A W Jones.
Submitted to the Astrophysical Journal (Letters), December 1981.

IR flashes from the X-ray rapid burster

A. W. Jones, M. J. Selby, C. M. Mountain & R. Wade

Astronomy Group, Blackett Laboratory, Imperial College, London SW7 2BZ, UK

C. Sánchez Magro & Mercedes Prieto Muñoz

Instituto de Astrofísica de Canarias, Universidad de La Laguna, Teberife Spain

We confirm here the report of Kulkarni *et al.*[1] who discovered IR bursts from the X-ray rapid burster, MXB1730−335. We observed two bursts at 2.2 μm, each of energy $\sim 10^{31}$ J, and a new feature; several bright, brief flashes ($\Delta t < 1$ s) superimposed on the burst continuum. The brevity, luminosity and inferred brightness temperature of the flashes ($T_B \geq 10^{10}$ K) imply a powerful, non-thermal emission mechanism. Simultaneous observations across the whole spectrum with high time resolution would be invaluable in understanding the emission process.

The rapid burster was discovered in 1976 by Lewin *et al.*[2] at MIT and is unique in producing $\sim 10^3$ X-ray bursts a day in its active periods. These periods occur about every 6 months and last 2–6 weeks[3]. Liller[4], and Kleinmann *et al.*[5] have shown that the source lies in a compact globular cluster, now called Liller 1, at a distance of 10 kpc. By 1978 it had become clear that the same cluster also produces 'special' bursts[6], similar to those from the more usual X-ray burst sources. They are characterised by a softening of the X-ray spectrum during decay and are now known as Type I bursts. The rapid bursts are classified as Type II. In April 1979 Kulkarni *et al.*[1], observing from Kavalur in India, detected six bursts at 1.6 μm which they attributed to the Type I X-ray bursts.

On 8 August 1979 Type II bursts were seen by the X-ray satellite Hakucho[7], heralding a new period of activity. We attempted IR observations in early September using the 1.5 m IR flux collector at Izaña, Tenerife. The detector was an indium antimonide diode cooled to 75 K. The cooled filter had an effective wavelength of 2.2 μm and a bandwidth of 0.4 μm. We used a two-mirror focal plane sky chopper[8] at 20 Hz, with one beam (20 arc s diameter) centred on Liller 1 and the reference beam 20 arc s to the north. For calibration we used ϕ Ophiuchi ($m_K = 2.27$) taking its flux as $F_\lambda = 4.8 \times 10^{-11}$ W m^{-2} μm^{-1} in accordance with Johnson's[9] absolute flux calibration.

Table 1 lists the dates and times of our observing periods; a total of 5 h 15 min. In this time we saw only two bursts, 1 min apart, on 5 September 1979 (Kulkarni *et al.* saw six in 2.5 h). The chart recording of the bursts is shown in Fig. 1. They appeared at 21 h 04 min 01 s and 21 h 04 min 55 s UT ± 1 s, and lasted 20 s and 10 s respectively. They are similar in shape to the Kavalur bursts, except for the seven sharp spikes accompanying them. Our nominal time resolution, set by the output filter of our phase-sensitive detector (PSD) was 0.3 s, but the widths of two of the spikes (1d and 2c) remain unresolved (see Table 2). The negative-going spike, marked A in Fig. 1, is probably an artefact of the PSD caused by a sudden, rapidly increasing signal. We have been able to reproduce this feature with a laboratory PSD. The other spikes do not seem to be spurious. They appear nowhere else on the chart trace and are closely associated with the structure of the bursts. Assuming they are real, we can properly describe them as flashes.

Table 1 IR observations of the rapid burster

Date (September 1979)	Times (UT) Start (h min)	Finish (h min)	Duration (h min)	No. of bursts
5	20 50	22 10	1 20	2
6	20 20	22 05	1 45	0
11	21 10	21 45	0 35	0
12	20 05	21 40	1 35	0
		Total	5 15	2

In Table 2 we list some observed and derived characteristics of the flashes assuming a distance of 10 kpc and an interstellar absorption of 1.1 mag (ref. 5). With the data from Table 2 and Fig. 1 we can make the following observations.

Why are IR bursts visible at all? The MIT group[10] have measured the spectra of several X-ray bursts, both Type I and Type II, and have fitted them to black-body curves of temperature $T \approx 2 \times 10^7$ K. The inferred radius of the X-ray emitting region is $R \approx 10^4$ m. If we extrapolate the black-body spectrum into the IR we would expect a flux $F_\lambda \sim 10^{-23}$ W m^{-2} μm^{-1} at 2.2 μm; a factor of 10^{11} below our observed value.

Two of the flashes are unresolved at our instrumental time resolution of 0.3 s, putting an upper limit on the size of the emitting region of $R = 10^8$ m. This implies an IR brightness temperature $T_B \geq 4 \times 10^{10}$ K. If we assume that the IR radiation is coming from the same small region as the X rays, T_B rises to an improbable 4×10^{18} K.

If the radiation is isotropic, then the IR burst energies in our 0.4-μm bandwidth are 9×10^{30} J and 6×10^{30} J, and the peak luminosity is 2.2×10^{30} W. This compares with $\sim 10^{32}$ J and $\sim 10^{31}$ W for the Type I X-ray bursts[3].

It may be significant that the three flashes in each burst occur at similar times after the initial rise (see Table 2), except

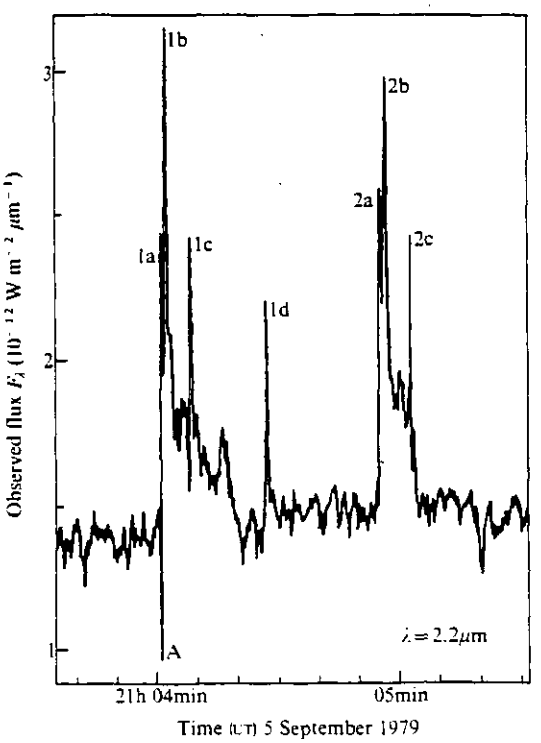

Fig. 1 Two IR bursts from the X-ray rapid burster, accompanied by seven brief flashes. The flux scale is not corrected for interstellar absorption. The feature at A is an artefact of the detection system.

Table 2 Details of the IR flashes

Flash no.	Time of peak (s±0.1)	Half-peak width (s±0.1)	In bandwidth 0.4 μm Luminosity (10^{30} W)	Energy (10^{30} J)
1a	0.0	0.5	1.3	0.6
1b	1.2	0.9	2.2	1.9
1c	7.0	0.8	1.3	1.0
1d	25.7	0.3	1.0	0.3
2a	54.2	0.6*	1.4	0.8
2b	55.6	1.5	1.9	2.8
2c	61.7	<0.3	1.2	<0.4

The half-peak widths, luminosities and energies were measured with respect to the background on either side of each burst. Isotropic radiation is assumed.
*This is the rise time: the half-peak width cannot be measured.

for the solitary flash 1d, which occurs in the space between the bursts.

Although we observed for 5 h 15 min the bursts appeared in the space of 1 min, suggesting that they may be physically associated. Kulkarni *et al.* noted similar groupings among some, but not all, of their bursts.

There are no clear spikes in the Kavalur bursts, but they did have a lower time resolution (0.6 s) and the signals were 2 or 3 times noisier than ours. It is not clear whether flashes would have been detected if they were there. The difference in wavelength could also be important. If the spectral index of the flashes is different from that of the burst continuum, then the flashes may be apparent at one wavelength but not at another.

We do not intend to go into the details of possible mechanisms, but we conclude: (1) As there have been no simultaneous X-ray/IR observations, we cannot say for certain that our bursts correspond to X-ray bursts; Type I X-ray bursts recur at intervals of hours, while the Type II bursts repeat at intervals of seconds or minutes. The IR bursts observed so far do not fit either category.

(2) If our observations do correspond to X-ray bursts, then the high brightness temperature and unexpectedly intense IR flux strongly suggest a non-thermal emission mechanism. The favoured explanation of the Type I X-ray bursts is a thermonuclear helium flash in accreted material on a neutron star[3,11]. This accounts for the observed X-ray behaviour very well, but does not predict an observable IR flux. Apparao and Chitre[12] propose that the IR bursts are produced by a 'cyclotron maser' operating above the poles of a magnetised neutron star in a close binary system.

Further observations at IR wavelengths should attempt time resolutions of <0.1 s to detect and resolve the flashes. Simultaneous observations at X-ray, optical and several IR wavelengths would be invaluable in understanding the emission process.

We thank Professor P. V. Kulkarni and N. M. Ashok for details of their bursts, and Professor F. Sánchez Martinez of the Cabezon Observatory of the Instituto de Astrofísica de Canarias, La Laguna, for cooperation. A.W.J. and C.M.M. were supported by SRC research studentships and R.W. by an SRC research fellowship.

Received 5 November; accepted 20 December 1979.

1. Kulkarni, P. V., Ashok, N. M., Apparao, K. M. V. & Chitre, S. M. *Nature* **280**, 819–820 (1979).
2. Lewin, W. H. G. *et al. Astrophys. J. Lett.* **207**, L95–L99 (1976).
3. Lewin, W. H. G. in *X-Ray Astronomy* (eds Baity, W. A. & Peterson, L. E.) 133–149 (Pergamon, Oxford, 1979).
4. Liller, W. *Astrophys. J. Lett.* **213**, L21–L23 (1977).
5. Kleinmann, D. E., Kleinmann, S. G. & Wright, E. L. *Astrophys. J. Lett.* **210**, L83–L86 (1976).
6. Hoffman, J. A., Marshall, H. L. & Lewin, W. H. G. *Nature* **271**, 630–633 (1978).
7. Oda, M. *IAU Circ.* No. 3392 (1979).
8. Selby, M. J., Wade, R. & Sánchez Magro, C. *Mon. Not. R. astr. Soc.* **187**, 553–566 (1979).
9. Johnson, H. L. *A. Rev. Astr. Astrophys.* **4**, 193–206 (1966).
10. Marshall, H. L., Ulmer, M. P., Hoffman, J. A., Doty, J. & Lewin, W. H. G. *Astrophys. J.* **227**, 555–562 (1979).
11. Joss, P. C. *Comments Astrophys.* **8**, 109–118 (1979).
12. Apparao, K. M. V. & Chitre, S. M. Preprint (1979).

(Reprinted from Nature, 283, 550-551, February 7 1980)

Printed in Great Britain by Macmillan Production Ltd., Basingstoke, Hampshire

QUASARS NEAR COMPANION GALAXIES: A REAPPRAISAL

A. W. JONES

Blackett Laboratory, Imperial College, London

Submitted to the Astrophysical Journal (Letters)
Received 1981 December 28, revised 1982 March 31

ABSTRACT

Near a sample of 34 companion galaxies, Arp (1981) has found 13 quasars with a combined probability of $\sim 10^{-17}$ of being chance associations. Quasar background densities of $N(20) > 100$ deg^{-2} would be required to bring this probability to a more reasonable level. This Letter argues that both these figures are almost entirely spurious. They are effects of rounding errors, adoption of lower limits for individual probabilities and an arbitrary definition of a close association. A better estimate of the combined probability is ~ 0.2, with $N(20) \lesssim 12$ deg^{-2}.

I. INTRODUCTION

Although the Hubble Law is now generally accepted, there is still controversy over whether all redshifts can be interpreted in this way. In particular the high redshifts of quasars ($z \gtrsim 0.1$), which imply extreme luminosities ($\sim 10^{40}$ W), are not yet corroborated by independent measurements of distance.

One approach to testing the universality of the Hubble Law is to look for apparent physical associations between objects of differing redshift. Interacting galaxies, rows of quasars, or quasars improbably close to low-redshift galaxies, have all been examined with this in mind. If two objects of different redshift can be shown to be at similar distances, then at least one of the redshifts cannot be wholly understood as a consequence of the Hubble expansion (the classic discussion on this is Field, Arp and Bahcall 1973). The difficulty with this approach is to distinguish a physical association from a chance line-of-sight alignment between objects at different distances. In general, this can only be done in a statistical sense; that is, by demonstrating that the frequency of observed associations is significantly greater than would be expected from chance alignments alone.

Recently Arp (1981) has tested his hypothesis that quasars tend to be associated with low-redshift companions to non-elliptical galaxies. He reports that in a sample of 34 companion galaxies he found 13 quasars, each close enough to a galaxy to have a probability of ≤ 0.01 of being there by chance. The combined probability of all these associations being chance is $\sim 10^{-17}$. Background quasar densities of > 100 deg^{-2} down to magnitude 20 would be required to bring this probability to a reasonable level. In this Letter I reanalyse Arp's data and argue that these two figures are almost entirely spurious.

II. REANALYSIS OF ARP'S DATA

We first rework Arp's calculation according to the method described in his paper and using the data from his Table 1.

A quasar of magnitude m is observed at an angular distance r from a galaxy. We wish to know the probability of this event occurring by chance. As there is no meaning to the probability of a quasar having a precise position and brightness, the best we can do is to calculate the probability of finding a quasar within some defined area and magnitude range. If quasars are distributed randomly and uniformly on the sky, then in an area A the expected number of quasars is NA, where N is the mean number per unit area. From Poisson statistics the probability of finding one or more quasars in A is

$$p(NA) = 1 - e^{-NA} \approx NA \quad (\text{for } NA \ll 1). \tag{1}$$

Following Arp for the present, we calculate the probability $p(r,m)$ of finding quasars closer than r and brighter than m from

$$p(r,m) = p(NA), \quad \text{where } NA = \pi r^2 N(20)\, 4^{m-20} \quad \text{and } N(20) = 10 \text{ deg}^{-2} \tag{2}$$

Where a range of m is given for a quasar, we take the lower value. The factor of 4 is an empirical scaling factor for the sky density of quasars.

Arp defines a "success" (i.e. an association) as a quasar with $p(r,m) \leq 0.01$. The 12 companion galaxies with 13 associated quasars are identified in columns 1, 2 and 3 of Table 1. Column 4 gives the p(r,m) quoted in Table 1 of Arp (1981). Column 5 lists p(r,m) calculated from equation (2), but given to two significant figures rather than to one only. This is the only evident difference between the present calculation and that of Arp (however, some of the figures in columns 4 and 5 have discrepancies over and above rounding errors). We note that the number of successes has fallen from 13 to 6 (none of Arp's "failures" becomes a success after this reworking).

Arp then uses the binomial distribution to estimate the combined probability of these associations occurring by chance. The form of the distribution is

$$P(q) = P(p_o,n,q) = \frac{n!}{q!(n-q)!} p_o^q (1-p_o)^{n-q} \qquad (3)$$

where $P(p_o,n,q)$ is the probability that a random sample of n objects will contain q marked items, when the proportion of marked items in the parent population is p_o. Arp puts n = 34 as the number of galaxies in the sample and $p_o = 0.01$ as the proportion of all galaxies with quasars close enough to be defined as "associated" (by a self-consistent argument). However, he identifies q with the number of associated quasars (13), rather than the number of galaxies with quasars (12). The sample consists of galaxies, not quasars. $P(12) = 4 \times 10^{-16}$, which is slightly larger than Arp's result, but putting in q = 6 from Table 1 we have $P(6) = 1 \times 10^{-6}$, some eleven orders of magnitude higher than Arp's 10^{-17}.

We now reconsider the two variables defining the probability in equation (1) : the area A, and the quasar sky density N.

Arp uses $A = \pi r^2$, which gives the probability of finding a quasar anywhere within a circle of radius r. But the quasar is on the edge of this circle, so A is the smallest area that still encloses it. Probabilities calculated with this A are therefore lower limits.

I propose that a better choice of A is $2\pi r^2$. This gives the probability of finding a quasar anywhere inside a circle of radius $\sqrt{2}r$, and therefore an equal probability of it being either closer or further than r. Column 6 of Table 1 lists p(r,m) calculated with this A. The number of successes reduces from 6 to 3, with a combined probability of $P(3) = 4 \times 10^{-3}$.

Next we consider Arp's correction for the magnitude of the quasar. Although there is a smaller chance of finding a bright quasar close to a galaxy than a faint one (because there are fewer bright ones), it does not follow that the sky density should be scaled to N(m). This gives the probability of observing a quasar of magnitude m or brighter, and so is the smallest N consistent with the quasar being seen at all. Probabilities calculated with N(m) are, once again, lower limits.

To avoid this pitfall we must assume that the environs of each galaxy were searched to some limiting quasar magnitude m_L (which could be different in each area). The appropriate sky density is then $N(m_L)$. Although Arp does not give any values of m_L, he does say that his investigation was "as complete as possible" in the sample of 34 galaxies. Since he lists quasars to $m \approx 20$, it seems reasonable to put $m_L = 20$ and use $N = N(20)$ to recalculate p(r,m), retaining $A = 2\pi r^2$. Column 7 in Table 1 shows that only one of the original successes survives, with a combined probability of $P(1) = 0.24$.

Similar results are obtained if the "success" criterion is varied. For example, we can choose $p_o = 0.005$ and find $P(q) = 6 \times 10^{-4}$, 0.01 and 0.84 for the three stages of the calculation corresponding to columns 5, 6 and 7. Similarly, if $p_o = 0.02$, then $P(q) = 5 \times 10^{-14}$, 5×10^{-5} and 0.12. It is curious that the less stringent criteria produce smaller combined probabilities.

Finally, we examine Arp's claim that sky densities of $N(20) > 100$ deg^{-2} are required for his associations to be chance. If we assume that the surroundings of each galaxy were searched out to the distance of its furthest quasar, then the total search area for the 27 quasars is 2.05 deg^2. In this region there are 24 quasars of $m \leq 20$, and so $N(20) = 12 \pm 2$ deg^{-2} (Poisson error). This is an upper limit because we do not know how much more sky was observed without finding quasars. It compares with 10 deg^{-2} assumed in Arp (1981) and in this Letter, and with 6-7 deg^{-2} reported in the unspecified control fields. On the face of it, there seems no need to postulate $N(20) >$ 100 deg^{-2} to account for the observed number of quasars.

III. DISCUSSION

Arp's impressively small combined probability of 10^{-17} is largely an artifact arising from rounding off $p(r,m)$ to 0.01 and adopting $p(r,m) \leq 0.01$ as the criterion for a "success". By simply carrying another decimal place in the calculation we can raise this probability by eleven orders of magnitude. With the correction of two sources of bias the combined probability becomes an unremarkable ~ 0.2.

This alarming range of results from the same data is a consequence of a fundamental flaw in this method of analysis. It is not logically sound to calculate the prior probability of an event using information that can only be known after the event. Therefore, the magnitude and distance of an observed quasar should not enter into the calculation of p ($p \neq p(r,m)$). The only strictly correct choice of A and N is the pre-determined search area around each galaxy, and the sky density corresponding to the pre-determined magnitude limit of the survey.

Unfortunately, Arp's paper does not provide the information required for a correct assessment. It is difficult to decide how many galaxies have been searched (34 appears to be an upper limit) and to what extent. Arp does not state his search procedure, nor the area searched around each galaxy, nor the limiting magnitude for the detection of quasars in each area. Therefore, we cannot be sure that either the companion galaxies or the quasars are random selections from their parent populations.

IV. CONCLUSIONS

1. Arp's combined probability of $\sim 10^{-17}$ that his observed arrangement of quasars and galaxies is random is almost entirely spurious. This small figure is an effect of rounding errors, adoption of lower limits on individual probabilities, and an arbitrary choice of what constitutes a "success". A strict replication of Arp's analysis produces a figure of $\sim 10^{-6}$.

2. Attempts to rework the analysis without these biases have resulted in combined probabilities > 0.1.

3. An estimate on the quasar sky density near the galaxies is $N(20) \lesssim 12\ \mathrm{deg}^{-2}$. This is consistent with the values adopted by Arp for his calculation, and with those measured in his control fields. There is no need to postulate $N(20) > 100\ \mathrm{deg}^{-2}$ to account for the observed number of quasars.

4. The present method of analysis is logically flawed. Although there may be a prima facie case for quasar-galaxy associations, a correct analysis is hindered by the uncertainties surrounding the data as presented in Arp (1981).

I wish to thank Dr N. A. Robertson for the help of her clear thinking, and Dr R. D. Joseph for encouraging me to write this paper.

REFERENCES

Arp, H. 1981, Ap. J., 250, 31.
Field, G. B., Arp, H., and Bahcall, J. N. 1973, The Redshift Controversy (Reading, Massachusetts: Benjamin).

TABLE 1

REANALYSIS OF THE 13 QUASAR-GALAXY ASSOCIATIONS IN ARP(1981)

MAIN GALAXY (NGC) (1)	COM-PANION (2)	QUASAR (3)	PROBABILITIES p(r,m) Arp (1981) (4)	Reworked to 2 s.f. (5)	$A = 2\pi r^2$ (6)	N = N(20) (7)
2549	1	BSO 1	0.01	0.0094	<u>0.019</u>	
2639	1	UB1	0.01	<u>0.016</u>		
2681	1	0846+51W1	0.001	8.7×10^{-5}	0.00017	0.00070
2701	1	UB1	0.01	<u>0.013</u>		
2841	1	UB2	0.01	<u>0.016</u>		
		UB3	0.0002	0.00092	0.0018	<u>0.21</u>
2859	1	UB1	0.004	0.0029	0.0057	<u>0.017</u>
	2	UB2	0.01	0.0069	<u>0.014</u>	
	3	UB3	0.01	<u>0.019</u>		
2903	1	UB2	0.01	<u>0.012</u>		
3031	1	0959+68W1	0.006	<u>0.024</u>		
3079	1	UB1	0.01	0.0060	<u>0.012</u>	
3184	1	UB4	0.009	<u>0.013</u>		
Number of "successes", q			12	6	3	1
Combined probabilties P(q)			4×10^{-16}	1×10^{-6}	4×10^{-3}	0.24

NOTE. - A "success" is defined as a galaxy with a quasar with $p(r,m) \leq 0.01$. Probabilities which fail to meet this criterion are set in italic.

REFERENCES

Allen, D A, 1973. Near infrared magnitudes of 248 early type emission line stars and related objects. Mon Not R Astron Soc, 161, 145-166.

Apparao, K M V, & Chitre, S M, 1980. Infrared bursts from Liller I/ MXB 1730-333. Astrophys Sp Sci, 72, 127-132.

AQ = Allen, C W, 1973. Astrophysical Quantities (3rd ed). Athlone Press, London.

Arp, H, 1965. Properties of the galactic nucleus in the direction of NGC 6522. Astrophys J, 141, 43-72.

Becklin, E E, & Neugebauer, G, 1967. Observations of an infrared star in the Orion Nebula. Astrophys J, 147, 799-802.

Becklin, E E, & Neugebauer, G, 1968. Infrared observations of the galactic center. Astrophys J, 151, 145-161.

Becklin, E E, & Neugebauer, G, 1969. 1.65 - 19.5 micron observations of the galactic center. Astrophys J (Letters), 157, L31-L36.

Becklin, E E, et al, 1978. Infrared observations of the galactic center. IV. The interstellar extinction. Astrophys J, 220, 831-835.

Blanco, V M, 1965. Distributions and motions of late-type giants. In: Blaauw, A, & Schmidt, M (eds). Galactic Structure (Stars and Stellar Systems Vol 5). University of Chicago Press, Chicago.

Bok, B J, 1937. The Distribution of the Stars in Space. University of Chicago Press, Chicago.

Bracewell, R, 1965. The Fourier Transform and its Applications. McGraw-Hill.

Brault, J W, & White, O R, 1971. The analysis and restoration of astronomical data via the Fast Fourier Transform. Astron Astrophys 13, 169-189.

Cline, T L, et al, 1980. Detection of a fast, intense and unusual gamma-ray transient. Astrophys J (Letters), 237, L1-L5.

Cominsky, L, et al, 1980. A search for pulsations and eclipses from X-ray burst sources. Astrophys J, 242, 1102-1106.

Grasdalen, G L, & Gaustad, J E, 1971. A comparison of the Two-Micron Survey with the Dearborn Catalogue of faint red stars. Astron J, 76, 231.

Hackwell, J A, et al, 1979. The detection of an optical burst coincident with an X-ray burst from MXB 1837+05 (Ser X-1). Astrophys J (Letters), 233, L115-L119.

Harwit, M, 1973. Astrophysical Concepts. Wiley, New York.

Hayakawa, S, et al, 1976. Infrared profile of the Milky Way at 2.4 μm. Nature, 261, 29-31.

Hayakawa, S, et al, 1977. Overall distribution of infrared sources in our Galaxy. Astron Astrophys, 58, 325-330.

Hayakawa, S, et al, 1978. Near-infrared observation of the Galaxy in the galactic anticentre direction. Publ Astron Soc Japan, 30, 369.

Hayakawa, S, et al, 1979. Near IR surface brightness of southern galactic plane. Nature, 279, 510-512.

Hayakawa, S, et al, 1980. Preprint of Hayakawa et al, 1981.

Hayakawa, S, et al, 1981. Distribution of near infrared sources in the galactic disk. Astron Astrophys, 100, 116-123.

Hoffman, J A, et al, 1978. Dual character of the Rapid Burster and a classification of X-ray bursts. Nature, 271, 630-633.

Hofmann, W, et al, 1977. Surface brightness of the central region of the Milky Way at 2.4 and 3.4 μm. Astron Astrophys, 57, 111-114.

Hofmann, W, et al, 1978. Mapping of the galactic centre and the Aquila region in the near infrared at balloon altitudes. Astron Astrophys, 70, 427-429.

Inoue, H, et al, 1980. A new mode of X-ray bursts from MXB 1730-335. Nature, 283, 358-360.

Ito, K, et al, 1976. Observation of the diffuse infrared radiation from our Galaxy at 2.4 μm. Publ Astron Soc Japan, 28, 427-436.

Ito, K, et al, 1977. Infrared profile of the central region of our Galaxy at 2.47 μm. Nature, 265, 517-518.

Johnson, H L, 1966. Astronomical measurements in the infrared. Annual Rev Astron Astrophys, 4, 193-206.

Johnson, H L, 1968. Interstellar extinction. In: Middlehurst, B M, & Aller, L H (eds). Nebulae and Interstellar Matter (Stars and Stellar Systems Vol 7). University of Chicago Press, Chicago.

Jones, A W, 1978. El Teide and the flux collector: infrared astronomy on Tenerife. J Brit Astron Assoc, 88, 257-266.

Jones, A W, et al, 1980. IR flashes from the X-ray Rapid Burster. Nature, 283, 550-551.

Jorden, P R, 1977. New Techniques and Measurements in Ground Based Infrared Astronomy. PhD thesis, University of London.

Joss, P C, 1977. X-ray bursts and neutron star thermonuclear flashes. Nature, 270, 310-314.

Kleinmann, D E, et al, 1976. The infrared source near the rapid-burst X-ray source MXB 1730-335. Astrophys J (Letters), 210, L83-L86.

Kleinmann, S G, et al, 1981. Preliminary results of the Air Force infrared sky survey. Annual Rev Astron Astrophys, 19, 411-456.

Klotz, I M, 1980. The N-ray affair. Sci American, 242, 122 (May).

Kulkarni, P V, et al, 1979. Discovery of IR bursts from Liller I/ MXB 1730-333. Nature, 280, 819-820.

Kurkarkin, B V, et al, 1970. General Catalogue of Variable Stars (3rd ed). Moscow State University.

Lamb, F K, et al, 1977. A model for bursting X-ray sources: time-dependent accretion by magnetic neutron stars and degenerate dwarfs. Astrophys J, 217, 197-212.

Lang, K R, 1974. Astrophysical Formulae. Springer, Berlin.

Lewin, W H G, 1977. X-ray burst sources. Mon Not R Astron Soc, 179, 43-53.

Lewin, W H G, 1979. What are X-ray burst sources? In: Baity, W A, & Peterson, L E (eds). X-Ray Astronomy. Pergamon.

Lewin, W H G, 1980. X-ray burst sources in globular clusters and the galactic bulge. In: Hanes, D, & Madore, B (eds). Globular Clusters. Cambridge University Press.

Lewin, W H G, & Joss, P C, 1977. X-ray burst sources. Nature, 270, 211.

Lewin, W H G, & Joss, P C, 1981. X-ray bursters and the X-ray sources of the galactic bulge. Sp Sci Rev, 28, 3-87.

Lewin, W H G, et al, 1976. The discovery of rapidly repetitive X-ray bursts from a new source in Scorpius. Astrophys J (Letters), 207, L95-L99.

Lewin, W H G, et al, 1980. Simultaneous IR and X-ray burst observation of Ser X-1. Nature, 287, 27-28.

Liller, W, 1977. Searches for the optical counterparts of the X-ray burst sources MXB 1728-34 and MXB 1730-33. Astrophys J (Letters), 213, L21-L23.

Lynn, P A, 1973. An Introduction to the Analysis and Processing of Signals. MacMillan, London.

MacGregor, A D, 1977. ICST Detector Testing Contract: Final Report. Royal Observatory, Edinburgh.

Maihara, T, et al, 1978. 2.4 micron observation of the Galaxy and the galactic structure. Publ Astron Soc Japan, 30, 1-19.

Maihara, T, et al, 1979. A balloon observation of diffuse far-infrared emission from the galactic plane. Astrophys J (Letters), 227, L129.

Malkan, M, et al, 1980. Infrared studies of globular clusters near the galactic center. Astrophys J, 237, 432-437.

Marshall, H L, et al, 1979. Further analysis of SAS-3 observations of the Rapid Burster (MXB 1730-335). Astrophys J, 227, 555-562.

McClintock, J E, et al, 1979. A 3-s delay in an optical burst from X-ray burst source MXB 1735-44. Nature, 279, 47-49.

Meikle, W P S, 1973. A Search for Radio Pulses of Astrophysical Origin. PhD thesis, University of Glasgow.

Neugebauer, G, and Leighton, R B, 1969. Two-Micron Sky Survey - A Preliminary Catalogue. NASA SP-3047, Washington DC.

Oda, N, et al, 1979. Cosmic dust in the central region of the Galaxy and an anomalous infrared source at $\ell = 355^\circ$, $b = -1^\circ$. Astron Astrophys, 72, 309-312.

Okuda, H, et al, 1977. 2.4 μm mapping of the galactic central region. Nature, 265, 515-516.

Okuda, H, 1981. The large scale infrared emission in the galactic plane - observations. In: Wynn-Williams, C G, & Cruikshank, D P (eds). Infrared Astronomy (IAU Symposium 96). Reidel, Dordrecht.

Oort, J H, 1977. The galactic center. Comments Astrophys, 7, 51-66.

Price, S D, & Walker, R G, 1976. The AFGL four color infrared sky survey - catalogue of observations at 4.2, 11.0, 19.8 and 27.4 μm. AFGL-TR-76-0208, USAF Geophysics Laboratory.

Sato, S, et al, 1980. No IR burst from the X-ray Rapid Burster MXB 1730-335. Nature, 286, 688-689.

Schmidt-Kaler, T, 1976. The spiral structure of our Galaxy - a review of current studies. Vistas in Astron, 19, 69-89.

Tyson, J A, & Giffard, R P, 1978. Gravitational wave astronomy. Annual Rev Astron Astrophys, 16, 521.

Ulmer, M P, et al, 1977. Some further information on the Rapid Burster MXB 1730-335. Astrophys J (Letters), L11-L15.

van Paradijs, J, 1978. Average properties of X-ray burst sources. Nature, 274, 650-653.

van Paradijs, J, 1981. Simultaneous optical/X-ray bursts. The Messenger, no 23, 1 (March).